NMDA- and asphyxia induced alterations of neurovascular responses in the cerebral cortex of newborn pigs, implications for the pathomechanism of neonatal hypoxic-ischemic encephalopathy

Ph.D. Thesis

Gábor Remzső, MS

Supervisor:
Ferenc Domoki, MD, Ph.D.

University of Szeged, Faculty of Medicine, Department of Physiology
Doctoral School of Theoretical Medicine

2021
Szeged

LIST OF PUBLICATIONS

Publications related to the thesis:

I. Gábor Remzső, János Németh, Viktória Varga, Viktória Kovács, Valéria Tóth-Szűki, Kai Kaila, Juha Voipio, Ferenc Domoki (2020). Brain interstitial pH changes in the subacute phase of hypoxic-ischemic encephalopathy in newborn pigs.
PLoS One. 2020; 15(5): e0233851.
DOI: 10.1371/journal.pone.0233851.
IF: 2.740.
Scimago ranking: Multidisciplinary area: 10/145, Q1 (D1)

II. Gábor Remzső, János Németh, Valéria Tóth-Szűki, Viktória Varga, Viktória Kovács, Ferenc Domoki (2019). NMDA attenuates the neurovascular response to hypercapnia in the neonatal cerebral cortex.
Scientific Reports 2019; 9(1):18900.
DOI: 10.1038/s41598-019-55468-1.
IF: 3.998.
Scimago ranking: Multidisciplinary area: 9/145, Q1 (D1)

TABLE OF CONTENTS

LIST OF PUBLICATIONS 1
TABLE OF CONTENTS 2
LIST OF FIGURES AND TABLES 4
LIST OF ABBREVIATIONS 5
SUMMARY 7
INTRODUCTION 8
Perinatal asphyxia (PA) and hypoxic-ischemic encephalopathy (HIE) 8
Pathophysiology of the HIE-induced brain damage 9
The role of PA-induced brain pH alterations in HIE pathophysiology 11
The newborn pig as an experimental model animal 12
Neurovascular unit dysfunction as a contributing factor to HIE pathophysiology 13
The study of cerebrocortical neuronal activity as a contributor to PA/HIE pathophysiology 16
AIMS 18
MATERIALS AND METHODS 19
Animals, surgery and protocol 19
Induction of graded hypercapnia 22
Induction of asphyxia 22
pH_{brain} measurements 22
LSCI measurements and analysis 23
Neurophysiological recordings 24
LFP spectral analysis 24
Spike sorting and unit classification 25
Statistical analysis 25
RESULTS 27
Effects of graded hypercapnia and asphyxia on physiological parameters 27
pH_{brain} changes during graded normoxic hypercapnia 32
pH_{brain} changes during PA and HIE development 34
The cerebrocortical microvascular response to graded hypercapnia and NMDA 35
LFP changes under graded hypercania 38
NMDA evokes delta (δ) oscillation 41
Altered laminar spiking activity in response to graded hypercapnia and NMDA 42
DISCUSSION 44
The translational value of the newborn pig 44
pH_{brain} acidosis in response to asphyxia and hypercapnia 45

pH_{brain} monitoring during HIE development 46
The cortical microvascular response to NMDA 47
The cortical neuronal response to NMDA 48
NMDA triggers SD-like suppression of the microvascular response to hypercapnia 49
CONCLUSION 52
ACKNOWLEDGEMENT 53
FUNDING 53
REFERENCES 54

LIST OF FIGURES AND TABLES

Figure 1. Pathophysiology of HIE. 7
Figure 2. Major pathways of the glutamate regulated cerebral blood flow 8
Figure 3. Experimental groups and protocol 1 11
Figure 4. Experimental groups and protocol 2 12
Figure 5. Hemodynamic and oxygenation changes under PA 18
Figure 6. Physiological parameters and blood chemistry changes during PA and the subsequent 24h reventilation period 20
Figure 7. Cortical blood flow (CoBF) changes to graded hypercapnia and NMDA 22
Figure 8. Summary of the cortical microvascular responses to graded hypercapnia and NMDA 23
Figure 9. Representative heat map images of delta (δ) and theta (θ) band power spectral densities (PSDs) 25
Figure 10. NMDA evokes delta (δ) oscillation in the upper cortical layers 27
Figure 11. Representative auto-correlograms and cross-correlograms 29
Figure 12. pH_{brain} changes during PA and the reventilation period 30
Figure 13. Neuronal injury evaluated at 24 hours after PA 31
Figure 14. Cerebral acidosis induced by graded normoxic hypercapnia 33
Table 1. Arterial pCO_2, pO_2, pH, HCO_3^-, base excess BE(b), oxygen saturation (SpO_2), mean arterial blood pressure (MABP) and heart rate (HR) values 17
Table 2. Power spectral density changes in the delta and the theta band 26

LIST OF ABBREVIATIONS

20-HETE	20-hydroxy-eicosatetraenoic acid
AA	arachidonic acid
AAAN	N-(4 S)-4-amino-5-[aminoethyl]-aminopentyl-N′-nitroguanidin
ACG	auto-correlogram
aCSF	artificial cerebrospinal fluid
aEEG	amplitude-integrated EEG
ANOVA	analysis of variance
AP	anterior-posterior
ATP	adenosine triphosphate
BBB	blood-brain barrier
BE(b)	base excess
CBF	cerebral blood flow
CCG	cross-correlogram
cEEG	conventional EEG
CoBF	cortical blood flow
COX-2	cyclooxygenase-2
CSD	current source density
EEG	electroencephalography
EET	epoxyeicosatrienoic acid
FFT	Fast Fourier Transformation
fMRI	functional magnetic resonance imaging
HIE	hypoxic-ischemic encephalopathy
HR	hearth rate
IIR	infinite impulse response
LFP	local field potential
LSCI	laser-speckle contrast imaging
MABP	mean arterial blood pressure
MEG	magnetoencephalography
mGluR	metabotropic glutamate receptor
ML	medial-lateral
MRI	magnetic resonance imaging
MRS	magnetic resonance spectroscopy

NICU	neonatal intensive care unit
NMDA	N-methyl-D-aspartate
NMDAR	N-methyl-D-aspartate receptor
nNOS	neuronal nitric oxide synthase
NOS	nitric oxide synthase
ODQ	guanylate cyclase inhibitor 1 H-[1,2,4]oxadiazolo[4,4,-a]quinoxalin-1-one
PA	perinatal asphyxia
PET	positron emission tomography
PG	prostaglandin
pH_{brain}	brain interstitial pH
PIP	peak inspiratory pressure
PLA_2	phospholipase A_2
PSD	power spectral density
RM ANOVA	repeated measure of analysis of variance
ROI	region of interest
ROS	reactive oxygen species
RR	respiration rate
SD	spreading depolarization
SpO_2	peripherial saturation
XO	xanthine oxidase

SUMMARY

Perinatal asphyxia (PA) is a major cause of neonatal mortality and it can also lead to hypoxic-ischemic encephalopathy (HIE) in the surviving newborns. Despite the availability of therapeutic hypothermia, HIE still results in long term disability in many infants, as hypothermia alone is often not sufficient to fully mitigate the HIE-caused neuronal damage. To find new adjunct therapies, further investigation of the neuronal and vascular pathomechanisms underlying HIE development is warranted, and the newborn pig used in our studies is one of the best large animal model for the preclinical translational study of PA/HIE.

To enhance the mechanistic understanding of neuronal injury in our previously established translationally valid PA/HIE model, first we aimed to determine the magnitude, the dynamics, and the mechanisms of PA on the brain interstitial pH (pH_{brain}) both during asphyxia and HIE development. Second, we investigated the effects of excessive glutamatergic activation by NMDA on neurovascular unit function using hypercapnia-induced vasodilation to test cerebrovascular reactivity. Third, we wanted to explore if NMDA could alter both the spontaneous and also the hypercapnia induced changes in cortical electrical activity.

Anesthetized and mechanically ventilated piglets were fitted with either open or closed cranial windows. pH_{brain}, cortical blood flow (CoBF), and neuronal activity was determined, with pH-sensitive microelectrodes, laser-speckle contrast imaging, and multi-channel intracortical microelectrodes, respectively. PA was elicited by ventilation with a hypoxic-hypercapnic gas mixture (6%O_2, 20%CO_2; 20min), then HIE development was observed up to 24h. NMDA was applied onto the cortical surface, graded (5-20%) hypercapnia was induced by ventilation with a normoxic-hypercapnic gas mixture.

pH_{brain} dropped below 6.0 during PA exceeding by ≅0.8 pH unit the acidosis in the blood highlighting its importance in neuronal injury. The respiratory component was responsible for only ≅40% of the developing acidosis. pH_{brain} was restored quickly after PA and remained stable throughout the observation period. Both graded hypercapnia and NMDA caused increases in CoBF, but NMDA also attenuated the response to hypercapnia in an NMDA-receptor and nitric oxide synthase (nNOS) dependent manner shown with respective inhibitors. NMDA induced neurovascular dysfunction was also shown by NMDA-induced perturbations in cortical neuronal activity and the altered electrophysiological response to graded hypercapnia as well.

Our findings suggest that severe acidosis as well as excitotoxic neurovascular unit dysfunction may play an important role in PA/HIE pathpohysiology in our translational PA/HIE model.

INTRODUCTION

Perinatal asphyxia (PA) and hypoxic-ischemic encephalopathy (HIE)

The neonatal period (the first 28 days of life) is the most vulnerable time for a child's survival. Infants face the highest risk of dying in their first month of life at an average global rate of 17 deaths/1.000 live births in 2019. Since 1990 mortality has been reduced by 52% from 38 deaths/1.000. In 2019, the probability of dying after the first month and before reaching age 1 was estimated at 11 deaths/1.000 and the probability of dying after reaching age 1 and before reaching age 5 was estimated at 10 deaths/1,000. In 2019, 2.4 million children died globally in the first month of life (approximately 6,700 deaths/day) with about a third of all neonatal deaths occurring within the first day after birth, and close to three-quarters occurring within the first week of life. Beside the neonatal mortality globally, there are marked disparities in the neonatal mortality across countries and regions. In 2019, the neonatal mortality rate was the highest in South Asia and in sub-Saharan Africa with a 25 and 27 deaths/1000 live births. According to the United Nations Inter-agency Group for Child Mortality Estimation (UN IGME) and the United Nations International Children's Emergency Fund (UNICEF), in Hungary the neonatal mortality rate was 2 deaths/1000 live births in 2019[1].

Perinatal asphyxia (PA), occuring around birth, is a clinical condition that causes gas exchange abnormalities in the newborn, leading to hypercapnia, hypoxemia and mixed respiratory-metabolic acidosis[2]. Due to the cardiovascular responses to asphyxia, the developing centralized circulation tries to maintain the O_2 and glucose levels in the brain and myocardium. Critical tissue hypoxia can occur when the compensatory mechanisms fail to prevent the metabolic crisis, which will lead to hypoxic-ischemic encephalopathy (HIE) in the survivors[3]. The antepartum risk factors of PA can include chromosomal abnormalities, intrauterine growth restrictions, multiple gestations, preeclampsia, hemorrhage. The intrapartum risk factors can be recognised more easily, which includes placental abrubtion, uterine rupture, umbilical cord compression, chorioamnionitis and maternal cardiac arrest. Asphyxia can also occur in the immediate postnatal period[4].

HIE can also be regarded as a subset of neonatal encephalopathy where the brain dysfunctions are indicated by the following clinical manifestations[5].

The diagnostic criteria of HIE include the presence of two or more of the following:

1. Severe acidosis in the umbilical artery blood (pH < 7.0)[6]
2. Base deficit > 12 mmol/l[6]
3. Low Apgar score[7]
4. The need of respiratory support in the first few minutes of life[8]
5. Neonatal neurological disorders (seizures)[6]
6. Multiple organ failure[6]
7. Presence of meconium stained amniotic fluid[9]

If these criteria are present at birth, it is most likely that PA is responsible for HIE and the caused brain damage. The term „neonatal encephalopathy" describes a broader spectrum of clinical representation of the neurological dysfunctions, which can include depression, reflex abnormalities and consciousness/coma[3]. Sometimes it's hard to distinguish the PA-induced HIE from the other types of neonatal encephalopaties because the symptoms are not specific for the PA aetiology[10]. In the first few minutes of life, the clinical status is determined by the Apgar score, which include assessment of the respiration, reflexes, hearth rate, appearance (skin color), and muscle tone[11]. However, this scoring is not specific enough for the PA. The Sarnat score is a much more accurate system which also determines the severity of the encephalopathy[12]. The Sarnat scoring system classifies the HIE into mild (Stage I.), moderate (Stage II.) and severe (Stage III.) stages, based on electroencephalography (EEG) and neurological findings.

Pathophysiology of the HIE-induced brain damage

Due to impaired cerebral blood flow[13], lack of oxygen and glucose delivery to the brain, the accumulation of carbon dioxide and metabolic acidosis, the pathologic events of HIE can develop. These events occur in two main phases: primary- and secondary energy failure.

The main cause of primary energy failure is the cerebral blood flow reduction. The decreased glucose and oxygen levels lead to adenosine triphosphate (ATP) depletion and increased lactate production[14]. The loss of ATP results in the failure of many cellular mechanisms.

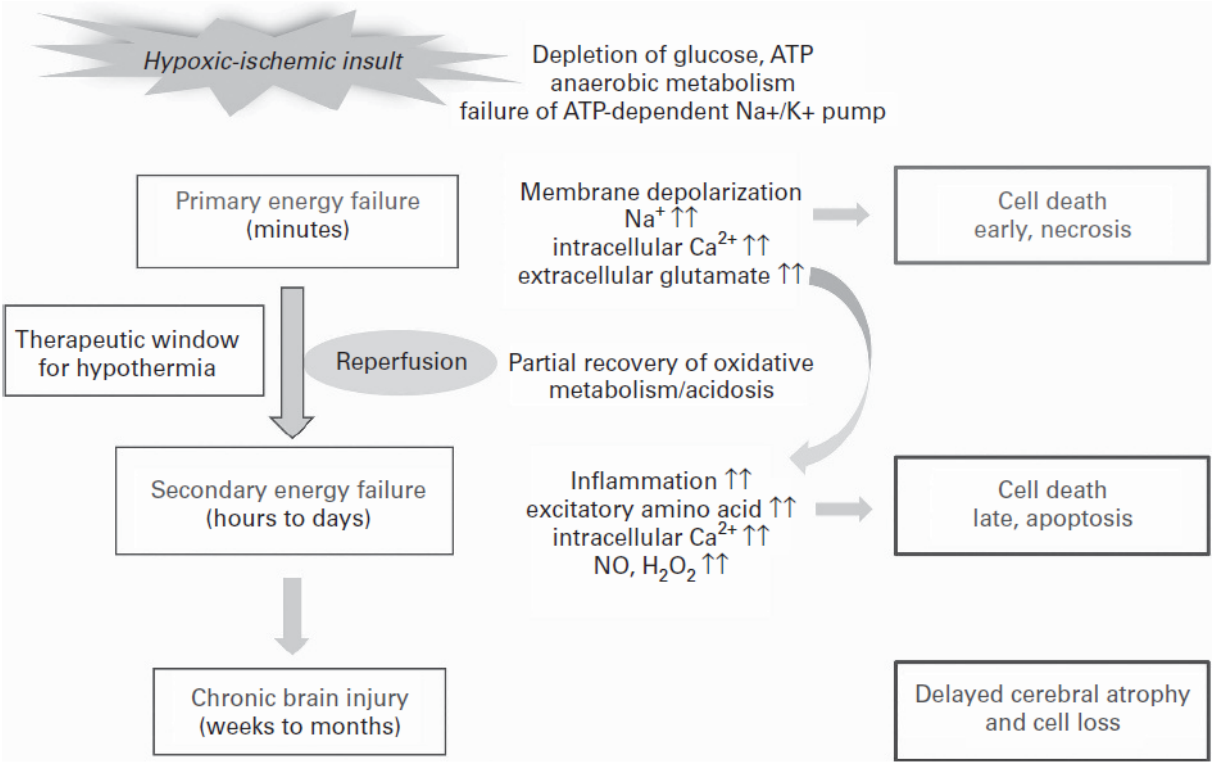

Figure 1. *Pathophysiology of HIE*[15]*. Hypoxic-ischemia is leading to cellular energy failure and cell death. The brain damage is caused by cerebral ischemia, which results in oxygen and glucose deprivation in the brain, driving the cells to anaerobic metabolism. The energy failure leads to ion channel dependent intracellular* Na^+ *accumulation, excitatory amino acid accumulation and uncontrolled glutamate receptor activation culminating in rapid cell swelling and necrosis. The reperfusion triggers further oxidative injury resulting in only partial recovery that marks the onset of the latent phase. Hours/days later the onset of the so-called secondary energy failure can be observed, characterized by repeated intracellular accumulation of* Ca^{2+} *and subsequent intracellular mechanisms, oxidative stress, neuroinflammation and delayed neuronal cell death. Further neuronal loss and cerebral atrophy appear in the tertiary phase.*

Most importantly the Na^+/K^+ pumps and the intracellular Ca^{2+} homeostasis maintatining mechanisms will be damaged[16]. Due to Na^+/K^+ pump failure, excessive Na^+ influx can lead to massive depolarization of the neurons. This will end up in excessive release of the excitatory neurotransmitter glutamate, which binds to its receptors and causes additional Na^+ and Ca^{2+} influx[17], leading to mitochondrial dysfunction[18]. The intracellular Ca^{2+} increase has a detrimental role in causing ischemia, cerebral edema and microvascular damage, resulting in necrosis and apoptosis[13,17,19]. These two types of cell deaths can occur under both primary and

secondary energy failure as well. Necrosis appears after severe ischemia and hypoxia[17]. Upon cell rupture, the cellular contents are released causing further inflammation[16]. The neuroinflammatory response will involve the activation and migration of microglia that scavenge tissue debris and release inflammatory mediators, which cause white matter damage and scar tissue formation[20]. If the insult is milder, the neurons may recover or progress to apoptosis (Fig.1).

The resuscitation regenerates the cerebral perfusion and partially decreases the excitotoxicity caused by the excessive glutamate level. This very short period of time called the latent period, its duration depends on the severity of the injury. Generally, the more severe the injury, the shorter the latent period is[21].

A secondary energy failure phase occurs 6-48 h after the injury which is highly related to inflammation, excitotoxicity and oxidative stress[13,17]. Oxidative stress can be described by the upregulation of the enzymes like cyclooxygenase-2 (COX-2), xanthine oxidase (XO) and nitric oxide synthase (NOS), which will lead to reactive oxygen species (ROS) overproduction, such as peroxynitrite- (ONOO-) and hydroxyl radical ($OH^{\bullet}$)[22]. Oxidative stress is harmful to the neonatal brain because the endogenous antioxidants are present at low levels and also due to the high concentration of unsaturated fatty acids that can produce more free radicals through lipid peroxidation than saturated fatty acids. The oxidative stress may result in sustained oxidative DNA damage[22]. After the antioxidant system exhaustion, the proteolytic caspase proteins will be activated. Furthermore, proinflammatory gene expression can also be observed, causing neutrophil granulocyte and microglia migration into the damaged area, leading to blood-brain barrier (BBB) disruption and microvascular injury[23].

Continuing pathological processes can occur in the survivors of PA/HIE up to weeks or even years which has been termed as tertiary brain injury. These persisting damaging mechanisms involve gliosis, epigenetic changes and persistent inflammatory receptor activation[24].

The role of PA-induced brain pH alterations in HIE pathophysiology

Primary and secondary pH_{brain} alterations can lead to neuronal injury in the newborn neocortex. The regulation of the pH is precise under physiological conditions, however the disturbances of the extracellular pH highly affect the neuronal excitability[25]. It is well documented that pH alteration modulates different types of ion channels. For instance, acidosis suppresses, while alkalosis facilitates the opening of NMDA receptors in rat hippocampal

neurons[26]. Furthermore, extracellular pH can also modify the currents through voltage-gated Na^+, K^+ and Ca^{2+} channels in rat hippocampus[27].

Helmy *et al.*[28] and Ala-Kurikka *et al.*[29] reported previously that asphyxia induced by hypoxic-hyperapnic gas mixtures (9% O_2 + 20% CO_2; 5-9% O_2 + 20% CO_2) evoked cerebral acidosis in spontaneously breathing newborn rats. Helmy *et al.* also reported that upon reventilation of the rat pups, pH_{brain} showed a shift into the alkalic direction, which was highly associated with the occurence of seizures[28]. Intermittent asphyxia triggering periodic hypoxic episodes have been suggested to enhance the neuronal excitability[30], which is manifested as hyperexcitability (lowered seizure threshold) and spontaneously occuring seizures. Seizures can be strongly suppressed by slowing down the pH_{brain} recovery with 5% CO_2 inhalation. The efficacy of CO_2 has also been demonstrated in translationally valid small-animal models of birth asphyxia in rats and guinea pigs, showing that gradual restoration of normocapnia had beneficial effects on cerebral metabolic acidosis, oxygen and lactate levels[31].

Several studies followed the pH_{brain} alterations during/after asphyxia, however we have very scarce knowledge about pH alterations in large animal models under the acute and subacute phase of PA/HIE.

The newborn pig as an experimental model animal

In preclinical research the animal models are mandatory to reveal the mechanisms of different pathophysiological processes - including PA/HIE as well - and to test the potential neuroprotective strategies. Primates and rodents have been the preferred species studying neuroscience. However in other fields, such as experimental surgery[32] the use of pigs has increased in the past few decades. Using a pig as an experimental model shows considerable resemblance of pigs to human physiology and anatomy. All agricultural and laboratory pigs are derived from the Eurasian *Sus scrofa*, however the different breeds have varying anatomy and physiology. The most common breeds are the Landrace, Hampshire, Yorkshire and Duroc[33]. There are also several minipig breeds used in laboratory research, such as the Yucatan, Hanford, Göttingen and Sinclair minipigs.

In the recent years, the domestic piglet has emerged as an excellent model animal for studying neurobehavior and neurodevelopment. Notably, the major brain growth spurt in pigs and as well as in humans, extends from the late prenatal to the postnatal period[34]. Other commonly used animal models have differences in growth spurt timing, in most the brain growth spurt can be observed postnatally[34]. In addition, the gross anatomical features, such as

the brain convolution and the distribution of the white and grey matter of the newborn piglet brain are similar to the human neonate[35,36]. The pig is a gyrencephalic species and the cortical surface is similar to the human gyrencephalic neocortex, in contrast with the rat cerebral cortex which is lissencephalic. The neonatal pig brain is very similar to the human neonate brain in anatomical, topological, developmental, cytoarchitectonical features as well. Furthermore, the maturation, myelination and electrical activity are also comparable to that of humans[37,38].The size of the newborn piglets allow the usage of the different neuroimaging techniques to be used in piglets, which are basically designed for humans. The experimental instrumentations which were already applied to piglets are: positron emission tomography (PET), magnetic resonance imaging (MRI), functional magnetic resonance imaging (fMRI), EEG, magnetic resonance spectroscopy (MRS) and magnetoencephalography (MEG)[37,38].

Based on the above described advantages, the neonatal piglet has become an excellent model for studying how the early life hypoxic-ischemic (HI) insults, such as PA, affect the brain and brain development. Several PA/HIE models have been used in the past few decades, however not all of them shows the major hallmarks of PA. In these models, the HI insults were evoked with increased intracranial pressure[39], vessel ligation[40], global asphyxiation[41] or cardiac arrest[42]. In light of the importance of CO_2 levels affecting neuronal excitability, recently the hypoxic ventilation combined with hypercapnia[31,43] has become our standard method for the induction of „true" PA.

Neurovascular unit dysfunction as a contributing factor to HIE pathophysiology

The neurovascular unit is a conceptual framework describing all the structural and functional connections among neuronal and vascular elements that assure the continuous adequate tissue perfusion to supply the metabolic demands of neuronal activity. Neurovascular unit dysfunction can be caused by HI injury including PA demonstrated by altered microvascular reactivity to N-methyl-D-aspartate (NMDA)[44]. The study of the mechanisms of NMDA-induced neurovascular effects in the cerebrocortical circulation requires the exploration of all contributors to the neurovascular unit. Synaptic release of glutamate or exogenous NMDA will activate the NMDA receptors (NMDAR), which leads to Ca^{2+} influx into the neurons and the activation of the neuronal nitric oxide synthase (nNOS). The NO release causes vasodilation[45] (Fig. 2) both *in vivo* and *in vitro* without astrocyte involvement. In the piglet, it has been described that nNOS positive neurons and NMDAR 2A/B expressing neurons are located in the cortical layer II/III[46]. However, the NMDAR 2A/B and nNOS coexistence was

not identified *in vivo* yet, only *in vitro*[47]. NMDAR localization is highly restricted in the cortex and its colocalization with nNOS depends on the developmental stage, anatomical location and species[46,48].

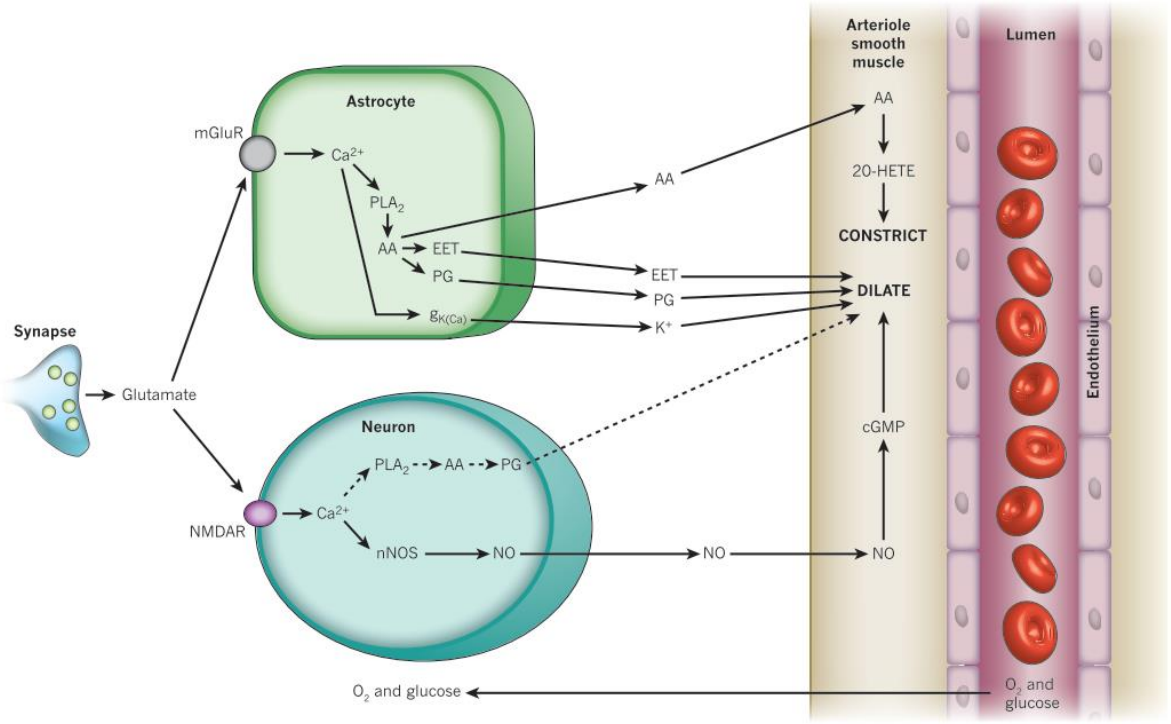

Figure 2. *Major pathways of the glutamate regulated cerebral blood flow*[49]*. Neuronal and astrocytic pathways regulate the cerebral blood flow via messengers, influencing the arteriolar smooth muscle, supplying the glucose and oxygen to the cells. In the neurons, the glutamate acts on NMDA receptors, increasing the intracellular* Ca^{2+}*, causing NO release by activating nNOS, which will activate the guanylate cyclase in the smooth muscle, generating cGMP and leading to vasodilation. The increased* Ca^{2+} *can also generate arachidonic acid (AA) from phospholipase* A_2 *(*PLA_2*), which is converted to prostaglandins (PG) by COX-2, causing vasodilation. In astrocytes, the glutamate activates the metabotropic glutamate receptors (mGluR), causing increased intracellular* Ca^{2+} *level, generating AA and three different types of metabolites. PGs and epoxyeicosatrienoic acids (EETs; produced by P450 epoxygenase) can elicit to vasodilation, however, 20-hydroxy-eicosatetraenoic acid (20-HETE) could cause vasoconstriction. Elevations in the astrocytic endfeet* Ca^{2+} *levels can not only trigger the synthesesis of vasoactive metabolites but it can also activate* Ca^{2+} *gated* K^+ *channels leading to vasodilation through the released* K^+ *ions.*

Inhibiton of the nNOS in the cerebral cortex reduces the blood flow increase which is associated with neuronal activity, proving the role of NO in the neurovascular coupling. By adding NO donors, it can restore the response, which means the presence of the NO is mandatory, however the dynamic NO increase in response to neuronal activity, not directly mediates the neuron to vessel signaling[50]. In this case the NO modulates the pathways in astrocytes, causing constriction or dilation of the blood vessels.

Astrocytes can dilate the vessels through a K^+-based mechanism. When the released glutamate escapes from the synaptic cleft, it can activate the mGluR on the astrocytes, causing intracellular Ca^{2+} increase. This elevated Ca^{2+} level can open the large conductance Ca^{2+} activated K^+ (BK) channels[51] and releasing K^+ from the astrocyte endfeet to the vessels (Fig.2). Yet another possible dilatory mechanisms in astrocytes is the activation of PLA_2 by the increased Ca^{2+} levels producing AA. The build-up of AA will lead to the production of PGs and epoxyeicosatrienoic acids (EETs), which dilate the arterioles[52,53]. However, the AA conversion to 20-hydroxy-eicosatetraenoic acid (20-HETE) is also possible, which will lead to vasoconstriction (Fig. 2). The vasodilatory or vasoconstrictive response is partially determined by the preexisting tone of the vessels[54] and also O_2 concentration has a key role in it, accordingly, vasodilation is enhanced by higher smooth muscle tone and tissue hypoxia.

Synaptic glutamate release raises intracellular Ca^{2+} in both neurons and astrocytes and some astrocytes show as fast Ca^{2+} increases as seen in neurons. The blood flow responses are highly correlated with local field potentials (LFP)[55,56]. The ionotropic glutamate receptor antagonists can decrease the blood flow responses and the LFP as well, after applying stimulation in the cortex, olfactory bulb or cerebellum. Glutamate release can generate LFPs and also activates the mGluRs on the astrocytes, which means the LFP amplitude can be also correlated with the receptor activation on astrocytes. Experimentally blocking the ionotropic glutamate receptors will decrease the neuronal firing and by blocking the glutamate release, it can prevent the release of astrocytic messengers.

The blood flow maintenance in the brain or the neurovascular unit's integrity can be disrupted due to pathological conditions. The NMDA caused cerebrovascular dilation is reduced or ceased by asphyxia[57], hypoxia/reoxygenation[46,58] or ischemia/reperfusion[59]. These altered mechanisms are highly connected to ROS production. The ROS's primary target appear to be the NMDARs themselves or the NMDAR-positive neurons, because the pial arteriolar responses to exogenous NO donors after the ischemic stress remain intact[47].

Interestingly, NMDARs can be not only a target but also a mediator of neurovascular unit dysfunction. Spreading depolarization (SD), a continuous wave of almost complete

neuronal depolarization accompanied by spreading depression of neuronal activity[60], can also induce neurovascular unit dysfunction and alter the microvascular reactivity. Even a single SD wave can abolish the normal microvascular response to hypercapnia in many species[61–63]. NMDA - the selective activator of the NMDAR - can trigger SD when topically applied onto the surface of the cortex in both adult rats[64] and mice[65]. The NMDAR involvement is required in evocation and propagation of the SD[66,67]. In neonates including newborn pigs, the SD cannot be yet elicited[64], despite the presence of functional NMDAR.

The study of cerebrocortical neuronal activity as a contributor to PA/HIE pathophysiology

Neuronal activity patterns in the neonatal brain are known to be important in shaping neuronal development and synaptogenesis, and they are extremely important for the postnatal survival of neurons as well. PA/HIE can elicit abnormal activity patterns that can themselves affect the long-term neurodevelopmental outcome of HIE patients. Although, there are several advanced neuroimaging methods that can be used to monitor mainly the structural/biochemical alterations in the neonatal brain, only the EEG allows the non-invasive assessment of cerebrocortical activty. A further advantage of the EEG that is far more available and less expensive as most/all of the imaging techniwques that require extensive equipment and maintenance. Despite the wide use of the newborn pig to study lesion outcome after PA/HIE, there is very scarce knowledge about cortical[68], intracortical[68] or hippocampal[69] neuronal activity in this species even under physiological let alone pathological conditions.

The neonatal EEG activity develops with the age and the pathophysiologic patterns are difficult to recognise. In the early neonatal period, the conventional EEG (cEEG) and the amplitude-integrated EEG (aEEG) are highly predictive of long term outcome. This predictive ability can help classifying and diagnose the HIE severity. Due to the need of long-term recordings of the EEG signals (often many days) in the neonatal intensive care unit (NICU), one or two channel aEEG is the most commonly used and preferred technique in clinical electrophysiology[70].

The normal cEEG background can be described by its most prominent features: frequency, amplitude, synchrony, symmetry and sleep wake state[71]. There are also important abnormalities in these features, such as electrical transients and seizures. These neonatal seizures are often subclinical or electrographic only or showing clinical manifestations which are hard to differentiate[72]. Electrographic seizures can be: unifocal, multifocal, lateralized, bilateral independent, bilateral, migrating and diffuse. The morphology of the ictal discharges

consist of rhythmic spikes, sharp waves or rhythmic delta, theta, alpha or beta waves. In neonates, the rhythmic delta waves are the most common in the ictal pattern[73]. Seizure semiology can also differentiate clonic-, tonic-, myoclonic seizures, epileptic spasms[74].

Due to the wide variety of seizure types and abnormal waveforms recorded in HIE suffered neonates, new methods need to be implemented in the clinical practice. Nowadays, the artificial intelligence (AI) based detection and prediction methods are more and more gaining acceptance into clinical use. All these AI-driven techniques are based on machine learning[75], deep learning and convolutional neural network (CNN) algorhytms[76], using neonatal EEG recordings.

AIMS

The major aim of our studies was to explore pathophysiological mechanisms in our translational large animal HIE model that may be of relevance for the development of adjunct neuroprotective therapies in the clinical management of HIE. The specific goals of our studies were the following:

1. We wanted to quantitatively determine the magnitude and the temporal dynamics of PA on pH_{brain} both during asphyxia and throughout the subacute phase of HIE development to be able assess the significance of pH alterations in our PA/HIE model and to allow comparison data from studies on rodents. We also wanted to determine the selective contribution of the respiratory component (the hypercapnia) in the PA-induced acidosis.
2. We wanted to determine if NMDA application alone (simulating generalized glutamatergic activation in the absence of PA) would affect the neurovascular unit function using hypercapnia-induced vasodilation as a test of cerebrovascular reactivity. As we proved NMDA-induced neurovascular dysfunction, we assessed if neuronal NO synthase activity plays a role in the mechanism.
3. Emanating from our results of specific goal #2, we wanted to start the electrophysiological exploration of cerebrocortical neuronal activity and connectivity in the piglet. Specifically, we studied if NMDA could alter both the spontaneous and also the hypercapnia-induced changes in electrical activity coinciding with its effect on cerebrovascular reactivity.

MATERIALS AND METHODS

Animals, surgery and protocol

Newborn (<24 h old) male Landrace piglets (n=47, body weight: 1.5-2 kg) were obtained from a local company (Pigmark Ltd., Co., Szeged, Hungary). The experimental procedures were approved by the National Ethical Committee on Animal Experiments (ÁTET, I.74-7/2015), and then the necessary permit to obtain the animals was issued by the National Food Chain Safety and Animal Health Directorate of Csongrád county, Hungary (permit nr: XIV./1414/2015). The procedures were performed according to the guidelines of the Scientific Committee of Animal Experimentation of the Hungarian Academy of Sciences (updated Law and Regulations on Animal Protection: 40/2013. (II. 14.) Gov. of Hungary), following the EU Directive 2010/ 63/EU on the protection of animals used for scientific purposes and reported in compliance with the ARRIVE guidelines.

The animals were restrained and anesthetized with intraperitoneal sodium thiopental injection (45 mg/kg; Sandoz, Kundl, Austria). The animals were placed on a servo-controlled heating pad (Blanketrol III, Cincinnati SUB-zero, Cincinnati, Ohio, USA), keeping their core temperature in the physiological range (38.5±0.5 °C). The piglets were intubated through a tracheostomy then mechanically ventilated with humidified medical air occasionally supplemented with oxygen (FiO_2: 0.21-0.25) with the following ventilation parameters: respiration rate (RR): 30-35/min; peak inspiratory pressure (PIP): 12-14 cmH_2O. A catheter was inserted into the right femoral vein under aseptic conditions and anesthesia/analgesia was switched to intravenous morphine (100 µg/kg bolus then 10 µg/kg/h; Teva, Petach Tikva, Israel) and midazolam (250 µg/kg bolus then 250 µg/kg/h; Torrex Pharma, Vienna, Austria) as used previously[77,78] along with supportive fluid therapy (0.45% NaCl, 5% glucose; 3 ml/kg/h). A second catheter was inserted into the right carotid artery for taking blood samples, monitoring the mean arterial blood pressure (MABP) and heart rate (HR). As shown previously, unilateral carotid artery occlusion does not affect cerebral blood flow (CBF) and preferable to catheterization of the femoral artery causing very severe hindlimb ischemic damage[79]. Blood samples (300 µl) were analyzed for pH, gases, electrolytes and metabolites with an epoc® Blood Analysis System (Epocal Inc., Ottawa, Canada). We monitored the peripheral saturation (SpO_2) using pulse oximetry.

After instrumentation, the heads of the animals were fixed into a stainless steel stereotactic frame (RWD Life Science, Shenzhen, Guangdong Province, China). For the LSCI

studies, we implanted a stainless steel closed cranial window (d=1.8 cm) over the parietal cortex which was sealed with bone wax and cemented with dental acrylic[80]. For the electrophysiology and the interstitial pH measuring studies, we obtained an open cranial window over the left parietal cortex for electrode insertion and we also drilled two holes into the frontal bone positioning the reference and the ground electrodes, respectively. The dura mater was carefully removed avoiding the blood vessels. If necessary, the smaller bridging veins were cauterized. The location of the cranial window and the electrode insertion point was determined by stereotactic reference points (window d=0.8 cm; measured from Bregma: anterior-posterior (AP) axis:-1.2-(-1.4) cm, medial-lateral (ML) axis: 1.1-1.3 cm). The subarachnoidal space was filled with warmed (37 °C) artificial cerebrospinal fluid (aCSF) containing 0.22 g/l KCl, 0.132 g/l $MgCl_2$, 0.221 g/l $CaCl_2$, 7.71 g/l NaCl, 0.402 g/l urea, 0.665 g/l dextrose and 2.066 g/l $NaHCO_3$, and was equilibrated with a gas mixture containing 6.3% O_2, 6.2% CO_2, and 87.5% N_2, respectively. At the end of the experiments the animals were euthanized with an overdose of pentobarbital sodium (300 mg, Release; Wirtschaftsgenossenschaft deutscher Tierärzte eG, Garbsen, Germany). According to the study protocols, we divided the animals into 2 and 4 groups, respectively (Fig. 3,4):

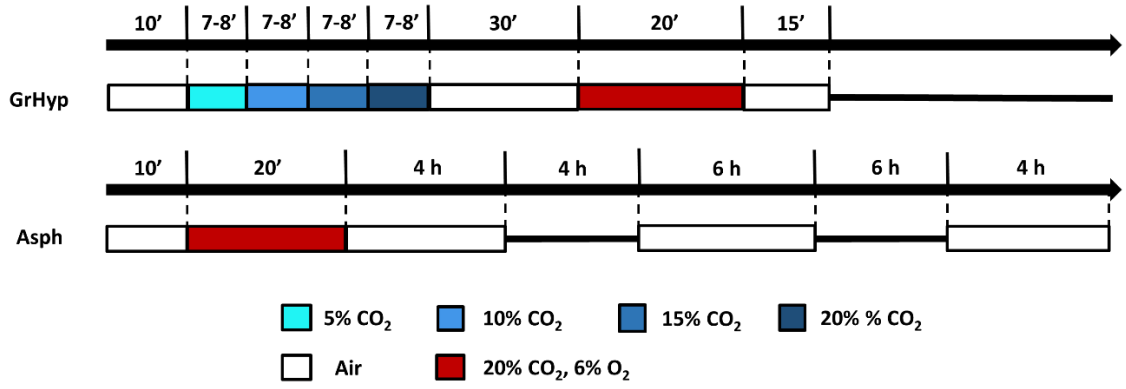

Figure 3. *Experimental groups and protocol 1. In the GrHyp group (Group 1) we induced graded hypercapnia with 5-20% CO_2, increased with 5% step-wise. In the Asph group (Group 2) we induced the asphyxia with 20% CO_2, 6% O_2 gas mixture (RR=15/min) and measured the cortical pH in different time windows.*

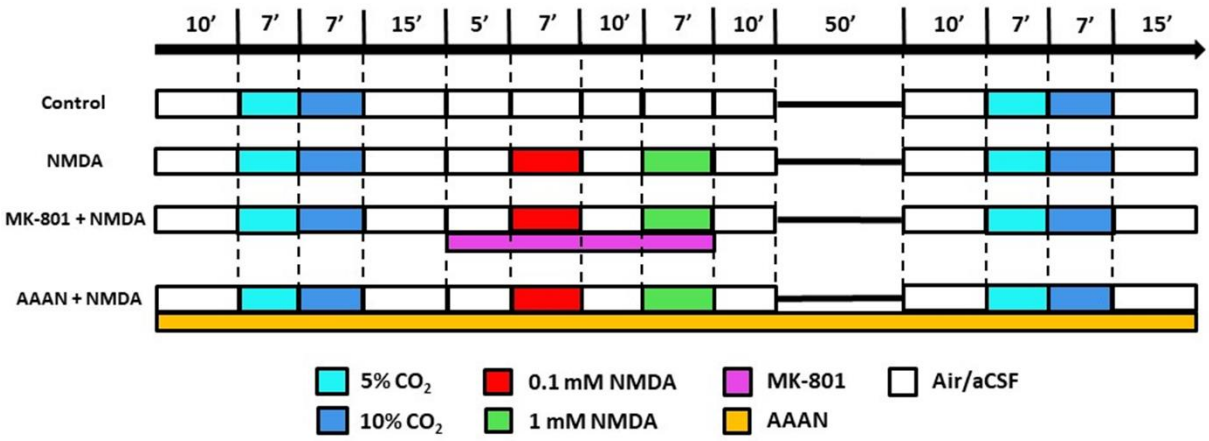

Figure 4. *Experimental groups and protocol 2. In the control group (Group 3) we repeated the graded hypercapnia with 5-10% CO_2. In the NMDA group (Group 4) we used 0.1 and 1 mM NMDA topically (dissolved in aCSF) between the two gaded hypercapnic stimulus. In MK-801 + NMDA group (Group 5) we pretreated the cortex and co-applied MK-801 with NMDA, strictly using the same stimuli as in Group 2. In AAAN + NMDA group (Group 6) the animals were treated with i.v. AAAN, then we repeated Group 2's stimuli.*

1.1 GrHyp group (Group 1, n=3): graded normoxic hypercapnia was elicited with 5% step-wise increase in CO_2 from 0% to 20%

1.2 Asph group (Group 2, n=13): we induced asphyxia with hypercapnic-hypoxic gas mixture (20% CO_2 and 6% O_2, RR=15/min) and recorded the cortical pH in different time windows (baseline, PA and the first 4 hours of reventilation (n=6), 8th-14th hours (n=8) and 20^{th}-24^{th} hours (n=3) of reventilation). HIE development was confirmed with previously estblished neuropathology assessment see details in Németh *et al*[77].

2.1 Control group (Group 3, n=6): we used repeated graded hypercapnia (5% and 10% CO_2) without NMDA stimulations

2.2 NMDA group (Group 4, n=14): between the two graded hypercapnia increasing concentrations (0.1 and 1 mM) of N-methyl-D-aspartate (NMDA; Sigma Aldrich, St. Louis, MO, US) dissolved in aCSF were topically washed onto the cortex under the closed cranial window to study CoBF (n=7) or the open cranial window to study LFP (n=7).

2.3 MK-801 + NMDA group (Group 5, n=4): we used the same stimuli as in Group 4, except we used NMDA-receptor antagonist MK-801 (0.1 mM dissolved in aCSF; Research

Biochemicals International, Natick, MA, US) to pretreat the cortex and co-applying with NMDA

2.4 AAAN + NMDA group (Group 6, n=7): selective neuronal nitric oxyde synthase (nNOS) inhibitor (N-(4S)-4-amino-5-[aminoethyl]aminopentyl-N'-nitroguanidin; AAAN; Santa Cruz Biotechnology, Dallas, TX, US; dissolved in saline, 0.4 mg/kg iv) [81] were given then we used the same stimuli as in Group 4

Induction of graded hypercapnia

In Group 1, before inducing PA, the effect of graded normoxic hypercapnia on pH_{brain} was evaluated by 5% step-wise increases in inhaled CO_2 from 0% to 20%, for 7 to 8 min each. After the graded hypercapnia, normocapnia was restored for 30 min. These animals were euthanized with an overdose of pentobarbital sodium (300 mg, Release; Wirtschaftsgenossenschaft deutscher Tierärzte eG, Garbsen, Germany) at 2 hours after PA.

Induction of asphyxia

In Group 2 after the surgery, a 1h recovery period allowed stabilization of the monitored physiological parameters prior to obtaining their baseline values. PA was induced by switching ventilation from medical air to a hypoxic-hypercapnic gas mixture (6% O_2, 20% CO_2, balance N_2) for 20 minutes, simultaneously reducing the RR to 15 1/min and stopping the fluid/glucose administration. Piglets (n=13) were reventilated (RR: 30 1/min) with medical air for the remaining time of the experiment.

pH_{brain} measurements

Measurements were performed inside a self-made Faraday cage with 4 Hz sampling rate. pH-selective microelectrodes (external tip diameter: 50 µm) were obtained from Unisense (Aarhus, Denmark), whereas glass reference microelectrodes (external tip diameter: ~20 µm and filled with 150 mM NaCl; resistance: ~4-5x10^{10} Ohm) were self-made and used with Ag/AgCl wire electrodes. The electrodes were mounted on stereotaxic manipulators for calibration in 3 different warmed (38°C) buffer solutions (pH: 6.10, 7.10, and 8.10, respectively) before each experiment. The piglet head was fixed in a stereotaxic frame and after retracting the scalp, two small circular craniotomies (Ø≅5 mm) were made over the fronto-

parietal cortex, and the dura mater was gently removed. The tips of the pH and reference microelectrodes were installed ~1-2 mm deep into the exposed cortex, and a Ag/AgCl ground electrode was placed under the scalp. The electrode signals were recorded, digitized and stored either using a custom-built differential electrometer (>10^{14} Ohm input impedance; 16 Hz low pass cut-off), a 16-bit analog-to-digital converter (National Instruments, Austin, TX) and WinEDR software (Dr. John Dempster, University of Strathclyde, UK), or using a Microsensor Multimeter and SensorTrace Logger software (Unisense, Aarhus, Denmark). Evaluation of the recordings was performed offline: by applying linear regression analysis, the signals from the calibration solutions were fitted with a curve and the data were converted to pH values using linear interpolation[28,82,83]. As the technique allows stable continuous pH_{brain} measurements reliably only for 3-4 hours, in different animals, different time windows were chosen to be assessed (baseline, PA and the first 4 hours of reventilation (n=6), 8^{th}-14^{th} hours (n=8) and 20^{th}-24^{th} hours (n=3) of reventilation as presented in the Results).

LSCI measurements and analysis

The brain was illuminated with near infrared polarized light (λ=808 nm, 200 mW) with a laser diode (DL-8141-002 SANYO Electric Co., Japan). The images were recorded with a monochrome camera (PL-B741F; PixeLINK® Ottawa, Canada; 1280×1024 pixels) which is using a polarizer and a color filter. The raw speckle images were sampled at 1 Hz, 1 ms exposure time with 1 frame/s rate during all the vascular stimuli.

The LSCI analysis was performed offline in LabVIEW (National Instruments Co., Austin, TX, USA). The contrast maps were calculated from the raw speckle images using a 5x5 pixel window. In each animal we selected 4 parenchymal region of interests (ROIs; 5x5 pixels ~1200 μm^2) over the cortical parenchyma avoiding pial vessels. The τ correlations were calculated using Equation (1), where K(T) is each ROIs' speckle contrast, β is the coherence factor and T is the exposure time.

$$K(T) = \sqrt{\beta}\left\{\frac{\tau^2}{2T^2}\left[exp\left(\frac{-2T}{\tau}\right) - 1 + \frac{2T}{\tau}\right]\right\}^{\frac{1}{2}} \quad \text{Equation (1)}$$

For each image, the calculated 1/τ values were normalized and expressed as percentages of the baseline, and values from all 4 ROIs were averaged in each animal.

Pial arteriolar diameters were determined at selected time points where peak changes in CoBF to the applied stimuli were detected. To obtain better resolution, 30 images were

averaged then the Otsu filtering method was applied to reduce noise. In each experiment, four arterioles were selected and the internal diameter of the arterioles were determined using edge detection and Euclidean distance measurement in MATLAB (Mathworks Inc., Natick, US)[84]. The arteriolar diameter data were normalized and expressed as percentages of the baseline, and values from all 4 arterioles were averaged in each animal.

Neurophysiological recordings

Electrophysiological recordings were taken with 16-channel, acute single shank planar silicone electrodes (l=10 mm, base width= 50 µm) with 177 μm^2 recording sites spaced 100 µm apart (A1x16-10mm-100-177-A16; Neuronexus Technologies. AnnArbor, MI, US, http://neuronexus.com/electrode-array/a1x16-10mm-100-177/). Data acquisition was performed with the RHD2000 Evaluation System. The recorded signals were preamplified with a 16-channel headstage/amplifier board (RHD2132 amplifier board, Intan Technologies, Los Angeles, US) under Faraday-cage then the signals were sent through an interface cable to the interface board (RHD2000 USB interface board, Intan Technologies, Los Angeles, US). All recorded data were sampled at 20 kHz, the broad band signals were filtered with a 1-9000 Hz bandpass filter and a notch filter was also applied to eliminate the 50 Hz electrical noise. All data were analyzed off-line in MATLAB environment with implemented toolboxes (Chronux, http://chronux.org/; FMAtoolbox, http://fmatoolbox.sourceforge.net) and custom written scripts.

LFP spectral analysis

The recorded broad band signals (20 kHz) were downsampled to 1250 Hz and filtered with an infinite impulse response (IIR) 4^{th} order Butterworth filter to generate the local field potential (LFP) and to eliminate spiking activity. After LFP generation, we decomposed the signal into the physiological frequency ranges - delta (1-4 Hz), theta (4-8 Hz), alpha (8-13 Hz), beta (13-30 Hz) – to calculate the power spectral density (PSD). We applied a 30 s window on the signals which moves onward with 1 s steps calculating the Fast Fourier Transform (FFT) of the signals using a Gaussian window. The PSDs were determined for each channels, frequency bands, conditions and animals using Welch's method. The calculated PSDs were summed for each frequency bands. All the PSDs were averaged and normalized to the baseline activity.

Addressing the 'inverse problem' of LFP, we computed the second spatial derivative, the current source density (CSD) to reveal how the different sources contribute to the mixed signal. We explored and segmented the data into 2.5 s epochs using Neuroscope[85]. We used the standard CSD method for the computation. All CSDs were calculated with the FMAtoolbox's built-in function and the spectra were averaged.

Spike sorting and unit classification

Spike sorting was done with the Klusta package (https://github.com/kwikteam/klusta) that performs automatic spike sorting and clustering. Single units were detected from digitally 1-5000 Hz high-pass filtered LFP using a threshold crossing-based algorithm (Spikedetekt2; https://github.com/klusta-team/spikedetekt2). The detected spikes were automatically clustered using masked Expectation-Maximization (EM) algorithm for Gaussian mixtures which is implemented into KlustaKwik2[86] (https://github.com/klusta-team/klustakwik2/). Clustering was followed by manual adjustment of the clusters using phy KwikGUI software (https://github.com/kwikteam/phy) which is an improved version of KlustaViewa[87]. The noise, as well as multi-unit and poor quality clusters were discarded from the analysis. The putative interneurons and pyramidal cells were identified by their waveform characteristics and auto-correlograms (ACG)[88,89,90] with the further examination of their cross-correlograms (CCG) to reveal the monosynaptic interactions with other single units[89,91].

Statistical analysis

All the LSCI statistical analysis were performed in IBM SPSS Statistics 22, using two-way ANOVA with repeated measures, followed by Tukey's *post hoc* test. All results show mean±SD, respective to the baseline. $p<0.05$* was considered as significant.

The electrophysiological statistical analysis was performed with IBM SPSS Statistics 22. We performed one-way ANOVA with repeated measures, followed by Bonferroni *post hoc* test. All results show mean±SD, respective to the baseline. $p<0.05$* and $p<0.01$** were considered as significant. For the Z-score computation we used MATLAB's statistics toolbox. Relative PSD changes were determined as significant above/below $Z\geq \pm 2$* and $Z\geq \pm 4$** with the further examination of the ANOVA results ($p<0.05$*, $p<0.01$**).

pH, hemodynamic and physiological parameters were analysed offline and plotted using SigmaPlot (v12.0, Systat Software Inc., San Jose, CA, USA) or a MATLAB environment

(Mathworks Inc., Natick, MA, USA). Data are expressed as mean±SEM. Normality was tested with the Shapiro-Wilk test. The correlation between P_aCO_2 and pH_{brain} data were calculated with MATLAB's polynomial curve fitting. Parametric data were compared with one-way repeated measure of analysis of variance (RM ANOVA) followed by the Student-Newman-Keuls *post hoc* test. Level of significance (p) was set at 0.05.

RESULTS

Effects of graded hypercapnia and asphyxia on physiological parameters

Ventilation with 5-10% CO_2 resulted in graded hypercapnia that was similar in all experimental groups both for LSCI and for electrophysiology experiments (Table 1). Graded elevations in arterial pCO_2 were accompanied by the expected development of marked respiratory acidosis and a slight increase in plasma HCO_3^- levels, however, arterial pO_2, blood oxygen saturation, MABP and HR were all maintained during graded hypercapnia. The stimulus was highly repeatable, repeated ventilation with 5-10% CO_2 resulted in virtually identical changes in blood gases compared to the first application (Table1).

	1st stimulus			**2nd stimulus**		
	Baseline	**5% CO_2**	**10% CO_2**	**Baseline**	**5% CO_2**	**10% CO_2**
pCO_2 (mmHg)	39±6	63±11	91±14	42±5	69±7	99±9
pO_2 (mmHg)	69±9	79±21	82±26	67±12	77±25	82±29
pH	7.51±0.06	7.32±0.07	7.17±0.05	7.48±0.05	7.29±0.06	7.15±0.05
HCO_3^-(mmol/l)	30.5±3.7	32.2±3.9	33.0±3.9	31.1±3.0	33.2±2.8	34.4±3.2
BE(b) (mmol/l)	6.9±3.6	5.1±3.8	3.3±3.6	7.0±3.1	5.6±3.1	4.0±3.5
SpO_2	97±2	95±4	94±3	96±3	94±4	94±4
MABP (mmHg)	62±9	70±10	75±14	55±8	67±11	74±14
HR (bpm)	139±18	147±28	161±29	140±17	149±25	168±29

Table 1. *Arterial pCO_2, pO_2, pH, HCO_3^-, base excess BE(b), oxygen saturation (SpO_2), mean arterial blood pressure (MABP) and heart rate (HR) values during the 1st and 2nd stimulation with graded hypercapnia (mean±SD) (n=31).*

During the 20 min asphyxia period, O_2 saturation fell to below 30% and HR increased from about 140 1/min to nearly 200 1/min within the first 2 min, after which they showed no major changes, whereas the response in MABP was biphasic with a transient rise to about 90 mmHg followed by a slower decrease to below baseline (Fig. 5). A rapid recovery of O_2 saturation to above 80% was seen during the first 2-3 min of reventilation, paralleled by transient increases in HR and MABP to above 240 1/min and 80 mmHg, respectively, after which the signals gradually recovered towards their normal values.

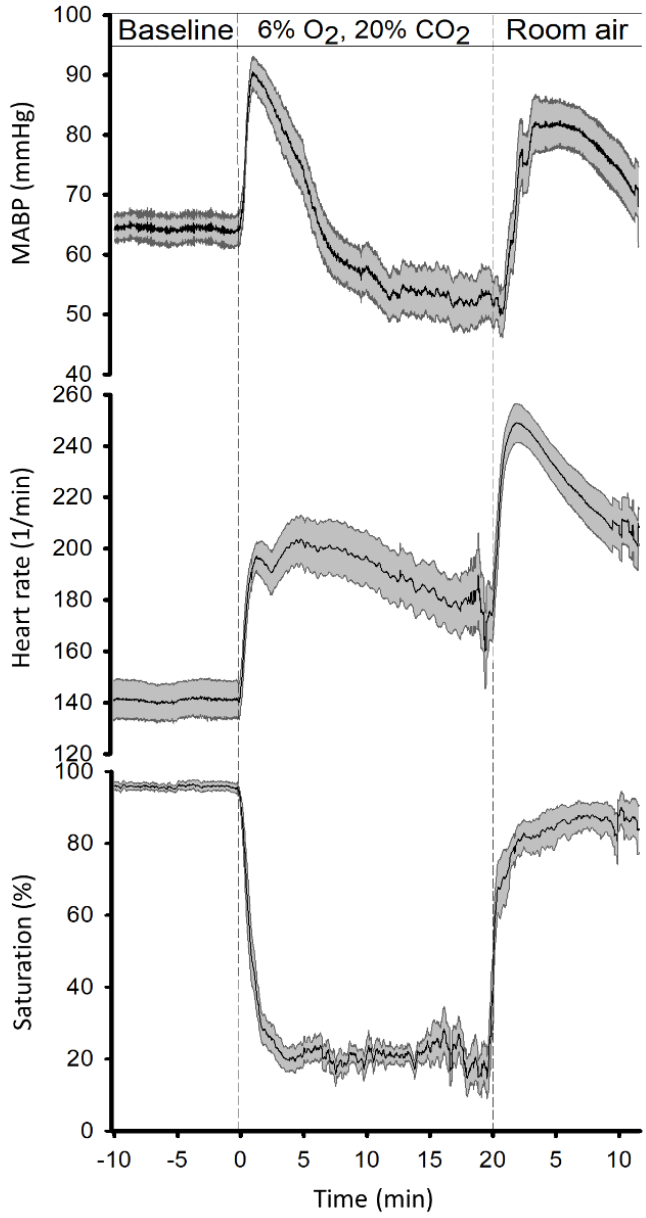

Figure 5. *Hemodynamic and oxygenation changes under PA. In all panels, solid lines indicate the mean and the grey shaded area the SEM. (n=13). After obtaining baselines, PA was initiated resulting first in the transient elevation of mean arterial blood pressure (MABP, top panel) and heart rate (HR, middle panel) accompanying the rapid fall in blood oxygen saturation (pulsoxymetry, bottom panel). While blood oxygen saturation remained ~20% throughout the asphyxia, after the initial peak, MABP fell continuously below baseline, whereas the drop in HR was more moderate and HR remained elevated. Reventilation with air quickly restored oxygen saturation and induced a second transient elevation in both MABP and HR.*

Longer-term monitoring of the physiological parameters reflected well the expected effects of PA and reventilation. Blood hemoglobin concentration (baseline: 8.0±0.3 g/dl; time course not illustrated), core body temperature (controlled by heating, see Methods), O_2 saturation, MABP and HR were within the normal range at baseline before PA and the values were not significantly different from baseline throughout the survival (Fig. 6A-D). In addition to the pulsoxymetry data, arterial blood gas analysis at the end of PA also confirmed the development of central haemoglobin desaturation (from 94±4 to 13±4%) along with severe acidosis, hypoxia and hypercapnia (Fig. 6E-H). Indeed, the fall in the arterial blood pH (pH_a) from 7.53±0.03 to 6.79±0.02 was substantial and paralleled by a rise in P_aCO_2 to 160±6 mmHg, however, pH_a remained more than 0.8 pH unit higher than pH_{brain}. Blood glucose and lactate levels were also profoundly raised (Fig. 6I,J)[92], indicating the metabolic response to PA. The large drop in base excess by 17.4±1.5 mmol/L and reduction in bicarbonate concentration (Fig. 6K,L) together with the low pH_a (6.79) at the end of PA indicate that asphyxia developed much beyond the key clinical criteria of severe BA in human neonates (pH <7.0 and base deficit ≥12 to 16 mmol/L[93,94]). Reventilation quickly restored normoxia in arterial blood, but P_aCO_2 levels remained slightly elevated, although the change was statistically significant only at 4 hours. Base excess was already normalized by this time point, and pH_a returned to 7.39±0.02, normal for piglets[95]. In a similar fashion, blood glucose and lactate levels also returned to baseline by 4 hours, although both were still significantly elevated at 1 hour after PA.

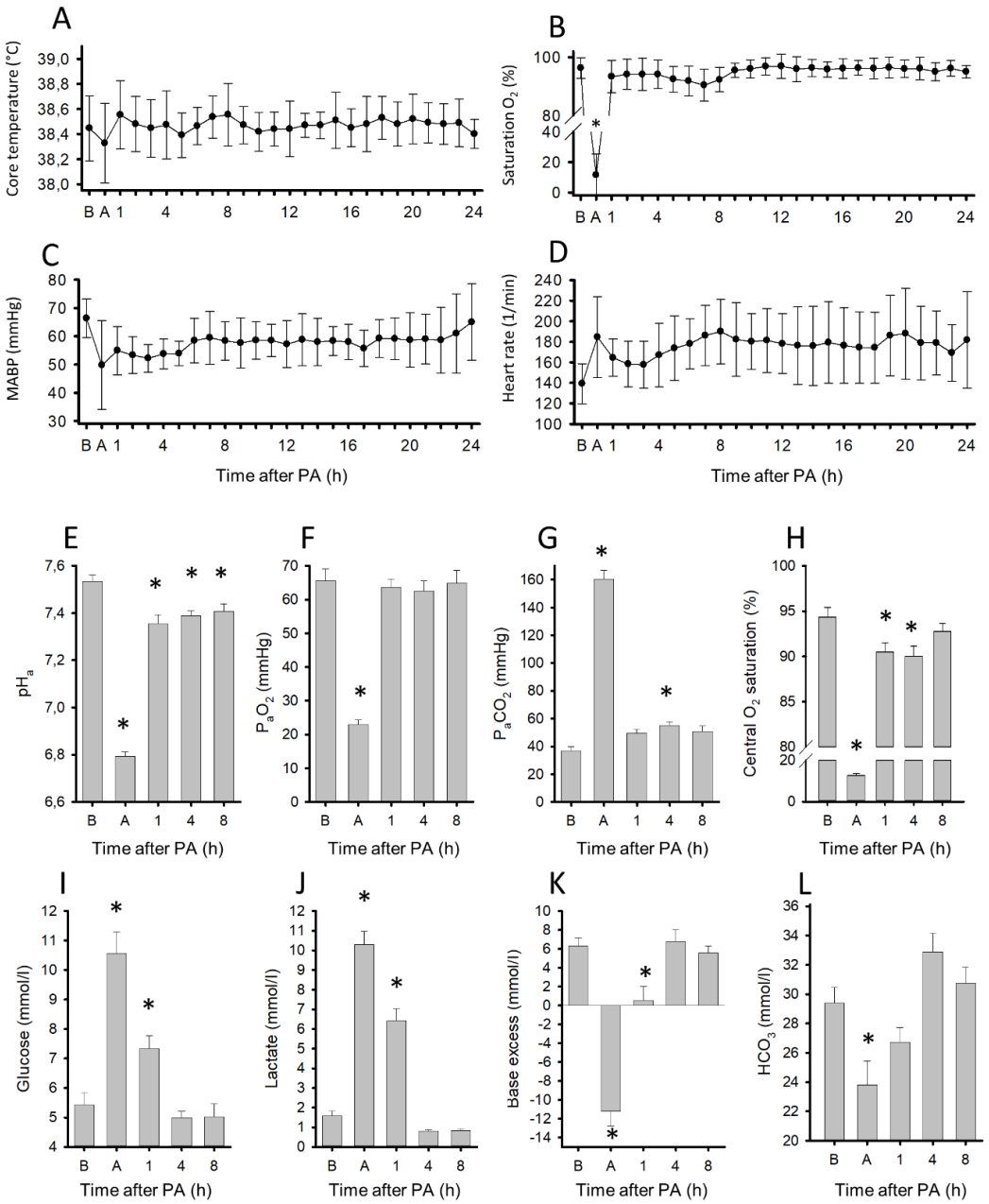

Figure 6. *Physiological parameters and blood chemistry changes during PA and the subsequent 24h reventilation period. Core temperature of the animals (n=13) was maintained in the physiologic range (38.5±0.5 °C) during the whole experiment (A). Blood oxygen saturation by pulse oxymetry (B) and mean arterial blood pressure (MABP, (C)) returned to baseline levels soon after asphyxia, however, the heart rate remained moderately elevated (D). Arterial blood gas analysis revealed that asphyxia resulted in severe acidosis (E), hypoxemia (F), hypercapnia (G), and central (arterial blood) desaturation (H). Plasma glucose (I) and lactate levels (J) were markedly elevated along with large drops in base excess (K) and significant reductions in blood bicarbonate concentrations (L). Reventilation restored most of the deranged parameters by 4 hours, and they were not significantly different from baseline*

levels afterwards, except for pH that was restored to the normal values[95] *and not to the slightly alkalotic baseline. B: baseline, A: at the end of 20 minute PA. Bars and whiskers represent mean±SEM, *p<0.05 vs. baseline values.*

Neuropathology analysis confirmed the development of HIE by revealing medium/severe neuronal damage in all examined neocortical regions (Fig. 7A,C), and also in the hippocampal CA1 region, the thalamus and the putamen (Fig. 7B). These findings are in accordance with previously reported neuronal injury using the same PA stress[77].

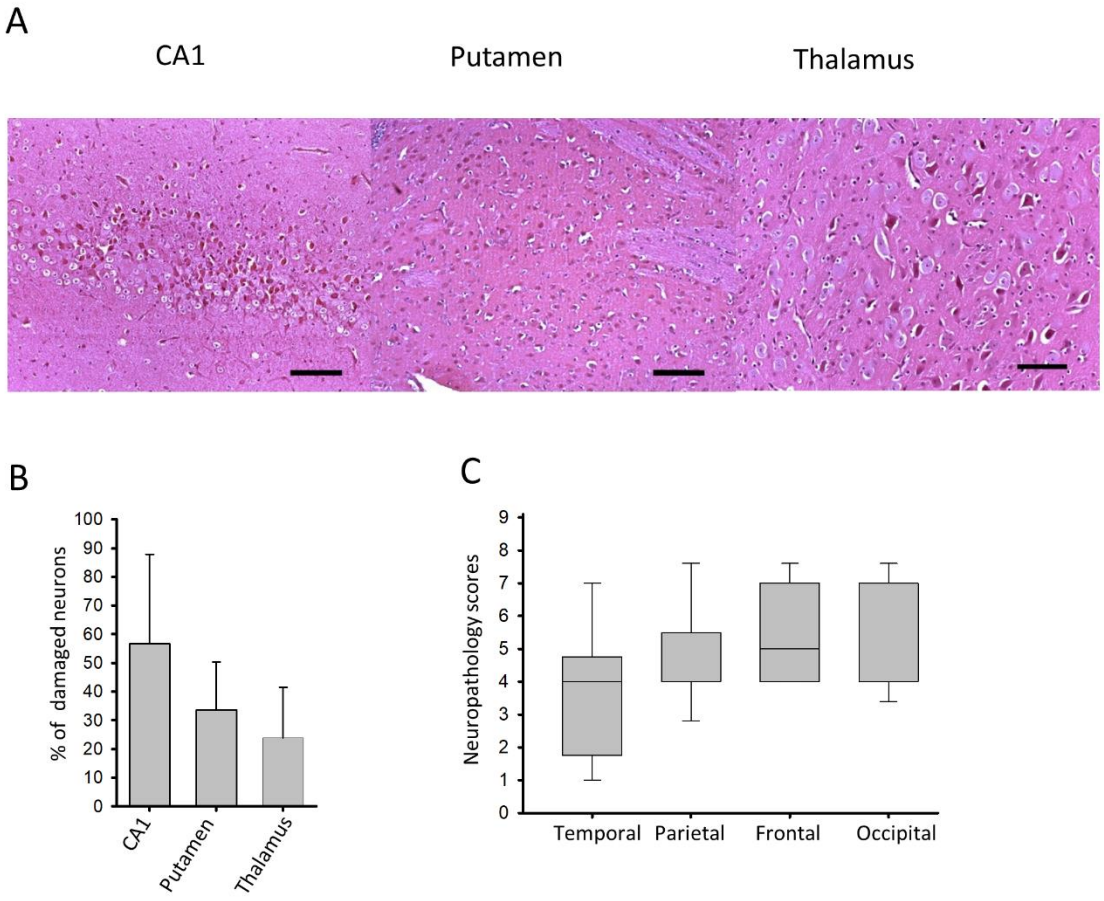

Figure 7. *Neuronal injury evaluated at 24 hours after PA. (A) Representative photomicrographs showing injured red neurons at 24-hours of after asphyxia in the CA1 hippocampal region, the putamen, and the thalamus (scale bar: 100µm) (B) Cell counting revealed moderate neuronal damage in these regions (n=8, mean±SEM). (C) Asphyxia also induced moderate/severe neocortical damage shown by medium/high neuropathology scores (lines, boxes, and whiskers represent the median, the 25th-75th, and the 5th-95th percentiles, respectively).*

pH_{brain} changes during graded normoxic hypercapnia

These experiments were performed to evaluate the contribution of the respiratory component to the pH_{brain} changes recorded during PA. Step-wise, 5% increases in inhaled CO_2 (Fig. 8A) resulted in proportional step-wise reductions in pH_{brain} (Fig. 8B,C). Arterial blood gas analysis revealed similar graded reductions in pH_a, thus the difference between pH_{brain} and pH_a remained unchanged during hypercapnia (Fig. 8B). Maximal changes were observed during the inhalation of 20% CO_2 when pH_a dropped from 7.52±0.06 to 6.98±0.02, whereas pH_{brain} from 7.32±0.01 to 6.77±0.02. The pH_{brain} and pH_a changes were fully reversed by restoration of normocapnia.

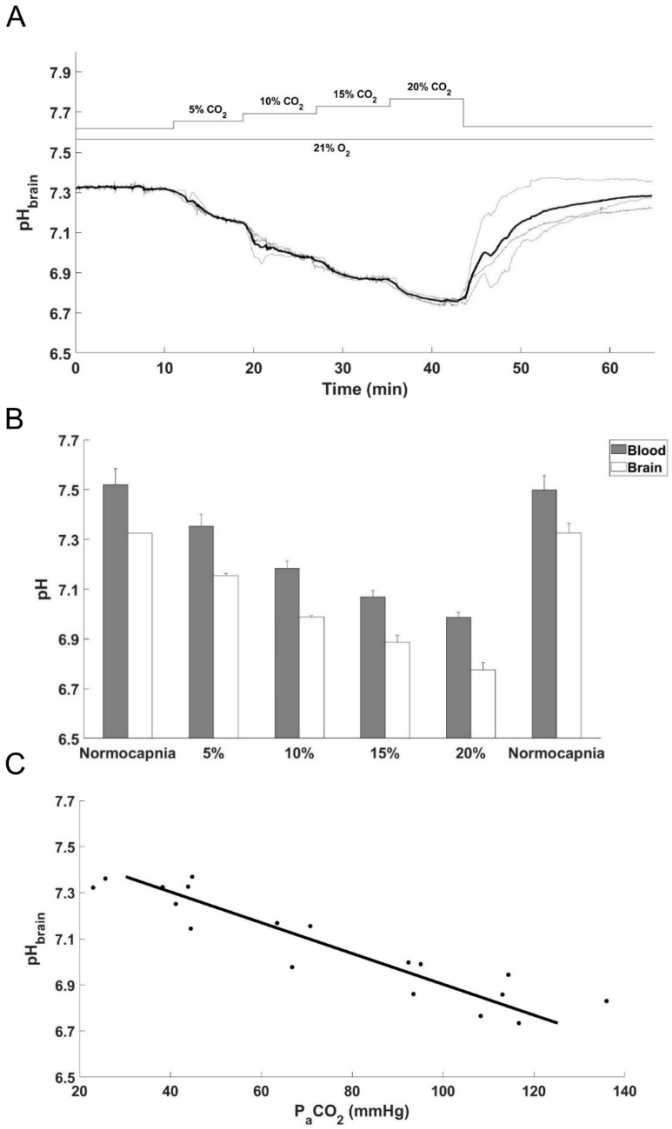

Figure 8. *Cerebral acidosis induced by graded normoxic hypercapnia. (A) pH_{brain} changes during graded normoxic hypercapnia induced by ventilation with 5-20% CO_2 followed by restoration of normocapnia (grey lines – individual tracings, bold black line – mean). (B) Simultaneous reductions in pH_a and pH_{brain} during graded normoxic hypercapnia were in accordance with the elevations in P_aCO_2, the values were (mmHg) 5%: 59.6±7.8, 10%: 84.7±9.0, 15%: 107.0±6.7, 20%: 120.3±8.2, (mean±SEM; n=3). Corresponding P_aO_2 values were (mmHg) 5%: 75.5±12.8, 10%: 78.2±11.3, 15%: 85.5±8.2, 20%: 84.5±9.8, (mean±SEM; n=3). (C) Linear regression shows close correlation between P_aCO_2 and pH_{brain} (R^2=0.8546) values obtained during graded hypercapnia (5-20% CO_2).*

pH_{brain} changes during PA and HIE development

Induction of PA elicited a reduction in pH_{brain} that continued without levelling off over the 20 min insult, during which pH_{brain} dropped from the baseline value of 7.21±0.03 to 5.94±0.11 by the end of asphyxia (n=6; Fig. 9A). Upon reventilation, pH_{brain} was restored to 7.0 in 29.4±5.5 minutes with subsequent stabilization at a level that was virtually indistinguishable from the original baseline. Thereafter, from 2 h onwards pH_{brain} remained slightly below baseline (on average, by 0.10±0.02 pH units) without showing any marked alterations at any observed time point within the 24-hour follow-up period (Fig. 9B).

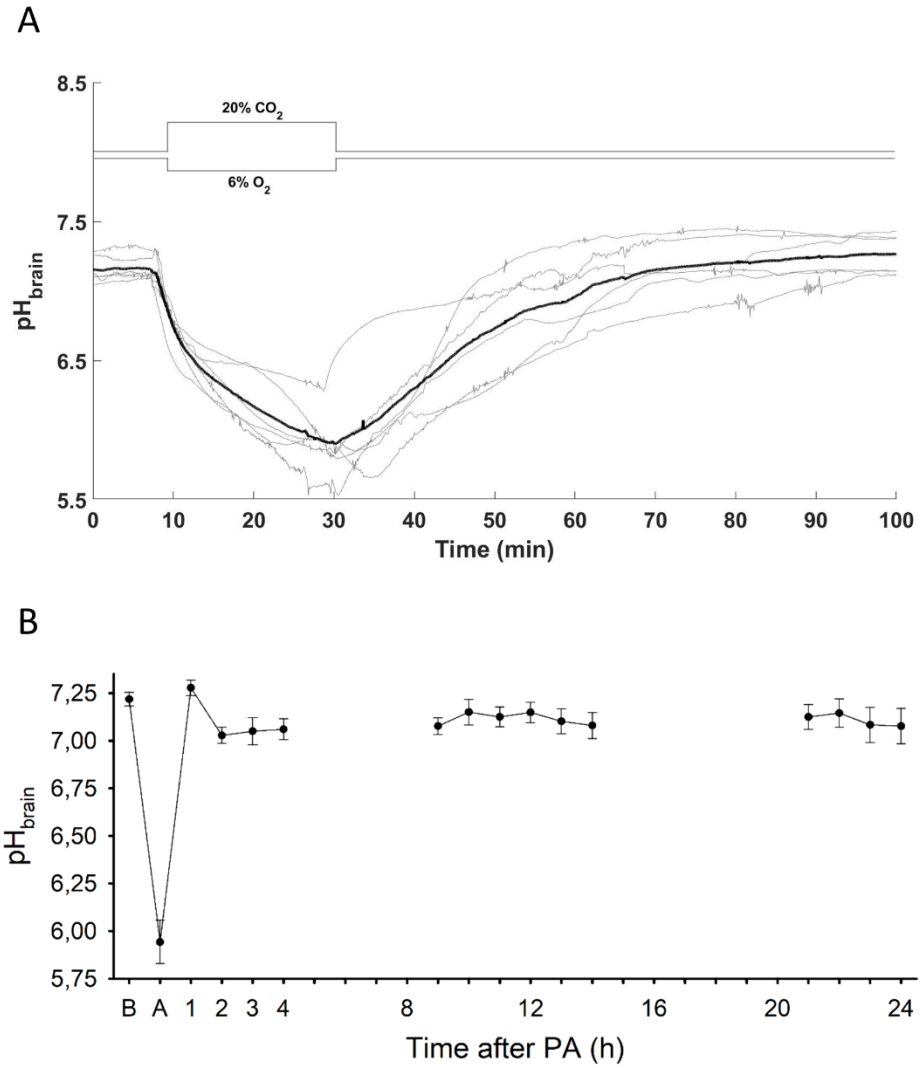

Figure 9. *pH_{brain} changes during PA and the reventilation period. (A) pH_{brain} changes (grey lines – individual tracings, bold black line – mean) are plotted 10 min prior the onset asphyxia, during asphyxia, and the first hour of of reventilation. pH_{brain} fell progressively during asphyxia showing severe cerebrocortical acidosis, by the end of the insult the pH drop exceeded 1.0 pH*

*unit virtually in all asphyxiated animals. Reventilation quickly restored pH_{brain} to baseline levels. (B) pH_{brain} alterations upon PA and over the 24-hour period after PA: after recovery from the PA-induced severe acidosis, no further significant pH_{brain} alterations were detected at the selected time intervals (n=6 at PA and between 1-4 hours; n=8 between 8-14 hours and n=3 between 20-24 hours; respectively). B: baseline, A: at the end of 20 minute PA. Panel B data points are presented as mean±SEM. *p<0.05 vs. baseline.*

The cerebrocortical microvascular response to graded hypercapnia and NMDA

LSCI provided two-dimensional maps of cortical perfusion (Fig. 10a-c) that served to determine changes in parenchymal perfusion (Fig. 10d-g, Fig. 11a-c) and pial arteriolar diameters (Fig. 11d).

The first exposure to graded hypercapnia resulted in similar, CO_2 concentration-dependent increases in CoBF in all groups (Fig. 10d-g), the peak CoBF values (Fig. 11a), the integrated hyperemic CoBF response (Fig. 11b), and the pial arteriolar diameter changes (Fig. 11d) were all similar.

Topical application of 0.1mM NMDA resulted in a significant increase in CoBF (peak CoBF was 151±14% of baseline) and pial arteriolar diameters (138±31% of baseline) that peaked within 3-4 min (Fig. 10e, Fig. 11abd), the elevated CoBF returned to baseline levels after perfusing the cranial window with aCSF. Repeating the stimulation with 1mM NMDA resulted only in slightly higher elevations both in the peak (172±23%) and the total CoBF responses and the arteriolar diameters (145±20%), and all these changes were reversible upon removal of NMDA. Topical application of the NMDA receptor inhibitor MK-801 did not affect CoBF (Fig. 10f), however, coapplication of MK-801 with either NMDA doses completely abolished the hyperemic and the pial arteriolar response to NMDA (Fig. 11abd). Systemic administration of the selective nNOS inhibitor AAAN did not affect the CoBF response to NMDA (Fig. 10g; Fig. 11ab), however, it caused a significant reduction in the pial arteriolar dilation to NMDA (Fig. 11d).

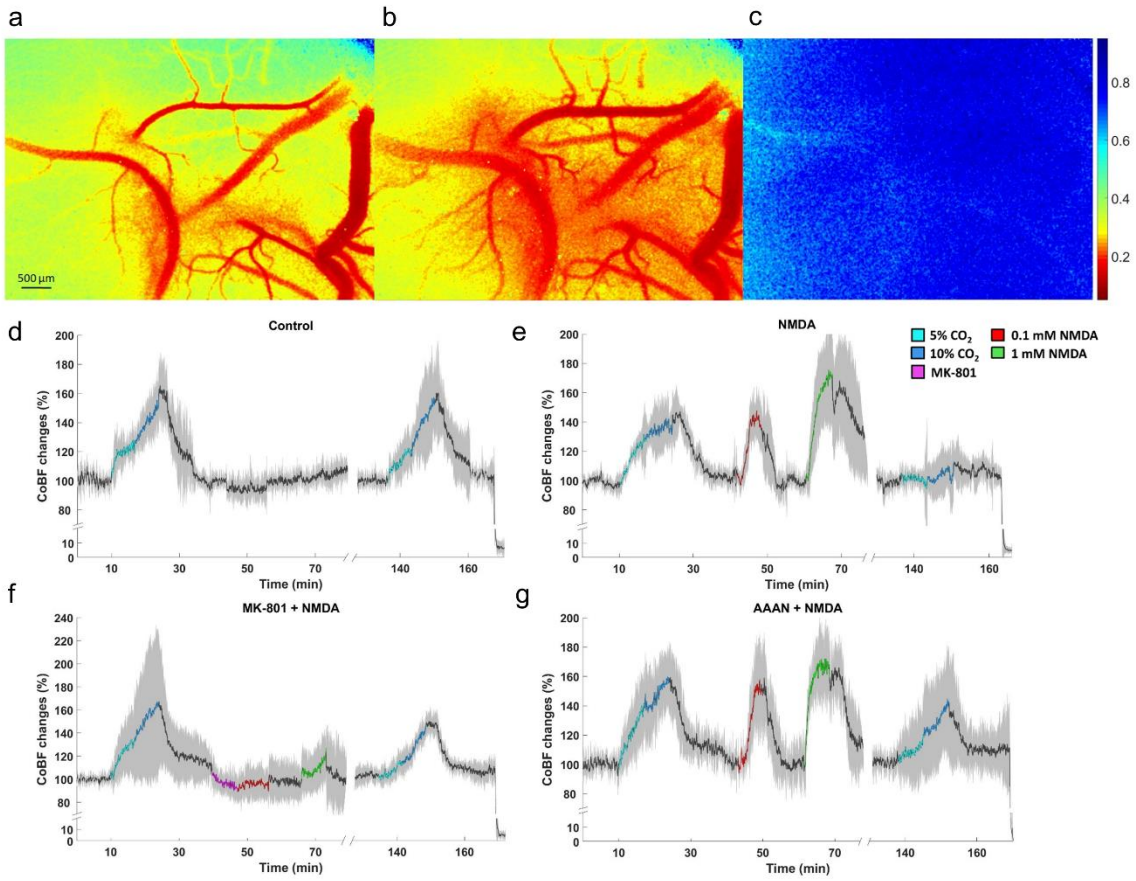

Figure 10. *Cortical blood flow (CoBF) changes to graded hypercapnia and NMDA using laser-speckle contrast imaging (LSCI) and analysis. (a-c): Representative LSCI contrast images obtained through the closed cranial window (a-c) with the corresponding contrast scales. Lower contrast values represent higher flow velocity in the cortical microcirculation. a): baseline condition; (b): NMDA (1mM) showing pial arteriolar vasodilation and increased parenchymal flow as well. (c): biological zero after euthanasia characterized by high and stable speckle contrast values marking the disappearance of the perfusion. (d-g): Summarized recordings of individual experiments, colored/black lines represent the group mean values during/between stimuli, the gray area represent the SD. (d): in the control group graded hypercapnia resulted in concentration-dependent repeatable increases in CoBF relative to the baseline. (e): Both doses of NMDA reversibly elevated CoBF, however, the CoBF response to graded hypercapnia was virtually absent after NMDA. (f): Pre- and co-treatment of MK-801 with NMDA abolished the CoBF response to NMDA and prevented the attenuation of the CoBF response to graded hypercapnia. (g): AAAN did not affect the CoBF response to hypercapnia or NMDA, however, at least partially prevented the attenuation of the microvascular response to graded hypercapnia by NMDA.*

In the control group, the CoBF response to the second exposure to graded hypercapnia was virtually identical to the first stimulation (Fig. 10d), the peak and the integrated CoBF values were very similar (Fig. 11ab), and the cerebrovascular reactivity to either CO_2 concentration was fully preserved (Fig. 11c). In sharp contrast, cerebrovascular reactivity to the second exposure to graded hypercapnia was abolished in the NMDA-treated group (Fig. 10e, Fig. 11). Pre- and coapplication of MK-801 with NMDA prevented the attenuation of the CoBF response to graded hypercapnia (Fig. 10f, Fig 11ab), cerebrovascular reactivity was preserved (Fig. 11c). In the nNOS inhibitor treated group, the CoBF response to graded hypercapnia was attenuated but not abolished after NMDA (Fig. 10g, Fig. 11ab), thus cerebrovascular reactivity was partially (68±35%) preserved in this group (Fig. 11c).

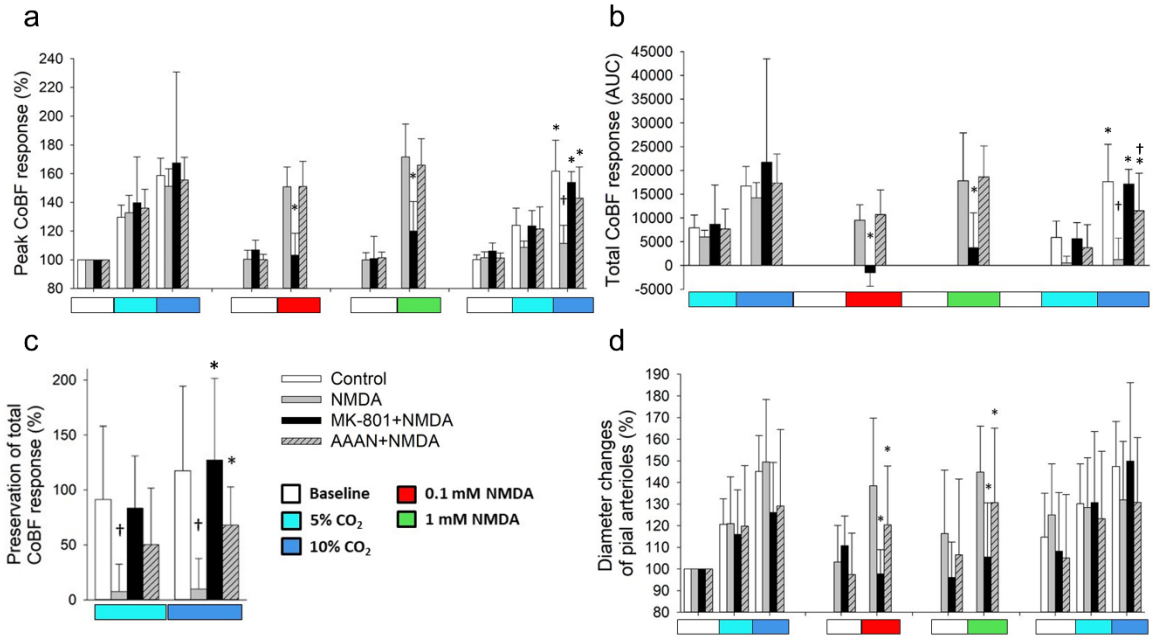

Figure 11. *Summary of the cortical microvascular responses to graded hypercapnia and NMDA assessed with laser-speckle contrast imaging and analysis. (a): Peak increases in CoBF to graded hypercapnia (n=6) were significantly blunted after NMDA-treatment (n=7) alone but not after MK-801+NMDA coapplication (n=4) or AAAN pretreatment (n=7). NMDA-induced peak increases in CoBF were also attenuated by MK-801 (F_{group}=3.785; η^2=0.066; p=0.012), but not by AAAN, furthermore AAAN clearly had no effect on the microvascular response to graded hypercapnia. (b): determination of the integrated (area under the curve, AUC) CoBF response shows also the severe attenuation of microvascular reactivity to graded hypercapnia in the NMDA-treated animals. Also, the inhibitory effect of MK-801 on NMDA-induced cortical*

*hyperemia is striking (F_{group}=4.464; η^2=0.411; p=0.0001). (c): Cortical microvascular reactivity to hypercapnia is expressed as the ratio of the total CoBF response to the first and second graded hypercapnia. The response was fully preserved in the control and in the MK-801+NMDA treated animals, however, virtually abolished in the animals exposed to NMDA alone. Pretreatment with AAAN resulted in a partial preservation of the response (F_{group}=8.428; η^2=0.441; p=0.0001). (d): Relative (%) changes in pial arteriolar diameters show that pial arteriolar responses to graded hypercapnia were not significantly different among the four groups. However, NMDA-induced pial arteriolar vasodilation was fully prevented by MK-801 and also significantly attenuated by AAAN (F_{group}=4.741; η^2=0.113; p=0.004),p<0.05, * vs. NMDA, † vs. control.*

LFP changes under graded hypercania

Induction of hypercapnia with 5% CO_2 elicited first increases then decreases in LFP power, especially in the delta (δ) and theta (θ) ranges (Fig. 12ab). Highest increases in δ were observed at cortical depths 100-400 μm and in θ at 100-600 and at 1000-1200 μm (Table 2). The subsequent reduction in power started in the deeper cortical layers (below 900 μm) gradually shifting upward. Switching to 10% CO_2 further reduced LFP power both in the δ and θ ranges (Fig. 12). These depressions were largely reversed upon restoration of normocapnia, and the LFPs were not significantly different from the baseline values. LFP power in the alpha (α) and beta (β) ranges was quite small under these experimental conditions and clear hypercapnia-related changes could not be observed (data not shown). LFP changes to graded hypercapnia following the stimulation with NMDA were markedly different, most strikingly the early increases in θ LFP power did not develop (Table 2, Fig. 12b). δ LFP powers were also significantly altered (Table 2), and the pattern of LFP changes appeared to have disorganized.

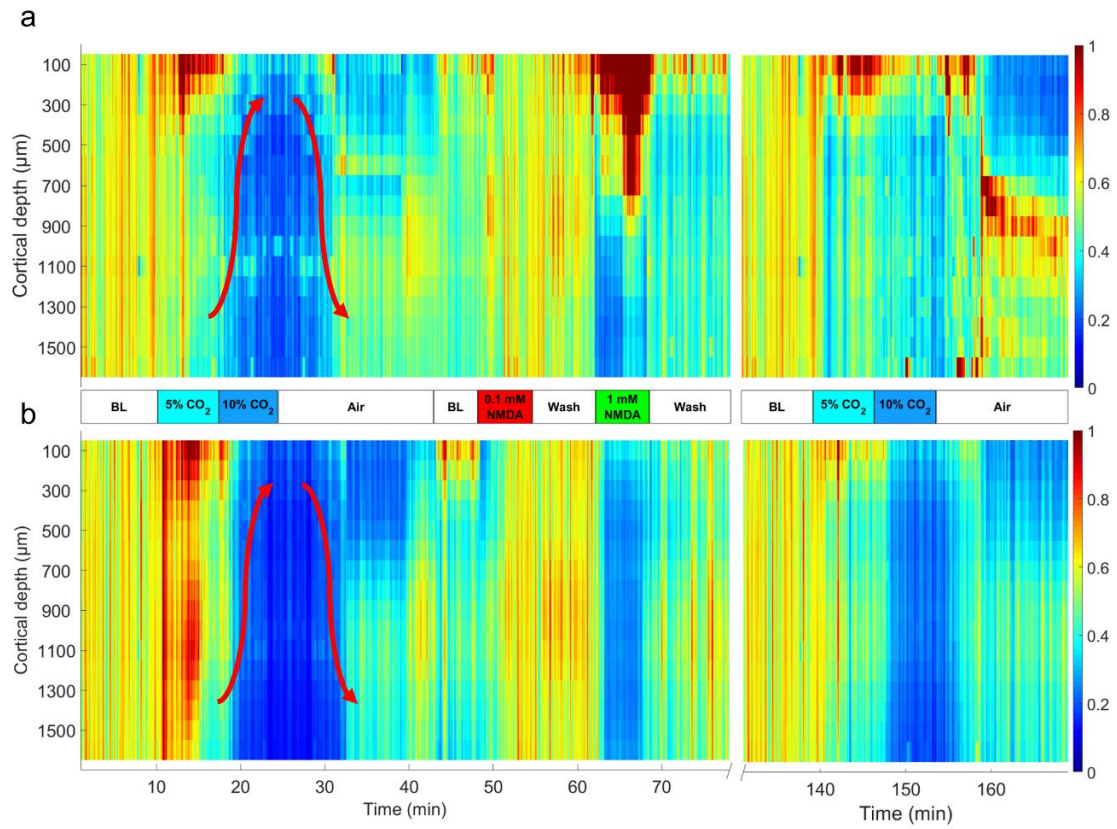

Figure 12. *Representative heat map images of (a): delta (δ) and (b): theta (θ) band power spectral densities (PSDs) obtained from the local field potential recordings with a 16-channel electrode representing 100-1600 µm cortical depths with the corresponding intensity scales (0-1) from an animal of the NMDA-treated group. (a): during hypercapnia, 5% CO_2 tended to increase δ in the superficial cortical layers, but activity diminished after switching to 10% CO_2 starting in the deep cortical layers gradually shifting upwards (arrow pointing up). After restoration of normocapnia, δ activity was also restored (arrow pointing down). NMDA, especially the higher dose strongly increased δ activity predominantly in the upper cortical layers (F_{group}=1363.103 (1 mM NMDA); η^2=0.8614; p=0.00001**). The second stimulation with graded hypercapnia showed a somewhat similar pattern, however, the δ depression during the deeper level of hypercapnia, and also the restoration of activity upon normocapnia was less clear-cut than before NMDA. (b): during hypercapnia, 5% CO_2 resulted in a quite widespread increase in cortical θ activity (F_{group}=726.632 (5% CO_2); η^2=0.7623; p=0.00001**) that was attenuated and reversed to depression after switching to 10% CO_2 similarly to the pattern observed for δ (arrows). NMDA (1mM) resulted in an almost complete suppression of θ in all cortical layers. After NMDA, the second graded hypercapnia lacked the θ activation associated with 5% CO_2. BL: baseline.*

Delta (%)						
Cortical depth (µm)	**5% CO_2**	**10% CO_2**	**0.1 mM NMDA**	**1 mM NMDA**	**5% CO_2**	**10% CO_2**
100	140.9±14.3*	58.6±17.4	76.2±10.2	252.1±54.3**	51.2±5.1	50.5±12.3
200	130.4±9.2*	20±3.1	44.7±5.1	243.6±49.2**	46.0±8.2	22.3±2.0
300	123.9±23.6*	18.7±3.1	46.8±4.1	187.0±14.3**	45.3±10.3	39.5±11.3
400	127.9±28.7*	46.5±8.2	113.4±11.3	305.0±78.9**	78.5±12.3	68.2±23.6
500	79.8±13.3	54.3±8.2	92.5±5.1	191.1±14.3**	66.6±11.3	59.6±18.4
600	71.1±7.2	44.1±12.3	90.3±7.2	197.7±15.4**	60.8±16.4	50.3±25.6
700	38.0±3.1	24.1±7.2	49.9±5.1	160.6±11.3**	24.4±2.0	34.8±8.2
800	73.4±14.3	60.4±29.7	113.0±10.2	140.9±18.4*	82.1±8.2	77.0±5.1
900	52.1±5.1	46.1±10.2	67.3±3.1	66.7±10.2	97.9±21.5	65.6±13.3
1000	29.7±4.1	26.6±6.1	37.7±1.0	54.2±7.2	31.6±8.2	31.0±6.1
1100	83.0±7.2	39.3±10.2	103.8±5.1	74.0±19.5	61.7±9.2	53.3±10.2
1200	40.8±6.1	31.5±10.2	33.7±3.1	40.7±7.2	27.2±4.1	52.1±14.3
1300	65.7±5.1	40.6±8.2	56.4±2.0	75.7±14.3	42.3±4.1	50.6±7.2
1400	55.3±6.1	41±7.2	45.1±2.0	80.8±21.5	38.4±3.1	65.3±12.3
1500	52.7±3.1	27.7±2.0	60.1±3.1	58.4±9.2	45.8±8.2	36.3±8.2
1600	64.2±5.1	35.2±4.1	61.6±7.2	84.0±14.3	40.1±4.1	34.5±7.2
Theta (%)						
Cortical depth (µm)	**5% CO_2**	**10% CO_2**	**0.1 mM NMDA**	**1 mM NMDA**	**5% CO_2**	**10% CO_2**
100	184.4±14.3**	32.1±5.1	61.9±3.1	59.0±11.3	43.2±4.1	24.7±3.1
200	174.2±13.3**	22.7±2.0	80.5±6.1	38.1±9.2	42.4±3.1	21.6±3.1
300	163.7±14.3**	19.1±1.0	59.0±4.1	51.3±8.2	37.9±3.1	31.5±4.1
400	160.1±18.4**	24.5±3.1	76.8±6.1	57.7±11.3	42.2±4.1	30.6±4.1
500	157.5±14.3**	30.3±5.1	51.2±3.1	42.5±8.2	31.3±3.1	29.1±6.1
600	165.4±18.4**	21.7±2.0	108.9±9.2	61.7±11.3	42.4±4.1	31.8±3.1
700	105.0±15.4	58.5±12.3	77.7±6.1	67.1±11.3	41.1±3.1	38.4±4.1
800	105.1±12.3	19.9±1.0	81.2±6.1	56.8±10.2	49.1±7.2	40.9±7.2
900	114.1±11.3	29.9±3.1	96.9±7.2	57.4±9.2	65.4±4.1	41.9±5.1
1000	167.5±11.3**	22.3±2.0	91.9±6.1	63.9±10.2	53.1±4.1	44.5±8.2
1100	157.7±12.3**	19.4±2.0	86.7±7.2	59.1±9.2	55.6±3.1	50.4±8.2
1200	154.0±12.3**	24.5±2.0	100.8±7.2	55.3±9.2	56.9±3.1	44.0±7.2
1300	114.5±15.4	22.3±2.0	98.1±6.1	54.0±7.2	64.3±4.1	61.9±1.0
1400	109.5±17.4	17.7±1.0	83.9±5.1	52.0±7.2	59.3±3.1	40.9±6.1
1500	101.5±16.4	19±2.0	82.0±6.1	45.8±7.2	60.4±4.1	32.4±4.1
1600	104.1±16.4	32.7±3.1	71.3±5.1	62.5±7.2	56.2±3.1	48.9±6.1

Table 2. *Power spectral density changes in the delta and the theta band during stimulations with graded hypercapnia and NMDA. Data are expressed as % of baseline (mean±SD). *p<0.05, **p<0.01.*

NMDA evokes delta (δ) oscillation

NMDA (1 mM) selectively increased δ LFP power only in the upper layers (100-700 µm; Fig. 12a; Table 1) however, activity in the θ range were simultaneously suppressed (Fig. 12b). Similar suppression was observed in the α and β ranges as well (e.g. at 600 µm cortical depth reductions were 58.8±1.2 and 44.9±1.7 % of baseline, respectively). This characteristic increase in the δ was identified as a ~2.5Hz δ oscillation) down to 600 µm (Fig. 13a). CSD analysis identifying the contributing sinks and sources of cortical extracellular currents showed that NMDA (1 mM) altered significantly the size of the sinks and sources (Fig. 13b) causing the activation first in layer I. then layer II/III and IV. This NMDA-induced activation was δ band-limited.

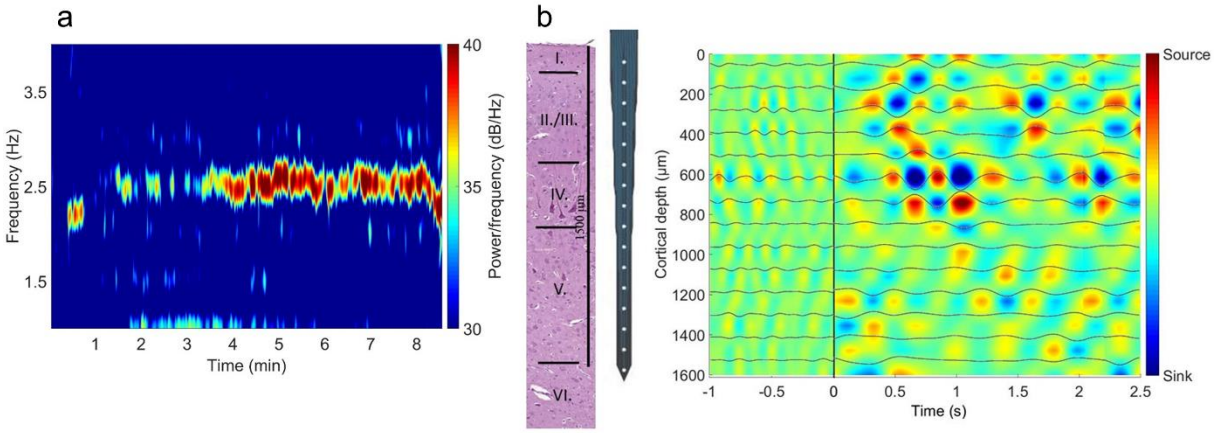

Figure 13. *NMDA evokes delta (δ) oscillation in the upper cortical layers. (a) Representative δ band spectrogram during NMDA (1 mM) stimulation recorded at 600 µm under the cortical surface. The heat map shows the appearance of a 2.5 Hz frequency oscillation. (b): Average current source density (CSD) map of the δ oscillations observed during NMDA (1 mM) stimulation with the δ-filtered LFP superimposed onto the image. The multi-channel electrode (http://neuronexus.com/electrode-array/a1x16-10mm-100-177/) and an H/E-stained section of the piglet cortex are also shown for orientation. CSD analysis show that the oscillation originates chiefly in layers III/IV where the largest amplitude currents appear.*

Altered laminar spiking activity in response to graded hypercapnia and NMDA

All recorded neurons (n=149; total spike count=152,089) fired with low frequency (~0.3-3 Hz, Fig. 14a-e). The ACGs identified major neuronal types of the parietal cortex such as interneurons (Fig. 14a), bursting (Fig. 14bde) and regular spiking pyramidal cells (Fig. 14c). CCGs helped to identify the most characteristic cell connections that were typically excitatory with 3-4 ms latency (Fig. 14g-i). We observed only a few inhibitory connections or reciprocal excitation/inhibition between the cells (Fig. 14h).

Graded hypercapnia and NMDA increased spiking activity mainly in the II/III. and IV. layers down to 900 μm. Increased firing allowed more precise identification of interneuronal connections, from the total 164 connections 71% have been associated with layer II/III including intralaminar connections as well. Under the first hypercapnia the recorded spike counts were much higher compared to baseline condition (5% CO_2: 36,245 spikes, 146/149 active cells; 10% CO_2: 24,043 spikes, 142/149 active cells). In the subsequent normocapnic period the spiking activity has returned almost to the baseline activity (19,443 spikes, 133/149 active cells). NMDA (1 mM) suppressed neuronal activity in ~60% of neurons, the number of active cells dropped to 73/149, but the remaining ~40% of neurons were excited that total spike count remained similar to the baseline (15,400 spikes). During the second hypercapnia, few cells remained responsive to CO_2 (5% CO_2: 8985 spikes, 41/149 active cells; 10% CO_2: 5130 spikes, 17/149 active cells).

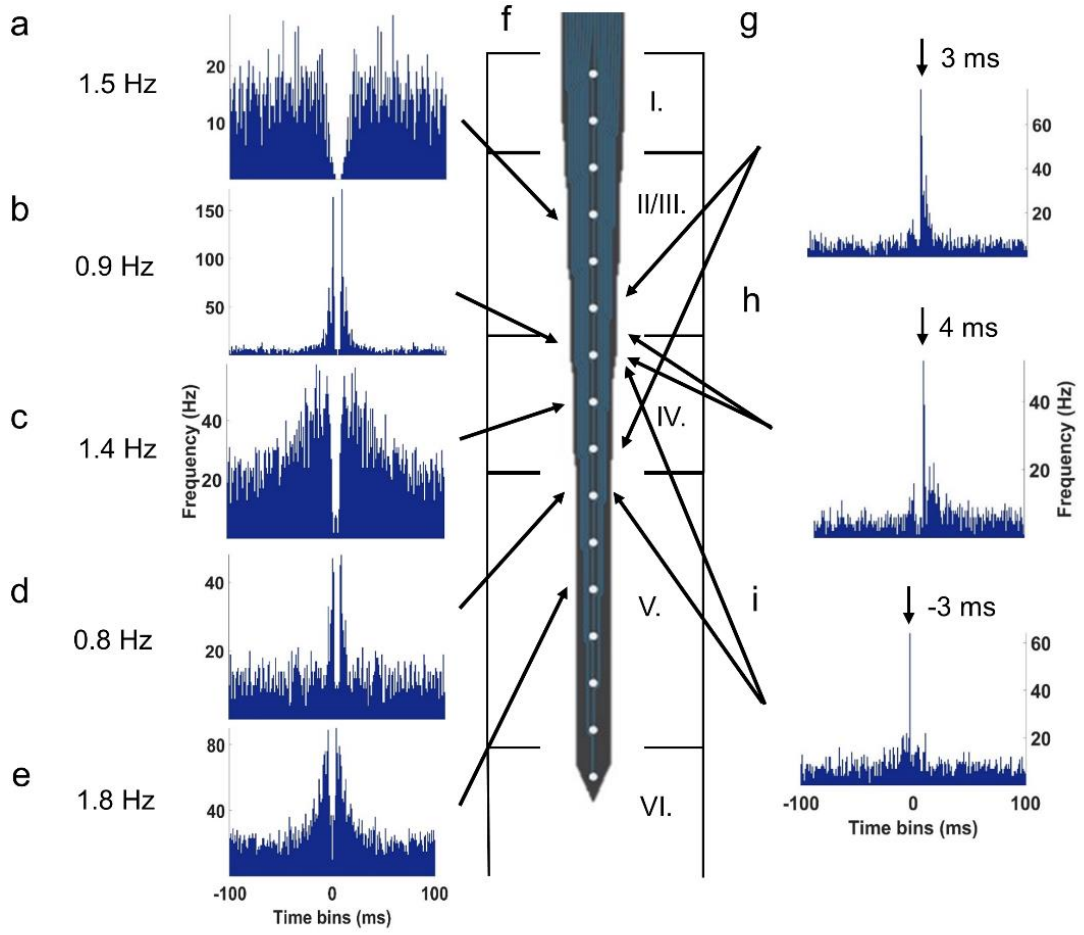

Figure 14. *Representative auto-correlograms (a-e) and cross-correlograms (g-i) of recorded cortical neurons and their connections with their highest firing rates. (a) Layer II/III. interneuron. (b) Layer IV. bursting pyramidal cell. (c) Layer IV. regular spiking pyramidal cell. (d, e) Layer V. bursting pyramidal cells. (f) Representative image of the recording electrode (http://neuronexus.com/electrode-array/a1x16-10mm-100-177/) with its position in the parietal cortex. Excitatory synapses between a (g) bursting and a regular spiking, (h) interneuron and bursting pyramidal cell, (i) two bursting pyramidal cells.*

DISCUSSION

The major findings of the present study are:

1. Our translational PA/HIE model shows the major hallmarks of the moderate/severe injury. Normoxic hypercapnia provided the opportunity to evaluate the respiratory component, which was responsible for ≅40% of the developing acidosis. Cerebrocortical pH dropped below 6.0 due to PA and the acidosis exceeded ≅0.8 pH unit lower in the brain, compared to the blood. Cerebrocortical pH remained stable after the reoxygenation throughout the 24h observation period, without observing any pH shift.
2. Graded hypercapnia caused concentration-dependent increase in CoBF which was attenuated by topical NMDA application. MK-801 fully-, while AAAN partially prevented the attenuation of the hemodynamic response which proves the involvement of the NMDA receptors and their mediation by nNOS activation.
3. Attenuation of the LFP's δ and θ bands under the repetition of hypercapnia was associated with the attenuated cerebrovascular response. NMDA evoked ~2.5 Hz δ oscillations 500-700 μm deep from the cortical surface, indicating the location of the major targets of NMDA.

The translational value of the newborn pig

The newborn pig is a well established translational large animal model of the term neonate. Studying the microvascular reactivity to different stimuli and their alterations following HI stress have been widely used in the field of experimental neonatology[96,97]. In cerebrocortical microcirculation research, the closed/open cranial windows and intravital microscopy are commonly used techniques. The major limitation of every PA/HIE model using postnatal animals is that under real-life conditions the PA usually precedes the cardiorespiratory adaptation to the extrauterine life. We believe that in our studies this disadvantage has been minimized by two factors. First, we use <24h old newborn piglets, thus their vulnerability to PA is unlikely to have considerably changed by postnatal development yet. Second, the evoked PA caused similar, severe alterations in the arterial blood gas and pH values, that are well-known indicators of brain injury and subsequent HIE development in humans. Indeed a clinical study reported significant alterations in the degree/severity of cord blood acidosis (pH_a:

6.75±0.18 vs 6.90±0.18) and hypercapnia (P_aCO_2: 141±37 vs P_aCO_2: 94±22 mmHg) between babies suffering from post-asphyxia HIE and those who were not affected[98]. The observed corresponding values in our piglet model were pH_a: 6.79±0.02 and P_aCO_2: 160±6 mmHg, similar to the human HIE patients' values. The translational value is further increased by the evidence that these values are identical in those piglets exposed to spontaneous PA during the delivery. Blood samples taken from umbilical artery show virtually identical values (pH_a: 6.69±0.04 and P_aCO_2: 156±4 mmHg) to both the human and our experimental data[99]. We have developed and used this PA/HIE protocol previously to test the putative neuroprotective effect of molecular hydrogen[77]. In the present study we report similar neocortical, hippocampal, and subcortical neuronal injury compared to those in[77]. Based on the similar neuropathology and microvascular findings, we can assume that the surgical manipulations did not affect HIE development or microvascular reactivity in this study, lending support to the translational value of the present findings.

pH_{brain} acidosis in response to asphyxia and hypercapnia

It is well known that the pH_{brain} has a determining role in the neurological outcome followed by hypoxic-ischemic stress[100]. However, experimental data on pH_{brain} changes during/after PA in piglet PA/HIE models are very scarce in the literature[101–103]. The similar technique was used in 1-3 days old piglets by Bender *et al.*[103], to assess the pH_{brain}. PA was elicited also with a hypoxic-hypercapnic gas mixture (5-8% O_2 and 7% CO_2) for 30 min. The PA stress resulted in the drop of the measured pH_{brain} to 6.26±0.14, which is 0.3 pH unit higher than in our study, due to the much lower P_aCO_2 values (61±1 *vs.* 160±6 mmHg[103], Bender *et al. vs* present study). After PA, the reventilation started with 100% O_2 ventilation, and additional sodium bicarbonate (2 mEq/kg, iv) was infused for rapid correction of arterial pH. These interventions decrease the translational value of the study by Bender *et al.*[103] as they are not included in the current neonatal caring guidelines, and they may have affected the recovery of pH_{brain}, which was restored under 90 min. They did not report significant neuronal injury compared to sham operated animals, except in those experiments where they combined the PA with hemorrhagic hypotension, suggesting that the PA alone was not severe enough to elicit HIE. The MRS study assessed by Corbett *et al.*[101], used 8±3 day old piglets to determine pH_i during and after ischemia but not under truly PA. Incomplete cerebral ischemia was elicited by the combination of hemorrhagic hypotension and bilateral carotid artery occlusion for 25 min followed by 90 min of reperfusion[102]. The developing severe acidosis during the ischemia was

dependent on blood glucose levels during the insult. In fed piglets the brain pH_i dropped below 5.6 and they responded with hyperglycemia (9.4-15 mmol/L) to the ischemia, whereas the fasted piglets responded with hypoglycaemia (1.4-2.6 mmol/L), so the nadir at the end of ischemia was mere $pH_i \cong 6.6$. Under the reperfusion period the pH_i was again normalized within the 90 min observation period.

We can conclude from the previously discussed studies that higher levels of hypercapnia, blood glucose and cerebral blood flow can all promote the development of cerebral acidosis during PA stress. The increased P_aCO_2 to 140-160 mmHg, which was observed in human and piglet PA as well, is able to reduce alone the pH_i to 6.5-6.6 under normoxic conditions[104]. In our present study, we provide evidence that the inhalation of 20% CO_2 alone (P_aCO_2:120 mmHg) under normoxic conditions can result in the drop of the pH_{brain} to 6.8. Applying linear regression (Fig. 8C), we calculated that the developing hypercapnia (at P_aCO_2: 160 mmHg) resulted in the drop of the pH_{brain} to 6.50 in our PA model, which is in a full agreement with the previous results. Further acidification during PA will be dominantly determined by the increases in the rate of anaerobic glycolysis fuelling the subsequent lactic acid production. The glucose delivery to the hypoxic brain limits the rate of glycolysis, as its reduction by either reducing cerebral blood flow[103] or blood glucose levels[102] attenuated the development of acidosis. In our previously shown PA model, significant cerebral ischemia did not develop[77] due to in most of the animals the MABP drop during the 20 min PA (Fig. 5) did not reach the lower limit of blood flow autoregulation[105]. In our model the PA was not long enough for the development of bradycardia and hypotension, which are commonly seen in severely asphyxiated infants, however, it represents well the acute PA phase before the cardiovascular adaptation mechanisms are disrupted and the most significant pH_{brain} alterations occur.

In summary, our study provides new experimental evidence that not only cerebral ischemia alone but PA combined with hypoxia, hypercapnia and hyperglycemia is adequate to elicit severe cerebral acidosis (pH_{brain} <6.0) which strongly affects on the neuronal viability[106]. The developing ≅0.8 pH unit difference between pH_{brain} and pH_a is a >6-fold H^+ gradient across the blood-brain barrier that is in accordance with previous newborn pig experimental findings that the blood-brain barrier is mature and not severely damaged by PA[107].

pH_{brain} monitoring during HIE development

pH_{brain} alteration has an important pathophysiological role during acute PA, and also after reventilation/reoxygenation. In piglets, the pH_{brain} was described earlier to remain stable after restoration from PA, but the observation lasted only for four hours after the recovery[103]. In contrast, we extended the post-asphyxia observation period to 24 hours. In our piglet PA/HIE model we didn't find any significant secondary alterations in pH_{brain} during the 24-hour period after PA. Our results are in total agreement with the previously reported pH_i data in a piglet MRS study where HI stress (hypoxic ventilation combined with carotid artery occlusion) was used instead of PA[108]. In that study, pH_i remained at baseline levels for 48 hours after restoration from the ischemic stress, furthermore, the pH_i alterations had no significant part in the development of secondary energy failure. A human MRS study also confirmed, that pH_i remained to be normal (7.13±0.05) in postasphyxial normocapnic newborns during the first day of life[109], which is in accordance with our study. In these newborn babies, the brain alkalosis developed during the following days, and then persisted for weeks, even months[109,110]. However, we would like to emphasize that our piglet model represents only a subgroup of asphyxiated babies who require intubation and respiratory support, but not those who can breathe spontaneously. The mechanically ventilated newborns stay normocapnic, while the spontaneously breathing babies may often develop hypocapnia[98] due to hyperventilation. This response can reflect a relative hyperventilation, secondary to the induction of hypoxic hypometabolism resulting in reduced CO_2 production[111]. Hyperventilation reduces the P_aCO_2 and tends to elevate pH_{brain}, which means that hypocapnia has been documented as an independent risk factor for adverse neurological outcome[112,113]. In piglets, moderate hypocapnia is needed to reduce the cerebral perfusion with an increase in pH and lactate levels even in the absence of asphyxia[114]. Our findings suggest that maintaining the normocapnia/ slight hypercapnia may have a role to prevent secondary pH_{brain} alterations. A translationally valid small-animal models of birth asphyxia in rats and guinea pigs established that higher P_aCO_2 levels during birth asphyxia and gradual restoration of normocapnia had beneficial effects on cerebral metabolic acidosis, oxygen and lactate levels[31]. Clearly, further studies are warranted to explore these effects in the piglet model. Our study limitations are that we have collected the pH_{brain} data from the neocortex using only one level of PA insult, leaving other brain regions and levels of stress unexplored.

The cortical microvascular response to NMDA

The NMDA induced pial arteriolar vasodilation was first described in newborn pigs[115], and later it was confirmed in different species[116,117]. The NMDA-induced pial arteriolar dilation is mediated by neuronal NO production in most of the animal models[45], according to its sensitivity to tetrodotoxin[118] and nNOS inhibitors[119,120]. In the present study we can confirm the previous experimental findings but some of them also conflict with the previous conclusions. In this study, the AAAN (0.4 mg/kg) caused nNOS inhibition resulted in a similar attenuation (~30-40%) of pial arteriolar dilation to NMDA described earlier by Bari *et al.* using 7-nitroindazole (50 mg/kg)[120]. However, we now presented that the attenuated arteriolar vasodilation to NMDA did not result in attenuated blood flow response in the underlying parenchyma, indeed the parenchymal flow response remained unchanged. We believe that the LSCI used in our study can give a good estimate of the NMDA-induced microvascular response to assess the cortical microvasculature. Our current results showing ~72% increase in CoBF to 1mM NMDA stimulation, which are in total agreement with our previous study showing identical increases in CoBF to 1mM NMDA using laser-Doppler flowmetry[64]. Our results suggest that dilation of intraparenchymal arterioles plays a more decisive role in determining the CoBF response and can compensate for the somewhat smaller pial arteriolar dilation in response to NMDA when nNOS activity is compromised. This finding is in contrast with an adult rat study, where also the CoBF response to NMDA was proved to be critically dependent on nNOS presence and activity[121], therefore this difference may well represent a species/age-dependent difference. Additional vasodilatory mechanisms may act predominantly on intraparenchymal vessels and must play an important role in mediating the observed increases in CoBF to NMDA in the piglet, which can be our further research subject. Based on microdialysis data[122], one of the possible mediator could be adenosine, because adenosine was proposed beside NO to contribute to the NMDA-induced CoBF response in the rat cerebral cortex. Exogenous adenosine reduces the pial arteriolar response to NMDA[46] in the piglet cortex, this latter finding presume that adenosine may have had a predominant action of intraparenchymal arterioles and their responses may largely independent of the pial vessels.

The cortical neuronal response to NMDA

In piglets, the cortical microvascular response to NMDA is thought to be mediated by exclusive activation of neuronal NMDA receptors. This finding is based on two evidence: isolated piglet cortical vessels do not respond to NMDA[123], and the functional NMDA receptors are not expressed in cerebrovascular endothelial cells or microvessels which were isolated from

rats, humans and piglets[124,125]. However, recent work suggests that the abluminally localized endothelial NMDA receptors in mice can contribute to functional hyperemia[126,127]. Unlike the painstakingly analyzed pial arteriolar response to NMDA, the changes in neuronal activity in response to topically applied NMDA were hardly tackled. Topically applied NMDA was proven to elicit SD, characterized by the SD-related DC potential shift simultaneously with pial arteriolar changes in adult mice, and the effect of NMDA was concentration-independently linked to the evoked SD[65]. In a following adult rat study, the topical NMDA was found to elicit SD, but the CoBF response after the SD-related hemodynamic response was demonstrated to act also NMDA-dose dependent manner[64]. The same experimental approach in piglets found only a dose-dependent CoBF response without any confounding SDs[64]. Immunohistochemistry studies in the piglet parietal cortex confirmed that layers II/III are the main zone of the nNOS-immunoreactive neurons and as these superficial cortical layers were also rich in NMDA-receptor expressing nerve cells[46], they seemed to be responsible for the observed effects of NMDA. Our present study is the first that studied the electrophysiological properties in all cortical layers to topically applied NMDA. Our present findings identified the superficial, and also the much deeper cortical structures to be affected by topical NMDA. Thus, the NMDA-induced robust 2.5 Hz δ-oscillation that have been found most prominent at 600-800 μm from the cortical surface suppressing LFP power in virtually all other frequency bands. NMDA also had opposing effects on neuronal firing, it suppressed or stimulated spiking in different neuronal populations. After NMDA stimulation, the LFP powers were restored to baseline levels, and also no abnormal spikes were recorded during/after NMDA application, suggesting that the cortex was not affected by significant excitotoxic stress during NMDA stimulation. This notion is in accordance with previous findings showing that the neurovascular response to topical NMDA is preserved in piglets (four applications in a 5 hours period)[59]. These results correspond well both with the previously observed SD-triggering and also with the tetrodotoxin-sensitive actions of topical NMDA application.

NMDA triggers SD-like suppression of the microvascular response to hypercapnia

The cortical microvascular response to graded hypercapnia has been extensively studied in the piglet, however just a few experiments have data about the pial arteriolar diameter and CoBF changes simultaneously[128]. In that study[128], both responses were unaltered by the general NOS inhibitor Nω-nitro-L-arginine methyl ester, indicating that NO plays minor role in the mediation of this response in the newborn pig. In pigs, the NO-independence is age-restricted

and the pial arteriolar response to hypercapnia is also NO-independent in newborns, but partially NO-dependent in juvenile (3-4 months old) pigs[129,130]. In rat, the soluble guanylate cyclase inhibitor 1H-[1,2,4]oxadiazolo[4,4,-a]quinoxalin-1-one (ODQ) had only effect on the response to NMDA[131] but had no effect on the response to hypercapnia. However, several rat studies highlight the role of nNOS-derived NO in the CoBF response to hypercapnia[132,133]. In the present study the nNOS inhibitor AAAN had no effect on the cortical microvascular response to graded hypercapnia, which is in agreement with the previous newborn pig studies.

The pial arteriolar response to graded hypercapnia is well known to be vulnerable to hypoxic/ischemic stress[134], endothelial injury[135], or seizures[136], which are good markers for identifying neurovascular unit dysfunction. SDs are also known to attenuate the microvascular response to hypercapnia in adult brains[62,63,61]. In the piglet cortex *bona fide* SDs are unable to be generated, however, a topically applied KCl induced 3-min long cortical depolarization (confirmed with DC recording) did not affect the microvascular response to hypercapnia and other assessed stimuli[137]. In the present study, in contrast with the previous findings, NMDA attenuated the response to graded hypercapnia in the newborn cerebral cortex, which is very similar to the occuring SDs effect in the adult cortex. The microvascular alteration appears to involve nNOS activity in its mechanism, but seems to be independent of the direct hemodynamic effect of NMDA-receptor activation. However, due to developmental differences we cannot conclude our findings to the adult cerebral cortex, because SDs are *de facto* unable to be triggered in the neonatal brain.

In our newborn pig study, we just started to explore the connections between the well-known cerebrovascular effects of hypercapnia and NMDA and the virtually uncharted neuronal effects of these stimuli in the cerebral cortex. Using multi-channel electrodes to study LFP and unit activity changes are widely used in the literature[138,139], as a state of the art method, although interpretation of LFP data is very difficult due to the lot of source contribution to the mixed signal[140,141]. There is very little information available about the LFP[68] or the unit activity[69] of the adult pig cerebral cortex let alone of the newborn piglet. Our electrophysiology data shows layer-specific and concentration-dependent effects of hypercapnia on the unit activity and the LFP as well, which are clearly altered after NMDA stimulation. Right now, we cannot make causative statements that the alterations in the neuronal response trigger the changes in microvascular reactivity or perhaps vice versa, however, our findings have a strong evidence that the mechanism of NMDA-induced attenuation of the microvascular response is not only limited to the cerebral vasculature. NMDA has suppressed all frequency bands of the LFP (similar to an SD in adult or old rats[142,143,144]), and it has also triggered a 2.5 Hz delta-

oscillation. The origin of the arising delta-oscillation is still unclear, however, it has been previously documented that these oscillations can be evoked by the stimulation of the cortex and different cell types can be responsible for the generation of abnormal oscillations in the cortex[145,146,147,148]. Furthermore, neuronal spiking was also suppressed in some, but triggered in other single units during NMDA exposure. All in all, we cannot determine the importance of these observations in the attenuation of microvascular response to hypercapnia, however, we can hypothesize that some aspects of the electrophysiological response to NMDA could participate in the attenuation of microvascular reactivity to hypercapnia and in the developing CoBF response. Clearly, further studies are needed to identify the specific and selective roles of the topically applied NMDA on the neuronal-vascular mechanisms.

CONCLUSION

HIE can result in lifelong disabilities and yet the only clinically approved neuroprotective possibility is the therapeutic hypothermia, which is not sufficient alone to mitigate severe brain damage caused by PA/HIE.

Our goal is to improve our understanding of PA/HIE pathophysiological mechanisms that may form a basis for the development of new neuroprotective therapeutic approaches combined with therapeutic hypothermia. To reach this goal, we advanced our knowledge by studying brain pH regulation, and the neurovascular unit function in the piglet cerebral cortex.

We found that:

- pH_{brain} drops below 6.0 in our translationally valid piglet PA model, the brain acidosis exceeding by ≅0.8 pH unit lower compared to the blood. The acidosis in the arterial blood highlighting the importance of severe acidosis in neuronal injury. The respiratory component is responsible for only ≅40% of the developing acidosis. In our animal model, no secondary pH shift (alkalosis) develops.
- NMDA elicits increases in CoBF but also triggers microvascular dysfunction by attenuating hypercapnia-induced cerebrovascular and neuronal responses. NMDA triggers an SD-like neuronal depression and neuronal excitation simultaneously evoking delta-oscillation in the cortex. These effects may contribute to the observed neurovascular dysfunction triggered by NMDA and may help the understanding of the similar neurovascular dysfunction triggered by SD.

ACKNOWLEDGEMENT

I would like to thank to Prof. Dr. Gábor Jancsó, the formal leader of the Theoretical Medicine Doctoral School, for accepting my application.

I would like to thank to Prof. Dr. Ferenc Bari, the leader of the Theoretical Medicine Doctoral School, for providing the circumstances to finish my PhD studies.

I would like to thank to Prof. Dr. Gyula Sáry for enabling my work in the Department of Physiology.

My eternal gratitude goes to my supervisor, Dr. Ferenc Domoki for giving me the opportunity to work in his lab, teaching me all the surgical and medical knowledge and helping me to improve my english skills.

I would like to thank to all my current and formal labmates Dr. Viktória Kovács, Dr. János Németh, Dr. Viktória Varga and Valéria Tóth-Szűki for their help in performing the experiments and giving advices.

I would like to express my thanks to all colleagues in the Department of Physiology for their support and kindness.

I am grateful to my family for their support and love. I am grateful to my mother, Éva Vass, who always stands beside me, no matter where the life drifts me away. I am the most grateful to my father, Attila Remzső who always inspired me for precise and hard work. Without them I couldn't reach my goals in life.

I am grateful to all my friends, Zoltán Molnár, Ádám Sulumán, Tamás Puskás, Henrik Somodi, Dr. Fanni Kelemen who always cheered me up when I needed them the most.

FUNDING

We are grateful for the financial funding of the following grants:

- EU-funded Hungarian grant GINOP (GINOP 2.3.2 15 2016 00034)
- EU-funded Hungarian grant EFOP (EFOP-3.6.1-16-2016-00008)
- Hungarian Brain Research Program 2.0 (2017-2.1 NKP 2017 00002)

REFERENCES

1. UNICEF. Neonatal mortality. https://data.unicef.org/topic/child-survival/neona (2020).
2. Bax, M. & Nelson, K. B. Birth Asphyxia : a Statement. *Dev. Med. Child Neurol.* **35**, 1022–1024 (1993).
3. Volpe, J. J. Neonatal encephalopathy: An inadequate term for hypoxic-ischemic encephalopathy. *Ann. Neurol.* **72**, 156–166 (2012).
4. Antonucci, R., Porcella, A. & Pilloni, M. D. Perinatal asphyxia in the term newborn. *J. Pediatr. Neonatal Individ. Med.* **3**, 1–14 (2014).
5. Kurinczuk, J. J., White-Koning, M. & Badawi, N. Epidemiology of neonatal encephalopathy and hypoxic-ischaemic encephalopathy. *Early Hum. Dev.* **86**, 329–338 (2010).
6. Hankins, G. D. V. & Speer, M. Defining the pathogenesis and pathophysiology of neonatal encephalopathy and cerebral palsy. *Obstet. Gynecol.* **102**, 628–636 (2003).
7. de Vries, L. S. & Cowan, F. M. Evolving Understanding of Hypoxic-Ischemic Encephalopathy in the Term Infant. *Semin. Pediatr. Neurol.* **16**, 216–225 (2009).
8. Cotten, C. M. & Shankaran, S. Hypothermia for hypoxic-ischemic encephalopathy. *Expert Rev. Obstet. Gynecol.* **5**, 227–239 (2010).
9. Kumar, S. & Paterson-Brown, S. Obstetric aspects of hypoxic ischemic encephalopathy. *Early Hum. Dev.* **86**, 339–344 (2010).
10. Nelson, K. B. & Leviton, A. How Much of Neonatal Encephalopathy Is due to Birth Asphyxia? *Am. J. Dis. Child.* **145**, 1325–1331 (1991).
11. Apgar, V. A proposal for a new method of evaluation of the newborn infant. *Curr. Res. Anesth. Analg.* **32**, 260–267 (1953).
12. Sarnat, H. B. & Sarnat, M. S. Neonatal encephalopathy following fetal distress. *Obstet. Gynecol. Surv.* **32**, 295–297 (1976).
13. Shalak, L. & Perlman, J. M. Hypoxic-ischemic brain injury in the term infant-current concepts. *Early Hum. Dev.* **80**, 125–141 (2004).
14. Hanrahan, J. D. *et al.* Cerebral metabolism within 18 hours of birth asphyxia: A proton magnetic resonance spectroscopy study. *Pediatr. Res.* **39**, 584–590 (1996).
15. Liao, Y., Cotten, M., Tan, S., Kurtzberg, J. & Cairo, M. S. Rescuing the neonatal brain from hypoxic injury with autologous cord blood. *Bone Marrow Transplant.* **48**, 890–900 (2013).
16. Volpe, J. J. *Neurology of the newborn*. (Saunders, 2008).
17. JOHNSTON, M. V. *et al.* Plasticity and Injury in the Developing Brain. *Brain Dev.* **31**, 1–10 (2009).
18. Hagberg, H., Mallard, C., Rousset, C. I. & Thornton, C. Mitochondria: Hub of injury responses in the developing brain. *Lancet Neurol.* **13**, 217–232 (2014).
19. Fatemi, A., Wilson, M. A. & Johnston, M. V. Hypoxic-Ischemic Encephalopathy in the Term

Infant. *Clin. Perinatol.* **36**, 835–858 (2009).

20. Alvarez-Díaz, A., Hilario, E., Goñi De Cerio, F., Valls-I-Soler, A. & Alvarez-Díaz, F. J. Hypoxic-ischemic injury in the immature brain - Key vascular and cellular players. *Neonatology* **92**, 227–235 (2007).
21. Iwata, O. *et al.* 'Therapeutic time window' duration decreases with increasing severity of cerebral hypoxia-ischaemia under normothermia and delayed hypothermia in newborn piglets. *Brain Res.* **1154**, 173–180 (2007).
22. Sanderson, T. H., Reynolds, C. A., Kumar, R., Przyklenk, K. & Hüttemann, M. Molecular mechanisms of ischemia-reperfusion injury in brain: Pivotal role of the mitochondrial membrane potential in reactive oxygen species generation. *Mol. Neurobiol.* **47**, 9–23 (2013).
23. Bhalala, U. S., Koehler, R. C. & Kannan, S. Neuroinflammation and neuroimmune dysregulation after acute hypoxic-ischemic injury of developing brain. *Front. Pediatr.* **2**, 1–12 (2015).
24. Hassell, K. J., Ezzati, M., Alonso-Alconada, D., Hausenloy, D. J. & Robertson, N. J. New horizons for newborn brain protection: Enhancing endogenous neuroprotection. *Arch. Dis. Child. Fetal Neonatal Ed.* **100**, F541–F551 (2015).
25. Casey, J. R., Grinstein, S. & Orlowski, J. Sensors and regulators of intracellular pH. *Nat. Rev. Mol. Cell Biol.* **11**, 50–61 (2010).
26. Tang, C. M., Dichter, M. & Morad, M. Modulation of the N-methyl-D-aspartate channel by extracellular H+. *Proc. Natl. Acad. Sci. U. S. A.* **87**, 6445–6449 (1990).
27. Tombaugh, G. C. & Somjen, G. G. Effects of extracellular pH on voltage-gated Na+, K+ and Ca2+ currents in isolated rat CA1 neurons. *J. Physiol.* **493**, 719–732 (1996).
28. Helmy, M. M., Tolner, E. A., Vanhatalo, S., Voipio, J. & Kaila, K. Brain alkalosis causes birth asphyxia seizures, suggesting therapeutic strategy. *Ann. Neurol.* **69**, 493–500 (2011).
29. Ala-Kurikka, T. *et al.* A physiologically validated rat model of term birth asphyxia with seizure generation after, not during, brain hypoxia. *Epilepsia* (2020) doi:10.1111/epi.16790.
30. Jensen, F. E. & Wang, C. Hypoxia-induced hyperexcitability in vivo and in vitro in the immature hippocampus. *Epilepsy Res.* **26**, 131–140 (1996).
31. Pospelov, A. S., Puskarjov, M., Kaila, K. & Voipio, J. Endogenous brain-sparing responses in brain pH and PO2 in a rodent model of birth asphyxia. *Acta Physiol.* e13467 (2020) doi:10.1111/apha.13467.
32. Richer, J. P. *et al.* Sacrococcygeal and transsacral epidural anesthesia in the laboratory pig: A model for experimental surgery. *Surg. Radiol. Anat.* **20**, 431–435 (1998).
33. Bollen, P., Hansen, A. K. & Rasmussen, H. J. *The laboratory swine*. (CRC Press, 2000).
34. Dobbing, J. & Sands, J. Comparative aspects of the brain growth spurt. *Early Hum. Dev.* **311**, 79–83 (1979).
35. Dickerson, J. W. & Dobbing, J. Prenatal and postnatal growth and development of the central

nervous system of the pig. *Proc. R. Soc. Lond. B. Biol. Sci.* **166**, 384–395 (1967).

36. Thibault, K. L. & Margulies, S. S. Age-dependent material properties of the porcine cerebrum: Effect on pediatric inertial head injury criteria. *J. Biomech.* **31**, 1119–1126 (1998).
37. Lind, N. M. *et al.* The use of pigs in neuroscience: Modeling brain disorders. *Neurosci. Biobehav. Rev.* **31**, 728–751 (2007).
38. Conrad, M. S. & Johnson, R. W. The Domestic Piglet: An Important Model for Investigating the Neurodevelopmental Consequences of Early Life Insults. *Annu. Rev. Anim. Biosci.* **3**, 245–264 (2015).
39. Leffler, C. W., Busija, D. W., Beasley, D. G., Armstead, W. M. & Mirro, R. Postischemic cerebral microvascular responses to norepinephrine and hypotension in Newborn Pigs. *Stroke* **20**, 541–546 (1989).
40. Kim, Y. B., Gidday, J. M., Gonzales, E. R., Shah, A. R. & Park, T. S. Effect of hypoglycemia on postischemic cortical blood flow, hypercapnic reactivity, and interstitial adenosine concentration. *J. Neurosurg.* **81**, 877–884 (1994).
41. Temesvari, P., Hencz, P. & Joo, F. Modulation of the blood-brain barrier permeability in neonatal cytotoxic brain edema: Laboratory and morphological findings obtained on newborn piglets with experimental pneumothorax. *Biol. Neonate* **46**, 198–208 (1984).
42. Martin, L. J., Brambrink, A., Koehler, R. C. & Traystman, R. J. Primary Sensory and Forebrain Motor Systems in the Newborn Brain Are Hypoxia-Ischemia. **285**, 262–285 (1997).
43. Kovács, V. *et al.* Inhaled H2 or CO2 do not augment the neuroprotective effect of therapeutic hypothermia in a severe neonatal hypoxic-ischemic encephalopathy piglet model. *Int. J. Mol. Sci.* **21**, 1–22 (2020).
44. Oláh, O., Tóth-Szűki, V., Temesvári, P., Bari, F. & Domoki, F. Delayed Neurovascular Dysfunction Is Alleviated by Hydrogen in Asphyxiated Newborn Pigs. *Neonatology* **104**, 79–86 (2013).
45. Busija, D. W., Bari, F., Domoki, F. & Louis, T. Mechanisms Involved in the Cerebrovascular Dilator Effects of N- methyl-D-aspartate in Cerebral Cortex. *Brain Res. Rev.* **56**, 89–100 (2007).
46. Bari, F., Thore, C. R., Louis, T. M. & Busija, D. W. Inhibitory effects of hypoxia and adenosine on N-methyl-D-aspartate-induced pial arteriolar dilation in piglets. *Brain Res.* **780**, 237–244 (1998).
47. Kim, W. K. *et al.* Attenuation of NMDA receptor activity and neurotoxicity by nitroxyl anion, NO-. *Neuron* **24**, 461–469 (1999).
48. Aoki, C., Rhee, J., Lubin, M. & Dawson, T. M. NMDA-R1 subunit of the cerebral cortex co-localizes with neuronal nitric oxide synthase at pre-and postsynaptic sites and in spines. *Brain Res.* **750**, 25–40 (1997).
49. Attwell, D. *et al.* Glial and neuronal control of brain blood flow. *Nature* **468**, 232–243 (2010).

50. Lindauer, U., Megow, D., Matsuda, H. & Dirnagl, U. Nitric oxide: A modulator, but not a mediator, of neurovascular coupling in rat somatosensory cortex. *Am. J. Physiol. - Hear. Circ. Physiol.* **277**, 799–811 (1999).
51. Filosa, J. A. *et al.* Local potassium signaling couples neuronal activity to vasodilation in the brain. *Nat. Neurosci.* **9**, 1397–1403 (2006).
52. Zonta, M. *et al.* Neuron-to-astrocyte signaling is central to the dynamic control of brain microcirculation. *Nat. Neurosci.* **6**, 43–50 (2003).
53. Metea, M. R. & Newman, E. A. Glial cells dilate and constrict blood vessels: A mechanism of neurovascular coupling. *J. Neurosci.* **26**, 2862–2870 (2006).
54. Blanco, V. M., Stern, J. E. & Filosa, J. A. Tone-dependent vascular responses to astrocyte-derived signals. *Am. J. Physiol. - Hear. Circ. Physiol.* **294**, 2855–2863 (2008).
55. Mathiesen, C., Caesar, K., Akgören, N. & Lauritzen, M. Modification of activity-dependent increases of cerebral blood flow by excitatory synaptic activity and spikes in rat cerebellar cortex. *J. Physiol.* **512**, 555–566 (1998).
56. Enager, P. *et al.* Pathway-specific variations in neurovascular and neurometabolic coupling in rat primary somatosensory cortex. *J. Cereb. Blood Flow Metab.* **29**, 976–986 (2009).
57. Busija, D. W. & Wei, M. Altered cerebrovascular responsiveness to N-methyl-D-aspartate after asphyxia in piglets. *Am. J. Physiol. - Hear. Circ. Physiol.* **265**, 389–394 (1993).
58. Bari, F., Errico, R. A., Louis, T. M. & Busija, D. W. Differential Effects of Short-term Hypoxia and Hypercapnia on N-Methyl-d-Aspartate–Induced Cerebral Vasodilatation in Piglets. *Stroke* 1634–1640 (1996).
59. Busija, D. W. *et al.* Effects of ischemia on cerebrovascular responses to N-methyl-D-aspartate in piglets. *Am. J. Physiol. - Hear. Circ. Physiol.* **270**, (1996).
60. Hartings, J. A. *et al.* The continuum of spreading depolarizations in acute cortical lesion development: Examining Leão's legacy. *J. Cereb. Blood Flow Metab.* **37**, 1571–1594 (2017).
61. Unekawa, M. *et al.* Dynamic diameter response of intraparenchymal penetrating arteries during cortical spreading depression and elimination of vasoreactivity to hypercapnia in anesthetized mice. *J. Cereb. Blood Flow Metab.* **37**, 657–670 (2016).
62. Piper, R. D., Lambert, G. A. & Duckworth, J. W. Cortical blood flow changes during spreading depression in cats. *Am. J. Physiol.* **261**, H96-102 (1991).
63. Lacombe, P., Sercombe, R., Correze, J. L., Springhetti, V. & Seylaz, J. Spreading depression induces prolonged reduction of cortical blood flow reactivity in the rat. *Exp. Neurol.* **117**, 278–286 (1992).
64. Lenti, L. *et al.* N-methyl-D-aspartate induces cortical hyperemia through cortical spreading depression-dependent and -independent mechanisms in rats. *Microcirculation* **16**, 629–639 (2009).
65. Ayata, C. & Moskowitz, M. A. Cortical spreading depression confounds concentration-

dependent pial arteriolar dilation during N-methyl-D-aspartate superfusion. *AJP Hear. Circ. Physiol.* **290**, H1837–H1841 (2006).

66. Marrannes, R., Willems, R., De Prins, E. & Wauquier, A. Evidence for a role of the N-methyl-d-aspartate (NMDA) receptor in cortical spreading depression in the rat. *Brain Res.* **457**, 226–240 (1988).
67. Lauritzen, M. & Hansen, A. J. The effect of glutamate receptor blockade on anoxic depolarization and cortical spreading depression. *J. Cereb. Blood Flow Metab.* **12**, 223–229 (1992).
68. Tanosaki, M., Ishibashi, H., Zhang, T. & Okada, Y. Effective Connectivity Maps in the Swine Somatosensory Cortex Estimated from Electrocorticography and Validated with Intracortical Local Field Potential Measurements. *Brain Connect.* **4**, 100–111 (2014).
69. Ulyanova, A. V. *et al.* Electrophysiological Signature Reveals Laminar Structure of the Porcine Hippocampus. *Eneuro* **5**, 1–15 (2018).
70. Walsh, B. H., Murray, D. M. & Boylan, G. B. The use of conventional EEG for the assessment of hypoxic ischaemic encephalopathy in the newborn: A review. *Clin. Neurophysiol.* **122**, 1284–1294 (2011).
71. Korotchikova, I. *et al.* EEG in the healthy term newborn within 12 hours of birth. *Clin. Neurophysiol.* **120**, 1046–1053 (2009).
72. Boylan, G. B., Stevenson, N. J. & Vanhatalo, S. Monitoring neonatal seizures. *Semin. Fetal Neonatal Med.* **18**, 202–208 (2013).
73. Fenichel MG. *Neonatal neurology*. (2006).
74. Ramantani, G. *et al.* Neonatal Seizures — Are We there Yet ? 280–293 (2019).
75. Pavel, A. M. *et al.* A machine-learning algorithm for neonatal seizure recognition: a multicentre, randomised, controlled trial. *Lancet Child Adolesc. Heal.* **4**, 740–749 (2020).
76. Raurale, S. A., Boylan, G. B., Lightbody, G. & O'Toole, J. M. Grading the severity of hypoxic-ischemic encephalopathy in newborn EEG using a convolutional neural network. *arXiv* 6103–6106 (2020).
77. Nemeth, J. *et al.* Molecular hydrogen affords neuroprotection in a translational piglet model of hypoxic-ischemic encephalopathy. *J. Physiol. Pharmacol.* **67**, 677–689 (2016).
78. Kovács, V. *et al.* Active forms of Akt and ERK are dominant in the cerebral cortex of newborn pigs that are unaffected by asphyxia. *Life Sci.* **192**, (2018).
79. Laptook, A. R., Stonestreet, B. S. & Oh, W. The effect of carotid artery ligation on brain blood flow in newborn piglets. *Brain Res.* **276**, 51–54 (1983).
80. Domoki, F. *et al.* Comparison of cerebrocortical microvascular effects of different hypoxic-ischemic insults in piglets: A laser-speckle imaging study. *J. Physiol. Pharmacol.* **65**, 551–558 (2014).
81. Ji, H. *et al.* Selective neuronal nitric oxide synthase inhibitors and the prevention of cerebral

palsy. *Ann. Neurol.* **65**, 209–217 (2009).

82. Voipio, J. & Kaila, K. Interstitial PCO2 and pH in rat hippocampal slices measured by means of a novel fast CO2/H+-sensitive microelectrode based on a PVC-gelled membrane. *Pflügers Arch. Eur. J. Physiol.* **423**, 193–201 (1993).
83. Voipio, J., Pasternack, M. & MacLeod, K. Ion-sensitive microelectrodes. in *Microelectrode Techniques – The Plymouth Workshop Handbook* vol. 17 275–316 (The Company of Biologists Limited, 1994).
84. Domoki, F. *et al.* Evaluation of laser-speckle contrast image analysis techniques in the cortical microcirculation of piglets. *Microvasc. Res.* **83**, 311–317 (2012).
85. Hazan, L., Zugaro, M. & Buzsáki, G. Klusters, NeuroScope, NDManager: A free software suite for neurophysiological data processing and visualization. *J. Neurosci. Methods* **155**, 207–216 (2006).
86. Kadir, S. N., Goodman, D. F. M. & Harris, K. D. High-Dimensional Cluster Analysis with the Masked EM Algorithm. *Neural Comput.* **26**, 2379–2394 (2014).
87. Rossant, C. *et al.* Spike sorting for large , dense electrode arrays. *Nat. Neurosci.* **19**, 634–641 (2016).
88. Csicsvari, J., Hirase, H. & Czurko, A. Reliability and State Dependence of Pyramidal Cell – Interneuron Synapses in the Hippocampus : an Ensemble Approach in the Behaving Rat. *Neuron* **21**, 179–189 (1998).
89. Mizuseki, K., Sirota, A., Pastalkova, E. & Buzsáki, G. Theta Oscillations Provide Temporal Windows for Local Circuit Computation in the Entorhinal-Hippocampal Loop. *Neuron* **64**, 267–280 (2008).
90. Stark, E. *et al.* Pyramidal cell-interneuron interactions underlie hippocampal ripple oscillations. *Neuron* **83**, 467–480 (2014).
91. Barthó, P. *et al.* Characterization of Neocortical Principal Cells and Interneurons by Network Interactions and Extracellular Features. *J. Neurophysiol.* **92**, 600–608 (2004).
92. Randall, G. C. B. Studies on the effect of acute asphyxia on the fetal pig in utero. *Biol. Neonate* **36**, 63–69 (1979).
93. Azzopardi, D. V. *et al.* Moderate hypothermia to treat perinatal asphyxial encephalopathy. *N. Engl. J. Med.* **361**, 1349–1358 (2009).
94. Thoresen, M. Who should we cool after perinatal asphyxia? *Semin. Fetal Neonatal Med.* **20**, 66–71 (2015).
95. Randall, G. C. B. pH Values and Blood-Gas Tensions in the Normal Piglet during the First 48 Hours of Life. *Biol. Neonate* **20**, 68–73 (1972).
96. Alonso-Alconada, D. *et al.* Brain cell death is reduced with cooling by 3.5°C to 5°C but increased with cooling by 8.5°C in a piglet asphyxia model. *Stroke* **46**, 275–278 (2015).
97. Sabir, H. *et al.* Xenon depresses aEEG background voltage activity whilst maintaining

cardiovascular stability in sedated healthy newborn pigs. *J. Neurol. Sci.* **363**, 140–144 (2016).

98. Engle, W. D., Laptook, A. R. & Perlman, J. M. Acute changes in arterial carbon dioxide tension and acid-base status and early neurologic characteristics in term infants following perinatal asphyxia. *Resuscitation* **42**, 11–17 (1999).
99. Randall, G. C. The relationship of arterial blood pH and pCO2 to the viability of the newborn piglet. *Can. J. Comp. Med.* **35**, 141–146 (1971).
100. Siesjö, B. K. Acid-Base Homeostasis in the Brain: Physiology, Chemistry, and Neurochemical Pathology. *Prog. Brain Res.* **63**, 121–154 (1985).
101. Corbett, R. J. T., Laptook, A. R., Nunnally, R. L., Hassan, A. & Jackson, J. Intracellular pH, Lactate, and Energy Metabolism in Neonatal Brain During Partial Ischemia Measured In Vivo by 31P and 1H Nuclear Magnetic Resonance Spectroscopy. *J. Neurochem.* **51**, 1501–1509 (1988).
102. Laptook, A. R., Corbett, R. J. T. & Nunnally, R. L. Effect of Plasma Glucose Concentration on Cerebral Metabolism During Partial Ischemia in Neonatal Piglets. *Stroke* **21**, 435–440 (1990).
103. Bender, T. M., Johnston, J. A., Manepalli, A. N. & Mink, R. B. Association between brain tissue pH and brain injury during asphyxia in piglets. *Resuscitation* **59**, 243–254 (2003).
104. Corbett, R. J. T., Laptook, A. R., Hassan, A. & Nunnally, R. L. Quantitation of acidosis in neonatal brain tissue using the 31P NMR resonance peak of phosphoethanolamine. *Magn. Reson. Med.* **6**, 99–106 (1988).
105. Laptook, A., Stonestreet, B. S. & Oh, W. Autoregulation of brain blood flow in the newborn piglet: Regional differences in flow reduction during hypotension. *Early Hum. Dev.* **6**, 99–107 (1982).
106. Li, P.-A., Shamloo, M., Katsura, K., Smith, M.-L. & Siesjö, B. K. Critical values for plasma glucose in aggravating ischaemic brain damage: correlation to extracellular pH. *Neurobiol. Dis.* **2**, 97–108 (1995).
107. Stonestreet, B. S., Burgess, G. H. & Cserr, H. F. Blood-brain barrier integrity and brain water and electrolytes during hypoxia/hypercapnia and hypotension in newborn piglets. *Brain Res.* **590**, 263–270 (1992).
108. Lorek, A. *et al.* Delayed ("Secondary") Cerebral Energy Failure after Acute Hypoxia-Ischemia in the Newborn Piglet: Continuous 48-Hour Studies by Phosphorus Magnetic Resonance Spectroscopy. *Pediatr. Res.* **36**, 699–706 (1994).
109. Hope, P. L. *et al.* Cerebral Energy Metabolism Studied With Phosphorus NMR Spectroscopy In Normal And Birth-Asphyxiated Infants. *Lancet* **324**, 366–370 (1984).
110. Robertson, N. J. *et al.* Cerebral Intracellular Lactic Alkalosis Persisting Months after Neonatal Encephalopathy Measured by Magnetic Resonance Spectroscopy. *Pediatr. Res.* **46**, 287–296 (1999).
111. Mortola, J. P. How newborn mammals cope with hypoxia. *Respiration Physiology* vol. 116 95–

103 (1999).

112. Lingappan, K., Kaiser, J. R., Srinivasan, C. & Gunn, A. J. Relationship between PCO2 and unfavorable outcome in infants with moderate-to-severe hypoxic ischemic encephalopathy. *Pediatr. Res.* **80**, 204–208 (2016).
113. Pappas, A. *et al.* Hypocarbia and adverse outcome in neonatal hypoxic-ischemic encephalopathy. *J. Pediatr.* **158**, 752–758 (2011).
114. Ringer, S. K., Clausen, N. G., Spielmann, N. & Weiss, M. Effects of moderate and severe hypocapnia on intracerebral perfusion and brain tissue oxygenation in piglets. *Paediatr. Anaesth.* **29**, 1114–1121 (2019).
115. Busija, D. W. & Leffler, C. W. Dilator effects of amino acid neurotransmitters on piglet pial arterioles. *Am. J. Physiol. Circ. Physiol.* **257**, H1200–H1203 (1989).
116. Faraci, F. M. & Breese, K. R. Nitric oxide mediates vasodilatation in response to activation of N- methyl-D-aspartate receptors in brain. *Circ. Res.* **72**, 476–480 (1993).
117. Mayhan, W. G. & Didion, S. P. Acute Effects of Ethanol on Responses of Cerebral Arterioles. *Stroke* **26**, 2097–2102 (1995).
118. Leffler, C. W., Parfenova, H., Fedinec, A. L., Tcheranova, D. & Basuroy, S. Contributions of astrocytes and CO to pial arteriolar dilation to glutamate in newborn pigs. *Am. J. Physiol. Circ. Physiol.* **291**, H2897–H2904 (2006).
119. Meng, W., Tobin, J. R. & Busija, D. W. Glutamate-Induced Cerebral Vasodilation Is Mediated by Nitric Oxide Through N-Methyl-D-Aspartate Receptors. *Stroke* **26**, 857–863 (1995).
120. Bari, F., Errico, R. A., Louis, T. M. & Busija, D. W. Interaction between ATP-sensitive K+ channels and nitric oxide on pial arterioles in piglets. *J. Cereb. Blood Flow Metab.* **16**, 1158–1164 (1996).
121. Girouard, H. *et al.* NMDA receptor activation increases free radical production through Nitric Oxide and NOX2. *J. Neurosci.* **29**, 2545–2552 (2009).
122. Kaiser, M. G. & During, M. J. Combining laser doppler flowmetry with microdialysis: a novel approach to investigate the coupling of regional cerebral blood flow to neuronal activity. *J. Neurosci. Methods* **60**, 165–173 (1995).
123. Simandle, S. A. *et al.* Piglet pial arteries respond to N-methyl-D-aspartate in vivo but not in vitro. *Microvasc. Res.* **70**, 76–83 (2005).
124. Morley, P. *et al.* Evidence that Functional Glutamate Receptors are not Expressed on Rat or Human Cerebromicrovascular Endothelial Cells. *J. Cereb. Blood Flow Metab.* **18**, 396–406 (1998).
125. Domoki, F., Kis, B., Gáspár, T., Bari, F. & Busija, D. W. Cerebromicrovascular endothelial cells are resistant to L-glutamate. *Am. J. Physiol. Integr. Comp. Physiol.* **295**, R1099–R1108 (2008).
126. Lu, L. *et al.* Astrocytes drive cortical vasodilatory signaling by activating endothelial NMDA

receptors. *J. Cereb. Blood Flow Metab.* **39**, 481–496 (2019).

127. Hogan-Cann, A. D., Lu, P. & Anderson, C. M. Endothelial NMDA receptors mediate activitydependent brain hemodynamic responses in mice. *Proc. Natl. Acad. Sci. U. S. A.* **116**, 10229–10231 (2019).
128. Domoki, F., Zimmermann, A., Tóth-Szűki, V., Busija, D. W. & Bari, F. Acetazolamide induces indomethacin and ischaemia-sensitive pial arteriolar vasodilation in the piglet. *Acta Paediatr.* **97**, 280–284 (2008).
129. Willis, A. P. & Leffler, C. W. NO and prostanoids: Age dependence of hypercapnia- and histamine- induced dilations of pig pial arterioles. *Am. J. Physiol. - Hear. Circ. Physiol.* **277**, 299–307 (1999).
130. Willis, A. P. & Leffler, C. W. Endothelial NO and prostanoid involvement in newborn and juvenile pig pial arteriolar vasomotor responses. *Am. J. Physiol. - Hear. Circ. Physiol.* **281**, 2366–2377 (2001).
131. Rosenblum, W. I., Wei, E. P. & Kontos, H. A. Dilation of rat brain arterioles by hypercapnia in vivo can occur even after blockade of guanylate cyclase by ODQ. *Eur. J. Pharmacol.* **448**, 201–206 (2002).
132. Iadecola, C. Does nitric oxide mediate the increases in cerebral blood flow elicited by hypercapnia? *Proc. Natl. Acad. Sci. U. S. A.* **89**, 3913–3916 (1992).
133. Wang, Q., Pelligrino, D. A., Baughman, V. L., Koenig, H. M. & Albrecht, R. F. The role of neuronal nitric oxide synthase in regulation of cerebral blood flow in normocapnia and hypercapnia in rats. *J. Cereb. Blood Flow Metab.* **15**, 774–778 (1995).
134. Leffler, C. W., Busija, D. W., Armstead, W. M., Mirro, R. & Beasley, D. G. Ischemia Alters Cerebral Vascular Responses to Hypercapnia and Acetylcholine in Piglets. *Pediatr. Res.* **25**, 180–183 (1989).
135. Leffler, C. W., Mirro, R., Shanklin, D. R., Armstead, W. M. & Shibata, M. Light/dye microvascular injury selectively eliminates hypercapnia-induced pial arteriolar dilation in newborn pigs. *Am. J. Physiol. Circ. Physiol.* **266**, H623–H630 (1994).
136. Carratu, P., Pourcyrous, M., Fedinec, A., Leffler, C. W. & Parfenova, H. Endogenous heme oxygenase prevents impairment of cerebral vascular functions caused by seizures. *Am. J. Physiol. Circ. Physiol.* **285**, H1148–H1157 (2003).
137. Domoki, F., Veltkamp, R., Bari, F., Louis, T. M. & Busija, D. W. Cerebrovascular reactivity remains intact after cortical depolarization in newborn piglets. *Pediatr. Res.* **45**, 834–837 (1999).
138. Berényi, A. *et al.* Large-scale , high-density (up to 512 channels) recording of local circuits in behaving animals. *J. Neurophysiol.* **111**, 1132–1149 (2014).
139. Fiáth, R. *et al.* Laminar analysis of the slow wave activity in the somatosensory cortex of anesthetized rats. *Eur. J. Neurosci.* **44**, 1935–1951 (2016).

140. Buzsáki, G., Anastassiou, C. A. & Koch, C. The origin of extracellular fields and currents-EEG, ECoG, LFP and spikes. *Nat. Rev. Neurosci.* **13**, 407–420 (2012).

141. Einevoll, G. T., Kayser, C., Logothetis, N. K. & Panzeri, S. Modelling and analysis of local field potentials for studying the function of cortical circuits. *Nat. Rev. Neurosci.* **14**, 770–785 (2013).

142. Hertelendy, P. *et al.* Advancing age and ischemia elevate the electric threshold to elicit spreading depolarization in the cerebral cortex of young adult rats. *J. Cereb. Blood Flow Metab.* **37**, 1763–1775 (2017).

143. Menyhárt, Á. *et al.* High incidence of adverse cerebral blood flow responses to spreading depolarization in the aged ischemic rat brain. *Neurobiol. Aging* **36**, 3269–3277 (2015).

144. Makra, P., Menyhárt, Á., Bari, F. & Farkas, E. Spectral and Multifractal Signature of Cortical Spreading Depolarisation in Aged Rats. *Front. Physiol.* **9**, 1–12 (2018).

145. Kiss, T., Feng, J., Hoffmann, W. E., Shaffer, C. L. & Hajós, M. Rhythmic theta and delta activity of cortical and hippocampal neuronal networks in genetically or pharmacologically induced N-methyl-d-aspartate receptor hypofunction under urethane anesthesia. *Neuroscience* vol. 237 255–267 (2013).

146. Gireesh, E. D. & Plenz, D. Neuronal avalanches organize as nested theta- and beta/gamma-oscillations during development of cortical layer 2/3. *Proc. Natl. Acad. Sci.* **105**, 7576–7581 (2008).

147. Minlebaev, M., Ben-Ari, Y. & Khazipov, R. NMDA receptors pattern early activity in the developing barrel cortex in vivo. *Cereb. Cortex* **19**, 688–696 (2009).

148. Matulewicz, P., Orzeł-Gryglewska, J., Kuśmierczak, M. & Jurkowlaniec, E. NMDA-glutamatergic activation of the ventral tegmental area induces hippocampal theta rhythm in anesthetized rats. *Brain Res. Bull.* **107**, 43–53 (2014).

I.

PLOS ONE

RESEARCH ARTICLE

Brain interstitial pH changes in the subacute phase of hypoxic-ischemic encephalopathy in newborn pigs

Gábor Remzső[1☯]*, János Németh[1☯], Viktória Varga[1], Viktória Kovács[1], Valéria Tóth-Szűki[1], Kai Kaila[2,3], Juha Voipio[2], Ferenc Domoki[1]

1 Department of Physiology, University of Szeged, Faculty of Medicine, Szeged, Hungary, **2** Faculty of Biological and Environmental Sciences, Molecular and Integrative Biosciences, University of Helsinki, Helsinki, Finland, **3** Neuroscience Center (HiLIFE), University of Helsinki, Helsinki, Finland

☯ These authors contributed equally to this work.
* remzso.gabor@med.u-szeged.hu

OPEN ACCESS

Citation: Remzső G, Németh J, Varga V, Kovács V, Tóth-Szűki V, Kaila K, et al. (2020) Brain interstitial pH changes in the subacute phase of hypoxic-ischemic encephalopathy in newborn pigs. PLoS ONE 15(5): e0233851. https://doi.org/10.1371/journal.pone.0233851

Editor: Mária A. Deli, Hungarian Academy of Sciences, HUNGARY

Received: January 27, 2020

Accepted: May 13, 2020

Published: May 29, 2020

Peer Review History: PLOS recognizes the benefits of transparency in the peer review process; therefore, we enable the publication of all of the content of peer review and author responses alongside final, published articles. The editorial history of this article is available here: https://doi.org/10.1371/journal.pone.0233851

Data Availability Statement: All experimental data are available at Open Science Framework (osf.io): DOI 10.17605/OSF.IO/MUTGA.

Abstract

Brain interstitial pH (pH_{brain}) alterations play an important role in the mechanisms of neuronal injury in neonatal hypoxic-ischemic encephalopathy (HIE) induced by perinatal asphyxia. The newborn pig is an established large animal model to study HIE, however, only limited information on pH_{brain} alterations is available in this species and it is restricted to experimental perinatal asphyxia (PA) and the immediate reventilation. Therefore, we sought to determine pH_{brain} over the first 24h of HIE development in piglets. Anaesthetized, ventilated newborn pigs (n = 16) were instrumented to control major physiological parameters. pH_{brain} was determined in the parietal cortex using a pH-selective microelectrode. PA was induced by ventilation with a gas mixture containing 6%O_2-20%CO_2 for 20 min, followed by reventilation with air for 24h, then the brains were processed for histopathology assessment. The core temperature was maintained unchanged during PA (38.4±0.1 *vs* 38.3±0.1˚C, at baseline *versus* the end of PA, respectively; mean±SEM). In the arterial blood, PA resulted in severe hypoxia (P_aO_2: 65±4 *vs* 23±1*mmHg, *p<0.05) as well as acidosis (pH_a: 7.53 ±0.03 *vs* 6.79±0.02*) that is consistent with the observed hypercapnia (P_aCO_2: 37±3 *vs* 160 ±6*mmHg) and lactacidemia (1.6±0.3 *vs* 10.3±0.7*mmol/L). Meanwhile, pH_{brain} decreased progressively from 7.21±0.03 to 5.94±0.11*. Reventilation restored pH_a, blood gases and metabolites within 4 hours except for P_aCO_2 that remained slightly elevated. pH_{brain} returned to 7.0 in 29.4±5.5 min and then recovered to its baseline level without showing secondary alterations during the 24 h observation period. Neuropathological assessment also confirmed neuronal injury. In conclusion, in spite of the severe acidosis and alterations in blood gases during experimental PA, pH_{brain} recovered rapidly and notably, there was no post-asphyxia hypocapnia that is commonly observed in many HIE babies. Thus, the neuronal injury in our piglet model is not associated with abnormal pH_{brain} or low P_aCO_2 over the first 24 h after PA.

Funding: JN,GR,VTSZ,VV,VK,FD; 2.0 1.3 2017 1,2.1 NKP 2017 00002; Hungarian Brain Research Program JN,GR,VTSZ,VV,VK,FD; EFOP-3.6.1-16-2016-00014; EU-funded Hungarian grant EFOP JN, GR,VTSZ,VV,VK,FD; GINOP 2.3.2. 15 2016 00034; GINOP The funders had no role in study design, data collection and analysis, decision to publish, or preparation of the manuscript.

Competing interests: The authors have declared that no competing interests exist.

Introduction

Perinatal asphyxia (PA), defined as O_2 deprivation around the time of delivery, is one of the primary causes of neonatal morbidity and mortality worldwide, affecting ~4 million neonates annually [1]. The interruption of the placental or pulmonary gas exchange induces immediate metabolic changes (hypoxemia, hypercapnia and mixed acidosis) that trigger cardiovascular responses in favour of maintaining O_2 delivery to the myocardium and the brain (i.e. centralized circulation). When these compensatory mechanisms are exhausted, critical tissue hypoxia/ischemia will occur, and the subsequent metabolic crisis will lead to hypoxic-ischemic encephalopathy (HIE) in the survivors [2].

Despite the partial efficacy of therapeutic hypothermia to mitigate the adverse outcome of PA/HIE [3,4], preclinical animal models are still required to study the precise pathophysiology of HIE development, and also to test putative neuroprotective approaches [5]. Similar to the heterogeneity of the aetiology, severity, and duration of the human PA/HIE syndrome, there is also considerable heterogeneity in the preclinical models, both in the species, the prenatal/postnatal age of the animals, the methodology to induce PA/HIE, and the length of the post-asphyxial observation period. These differences do not allow easy comparison and translation of the accumulated data. The newborn pig has long been identified and accepted as a general preclinical model to study the term human neonate [6,7]. There are a number of important similarities between the two species in brain structure, metabolism, development [8,9], and in cerebrovascular physiology [10] that make piglets adequate for translational PA/HIE research. We have recently published a newborn piglet PA/HIE model [11] that produced major hallmarks of human PA/HIE and was able to elicit significant neuronal injury, but did not include manipulations that occur never or very rarely in humans such as bilateral carotid artery occlusion or transient hemorrhagic hypotension.

In the present study, we set out to investigate the course of brain interstitial pH (pH_{brain}) changes during PA and the subacute phase of HIE development in our piglet model. In HIE patients using magnetic resonance spectroscopy (MRS) techniques at < 2 weeks of age, brain intracellular pH (pH_i) levels were found to be rather elevated [12]. This alkalosis persisted for months and correlated with adverse neurological outcome, and the described pH alteration may be one of the features of the so-called secondary energy failure [13,14]. However, changes in pH_i may not truthfully reflect pH_{brain} alterations as transmembrane pH gradients are subject to change during HIE development, and furthermore, intracellular and extracellular pH have different targets via which they may change brain activity and energy consumption [15]. There are very limited data on pH_{brain} changes elicited by PA/HIE from piglets [16], and these studies did not follow the course of pH_{brain} beyond 4 hours after the completion of the hypoxic-ischemic stress. We now report quantitative cerebrocortical pH_{brain} data in our well-characterized piglet PA/HIE model both during the PA and the first 24 hours of HIE development.

Materials and methods

All experimental procedures involving animals were approved in a three-step process. First, the detailed experimental plan was carefully reviewed and approved by the Institutional Animal Care and Use Committee of the University of Szeged (IACUC, in Hungarian: SZTE Munkahelyi Állatjóléti Bizottság). Second, the approval of the IACUC-endorsed experimental plan was requested from the National Ethical Committee on Animal Experiments (in Hungarian: Állatkísérletes Tudományos Etikai Tanács, ÁTET). Third, the National Food Chain Safety and Animal Health Directorate of Csongrád county, Hungary on behalf of the Hungarian Government issued the permit based on the ÁTET recommendation (permit nr: XIV./1414/2015). All animal experiments complied with (1) the guidelines of the Scientific Committee of Animal

Experimentation of the Hungarian Academy of Sciences (updated Law and Regulations on Animal Protection: 40/2013. (II. 14.) Gov. of Hungary), (2) the EU Directive 2010/ 63/EU on animal protection used for scientific research, and (3) with the ARRIVE guidelines. Furthermore, we state that all procedures in the present study were performed on anesthetized animals, also that all animals were anesthetized and treated with analgetics along with intensive monitoring of vital signs throughout the observation period (24 h) without expected or observed mortality. At the end of the experiments the animals were euthanized with an overdose of pentobarbital sodium (300 mg, Release; Wirtschaftsgenossenschaft deutscher Tierärzte eG, Garbsen, Germany).

Newborn ($\leq$1 day old) male Landrace pigs (body weight: 1.5–2.5 kg, n = 16) were obtained from a local company (Pigmark Ltd., Co., H-6728, Rózsamajor út 13., Szeged, Hungary) and delivered to the laboratory on the morning of the experiments. Anaesthesia was induced by sodium thiopental (45 mg/kg ip; Sandoz, Kundl, Austria). Piglets were intubated via tracheotomy and artificially ventilated by a pressure-controlled small animal respirator with warmed, humidified medical air (21% O_2, balance N_2) that could be optionally supplemented with O_2. Respiratory settings (fraction of inspired O_2: 0.21–0.25; respiratory rate (RR): 30–35 1/min, peak inspiratory pressure: 120–135 mmH_2O) were adjusted to maintain blood gas values and O_2 saturation in the physiologic range. The right femoral vein was catheterized under aseptic conditions to maintain anaesthesia/analgesia with a bolus injection of morphine (100 μg/kg; Teva, Petach Tikva, Israel) and midazolam (250 μg/kg; Torrex Pharma, Vienna, Austria), then with continuous infusion of morphine (10 μg/kg/h), midazolam (250 μg/kg/h) and fluids (5% glucose, 0.45% NaCl 3–5 ml/kg/h). A second catheter was placed into the right carotid artery for continuous monitoring of mean arterial blood pressure (MABP) and heart rate (HR). This artery was chosen as ligation of the femoral artery would have resulted in critical ischemia of the hindlimb over the 24h reventilation period (personal observations), in contrast, unilateral carotid artery occlusion has been shown not to affect cerebral blood flow [17]. Rectal temperature was measured continuously and kept in the physiologic range (38.5±0.5˚C) with a servo-controlled water circulation heating-cooling pads (Blanketrol III., Cincinnati Sub-Zero, Cincinnati, Ohio, USA). O_2 saturation, MABP and HR were continuously monitored using a Hewlett-Packard M1094 monitor (Palo Alto, California, USA) and recorded online (Mecif-View, Arlington, Mass., USA). These parameters were recorded at baseline, during PA and and then for 10 minutes at the beginning of each reventilation hour. Arterial blood samples (~300 μl/sample) were analysed with a blood analysis system (EPOC Blood Analysis, Epocal Inc., Ottawa Canada) at baseline, at the end of asphyxia; then at selected intervals up to 20 hours to determine arterial blood pH, gas tensions, base excess, central oxygen saturation, hemoglobin, bicarbonate, glucose and lactate concentrations. Prophylactic antibiotics were given iv.: penicillin (50 mg/kg/12 h, Teva, Petah Tikva, Israel) and gentamicin (2.5 mg/kg/12 h, Sanofi, Paris, France). The urinary bladder was tapped by suprapubic puncture at 12 hour after asphyxia.

pH_{brain} measurements

Measurements were performed inside a self-made Faraday cage with 4 Hz sampling rate. pH-selective microelectrodes (external tip diameter: 50 μm) were obtained from Unisense (Aarhus, Denmark), whereas glass reference microelectrodes (external tip diameter: ~20 μm and filled with 150 mM NaCl; resistance: ~4-5x10^{10} Ohm) were self-made and used with Ag/AgCl wire electrodes. The electrodes were mounted on stereotaxic manipulators for calibration in 3 different warmed (38˚C) buffer solutions (pH: 6.10, 7.10, and 8.10, respectively) before each experiment. The piglet head was fixed in a stereotaxic frame and after retracting the scalp, two

small circular craniotomies (Ø≅5 mm) were made over the fronto-parietal cortex, and the dura mater was gently removed. The tips of the pH and reference microelectrodes were installed ~1–2 mm deep into the exposed cortex, and a Ag/AgCl ground electrode was placed under the scalp. The electrode signals were recorded, digitized and stored either using a custom-built differential electrometer ($>10^{14}$ Ohm input impedance; 16 Hz low pass cut-off), a 16-bit analog-to-digital converter (National Instruments, Austin, TX) and WinEDR software (Dr. John Dempster, University of Strathclyde, UK), or using a Microsensor Multimeter and SensorTrace Logger software (Unisense, Aarhus, Denmark). Evaluation of the recordings was performed offline: by applying linear regression analysis, the signals from the calibration solutions were fitted with a curve and the data were converted to pH values using linear interpolation [15,18,19]. As the technique allows stable continuous pH_{brain} measurements reliably only for 3–4 hours, in different animals, different time windows were chosen to be assessed (baseline, PA and the first 4 hours of reventilation (n = 6), 8^{th}-14^{th} hours (n = 8) and 20^{th}-24^{th} hours (n = 3) of reventilation as presented in the Results).

Induction of asphyxia

After surgery, a 1h recovery period allowed stabilization of the monitored physiological parameters prior to obtaining their baseline values. PA was induced by switching ventilation from medical air to a hypoxic-hypercapnic gas mixture (6% O_2, 20% CO_2, balance N_2) for 20 minutes, simultaneously reducing the RR to 15 1/min and stopping the fluid/glucose administration. Piglets (n = 13) were reventilated (RR: 30 1/min) with medical air for the remaining time of the experiment.

In three additional animals, before inducing PA, the effect of graded normoxic hypercapnia on pH_{brain} was evaluated by 5% step-wise increases in inhaled CO_2 from 0% to 20%, for 7 to 8 min each. After the graded hypercapnia, normocapnia was restored for 30 min. These animals were euthanized with an overdose of pentobarbital sodium (300 mg, Release; Wirtschaftsgenossenschaft deutscher Tierärzte eG, Garbsen, Germany) at 2 hours after PA.

Neuropathology

The objective of the neuropathology examination was to test if the asphyxia-induced neuronal injury was similar to what we reported previously using this PA/HIE model at 24 hours after asphyxia [11]. Accordingly, out of the 13 piglets exposed to PA, only those animals which were maintained for 24 hours (n = 8) were included. The brains of the eight anesthetized animals were perfused with cold (4˚C) physiological saline through the catheterized common carotid arteries 24 hours after the end of asphyxia. The brains were gently removed and immersion-fixed in 4˚C, 4% paraformaldehyde solution before further processing. Paraffin embedded, 4 μm sections were stained with haematoxylin-eosin, and neuropathology was assessed by light microscopic evaluation (Leica Microsystems, Wetzlar, Germany). Damaged neurons were identified using the major hallmarks of dark eosinophilic cytosol, as well as pyknotic or disrupted nuclei. The degree of cerebrocortical neuronal damage in the frontal, parietal, temporal, and occipital cortices was determined adapting a previously published scoring system [11,20]. Briefly, the pattern of neuronal injury (none < scattered < grouped < panlaminar) was determined in 20–20 non-overlapping fields of vision under 20x magnification in each assessed cortical region. Then, scores (0–9) were given to each region based on the frequency (% of 20 examined fields) of the most severe pattern of injury observed. The neuronal damage in the putamen, thalamus and the hippocampal CA1 regions was assessed with cell counting in non-overlapping areas (in 5-5-3 fields of vision respectively; under 200x magnification) as in [11,21]. Neuronal injury in these regions was expressed as the percentage of damaged neurons.

Statistical analysis

Results were analysed offline and plotted using SigmaPlot (v12.0, Systat Software Inc., San Jose, CA, USA) or a MATLAB environment (Mathworks Inc., Natick, MA, USA). Neuropathology scores are expressed as median, 25–75 and 5–95 percentiles. All other data are expressed as mean±SEM. Normality was tested with the Shapiro-Wilk test. The correlation between P_aCO_2 and pH_{brain} data were calculated with MATLAB's polynomial curve fitting. Parametric data were compared with one-way repeated measure of analysis of variance (RM ANOVA) followed by the Student-Newman-Keuls *post hoc* test. Level of significance (p) was set at 0.05.

Results

pH_{brain} changes during PA and HIE development

Induction of PA elicited a reduction in pH_{brain} that continued without levelling off over the 20 min insult, during which pH_{brain} dropped from the baseline value of 7.21±0.03 to 5.94±0.11 by the end of asphyxia (n = 6; Fig 1A). Upon reventilation, pH_{brain} was restored to 7.0 in 29.4±5.5 minutes with subsequent stabilization at a level that was virtually indistinguishable from the original baseline. Thereafter, from 2 h onwards pH_{brain} remained slightly below baseline (on average, by 0.10±0.02 pH units) without showing any marked alterations at any observed time point within the 24-hour follow-up period (Fig 1B).

During the 20 min asphyxia period, O_2 saturation fell to below 30% and HR increased from about 140 1/min to nearly 200 1/min within the first 2 min, after which they showed no major changes, whereas the response in MABP was biphasic with a transient rise to about 90 mmHg followed by a slower decrease to below baseline (Fig 2). A rapid recovery of O_2 saturation to above 80% was seen during the first 2–3 min of reventilation, paralleled by transient increases in HR and MABP to above 240 1/min and 80 mmHg, respectively, after which the signals gradually recovered towards their normal values.

Longer-term monitoring of the physiological parameters reflected well the expected effects of PA and reventilation. Blood hemoglobin concentration (baseline: 8.0±0.3 g/dl; time course not illustrated), core body temperature (controlled by heating, see Methods), O_2 saturation, MABP and HR were within the normal range at baseline before PA and the values were not significantly different from baseline throughout the survival (Fig 3A–3D). In addition to the pulsoxymetry data, arterial blood gas analysis at the end of PA also confirmed the development of central haemoglobin desaturation (from 94±4 to 13±4%) along with severe acidosis, hypoxia and hypercapnia (Fig 3E–3H). Indeed, the fall in the arterial blood pH (pH_a) from 7.53±0.03 to 6.79±0.02 was substantial and paralleled by a rise in P_aCO_2 to 160±6 mmHg, however, pH_a remained more than 0.8 pH unit higher than pH_{brain}. Blood glucose and lactate levels were also profoundly raised (Fig 3I and 3J) [22], indicating the metabolic response to PA. The large drop in base excess by 17.4±1.5 mmol/L and reduction in bicarbonate concentration (Fig 3K and 3L) together with the low pH_a (6.79) at the end of PA indicate that asphyxia developed much beyond the key clinical criteria of severe BA in human neonates (pH $<$7.0 and base deficit $\geq$12 to 16 mmol/L [3,4]). Reventilation quickly restored normoxia in arterial blood, but P_aCO_2 levels remained slightly elevated, although the change was statistically significant only at 4 hours. Base excess was already normalized by this time point, and pH_a returned to 7.39 ±0.02, normal for piglets [23]. In a similar fashion, blood glucose and lactate levels also returned to baseline by 4 hours, although both were still significantly elevated at 1 hour after PA.

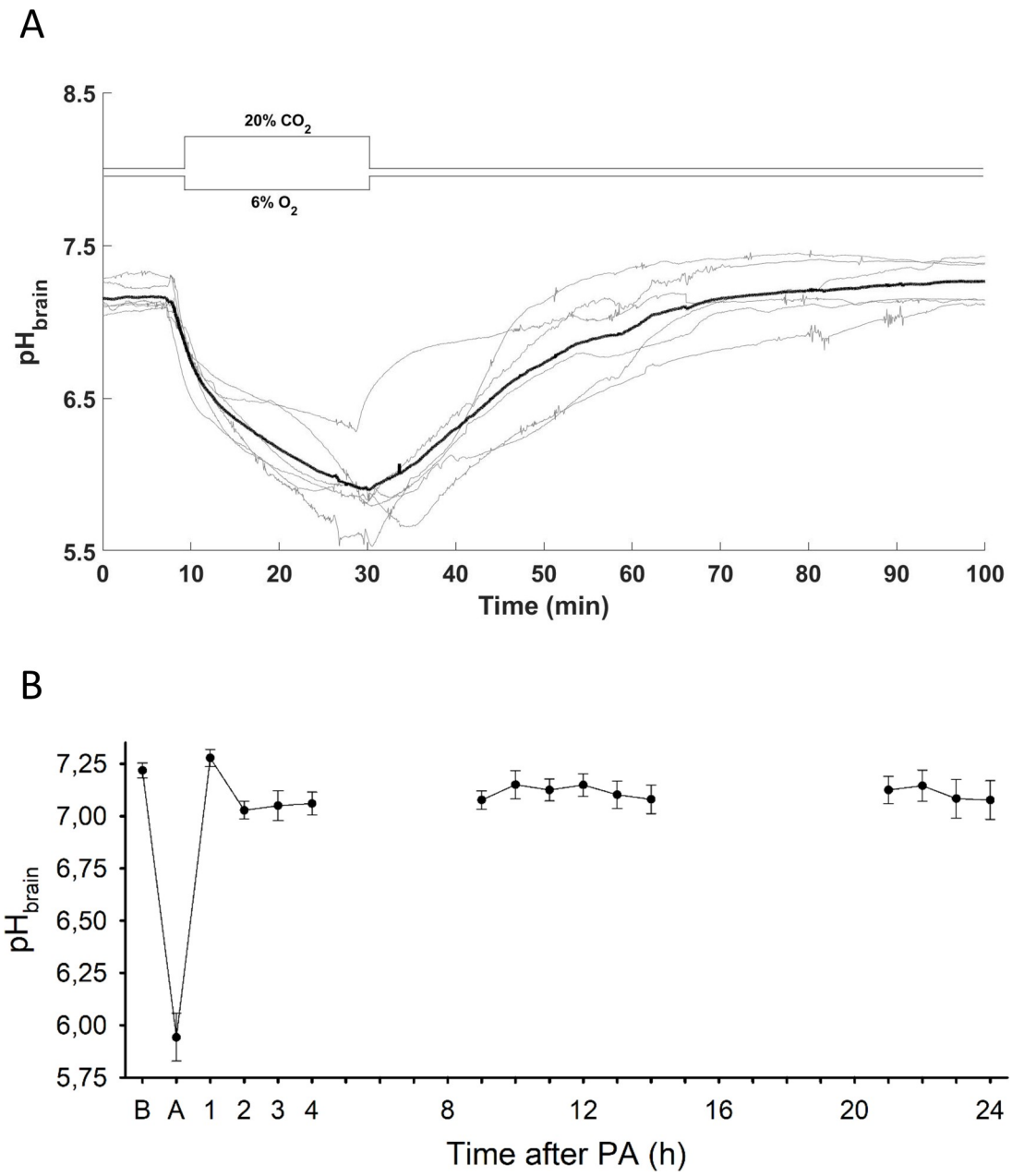

Fig 1. pH_{brain} changes during PA and the reventilation period. (A) pH_{brain} changes (grey lines–individual tracings, bold black line–mean) are plotted 10 min prior the onset asphyxia, during asphyxia, and the first hour of reventilation. pH_{brain} fell progressively during asphyxia showing severe cerebrocortical acidosis, by the end of the insult the pH drop exceeded 1.0 pH unit virtually in all asphyxiated animals. Reventilation quickly restored pH_{brain} to baseline levels. (B) pH_{brain} alterations upon PA and over the 24-hour period after PA: after recovery from the PA-induced severe acidosis, no further significant pH_{brain} alterations were detected at the selected time intervals (n = 6 at PA and between 1–4 hours; n = 8 between 8–14 hours and n = 3 between 20–24 hours; respectively). B: baseline, A: at the end of 20 minute PA. Panel B data points are presented as mean±SEM. *$p<0.05$ *vs.* baseline.

https://doi.org/10.1371/journal.pone.0233851.g001

Neuropathology analysis confirmed the development of HIE by revealing medium/severe neuronal damage in all examined neocortical regions (Fig 4A and 4C), and also in the hippocampal CA1 region, the thalamus and the putamen (Fig 4B). These findings are in accordance with previously reported neuronal injury using the same PA stress [11].

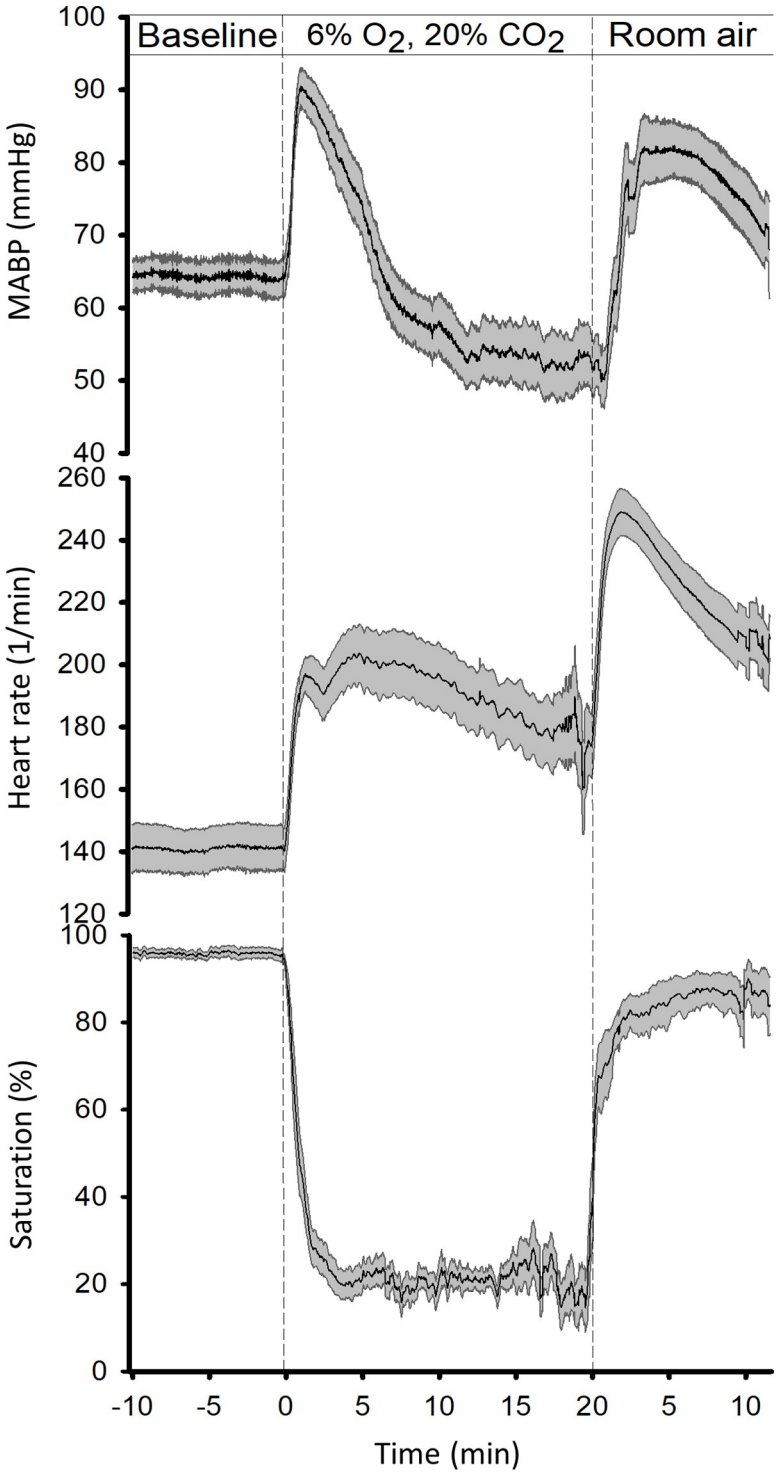

Fig 2. Hemodynamic and oxygenation changes during PA. In all panels, solid lines indicate the mean and the grey shaded area the SEM. (n = 13). After obtaining baselines, PA was initiated resulting first in the transient elevation of mean arterial blood pressure (MABP, top panel) and heart rate (HR, middle panel) accompanying the rapid fall in blood oxygen saturation (pulsoxymetry, bottom panel). While blood oxygen saturation remained ~20% throughout the asphyxia, after the initial peak, MABP fell continuously below baseline, whereas the drop in HR was more moderate and HR remained elevated. Reventilation with air quickly restored oxygen saturation and induced a second transient elevation in both MABP and HR.

https://doi.org/10.1371/journal.pone.0233851.g002

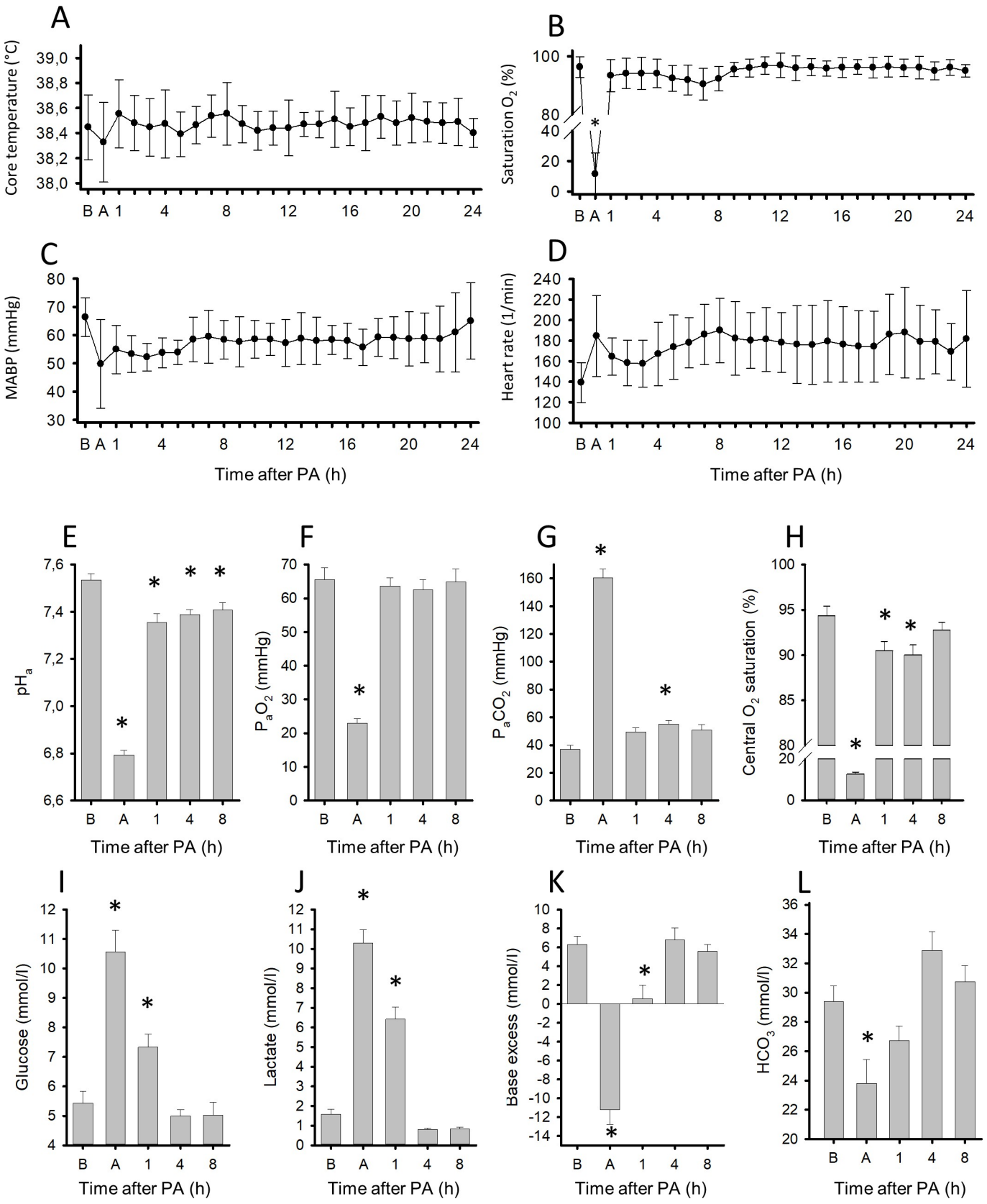
A
Core temperature (°C)
39,0
38,8
38,6
38,4
38,2
38,0
B A 1 4 8 12 16 20 24
B
Saturation O2 (%)
100
80
40
20
0
*
B A 1 4 8 12 16 20 24
C
MABP (mmHg)
80
70
60
50
40
30
B A 1 4 8 12 16 20 24
Time after PA (h)
D
Heart rate (1/min)
240
220
200
180
160
140
120
100
B A 1 4 8 12 16 20 24
Time after PA (h)
E
pHa
7,6
7,4
7,2
7,0
6,8
6,6
B A 1 4 8
Time after PA (h)
F
PaO2 (mmHg)
70
60
50
40
30
20
10
0
B A 1 4 8
Time after PA (h)
G
PaCO2 (mmHg)
160
140
120
100
80
60
40
20
0
B A 1 4 8
Time after PA (h)
H
Central O2 saturation (%)
100
95
90
85
80
20
0
B A 1 4 8
Time after PA (h)
I
Glucose (mmol/l)
12
11
10
9
8
7
6
5
4
B A 1 4 8
Time after PA (h)
J
Lactate (mmol/l)
12
11
10
9
8
7
6
5
4
3
2
1
0
B A 1 4 8
Time after PA (h)
K
Base excess (mmol/l)
10
8
6
4
2
0
-2
-4
-6
-8
-10
-12
-14
B A 1 4 8
Time after PA (h)
L
HCO3 (mmol/l)
36
34
32
30
28
26
24
22
20
B A 1 4 8
Time after PA (h)

Fig 3. Physiological parameters and blood chemistry changes during PA and the subsequent 24h reventilation period. Core temperature of the animals (n = 13) was maintained in the physiologic range (38.5±0.5˚C) during the whole experiment (A). Blood oxygen saturation by pulsoxymetry (B) and mean arterial blood pressure (MABP, (C)) returned to baseline levels soon after asphyxia, however, the heart rate remained moderately elevated (D). Arterial blood gas analysis revealed that asphyxia resulted in severe acidosis (E), hypoxemia (F), hypercapnia (G), and central (arterial blood) desaturation (H). Plasma glucose (I) and lactate levels (J) were markedly elevated along with large drops in base excess (K) and significant reductions in blood bicarbonate concentrations (L). Reventilation restored most of the deranged parameters by 4 hours, and they were not significantly different from baseline levels afterwards, except for pH that was restored to the normal values [23] and not to the slightly alkalotic baseline. B: baseline, A: at the end of 20 minute PA. Bars and whiskers represent mean ±SEM, $^{*}p<0.05$ *vs*. baseline values.

https://doi.org/10.1371/journal.pone.0233851.g003

pH_{brain} changes during graded normoxic hypercapnia

These experiments were performed to evaluate the contribution of the respiratory component to the pH_{brain} changes recorded during PA. Step-wise, 5% increases in inhaled CO_2 (Fig 5A) resulted in proportional step-wise reductions in pH_{brain} (Fig 5B and 5C). Arterial blood gas

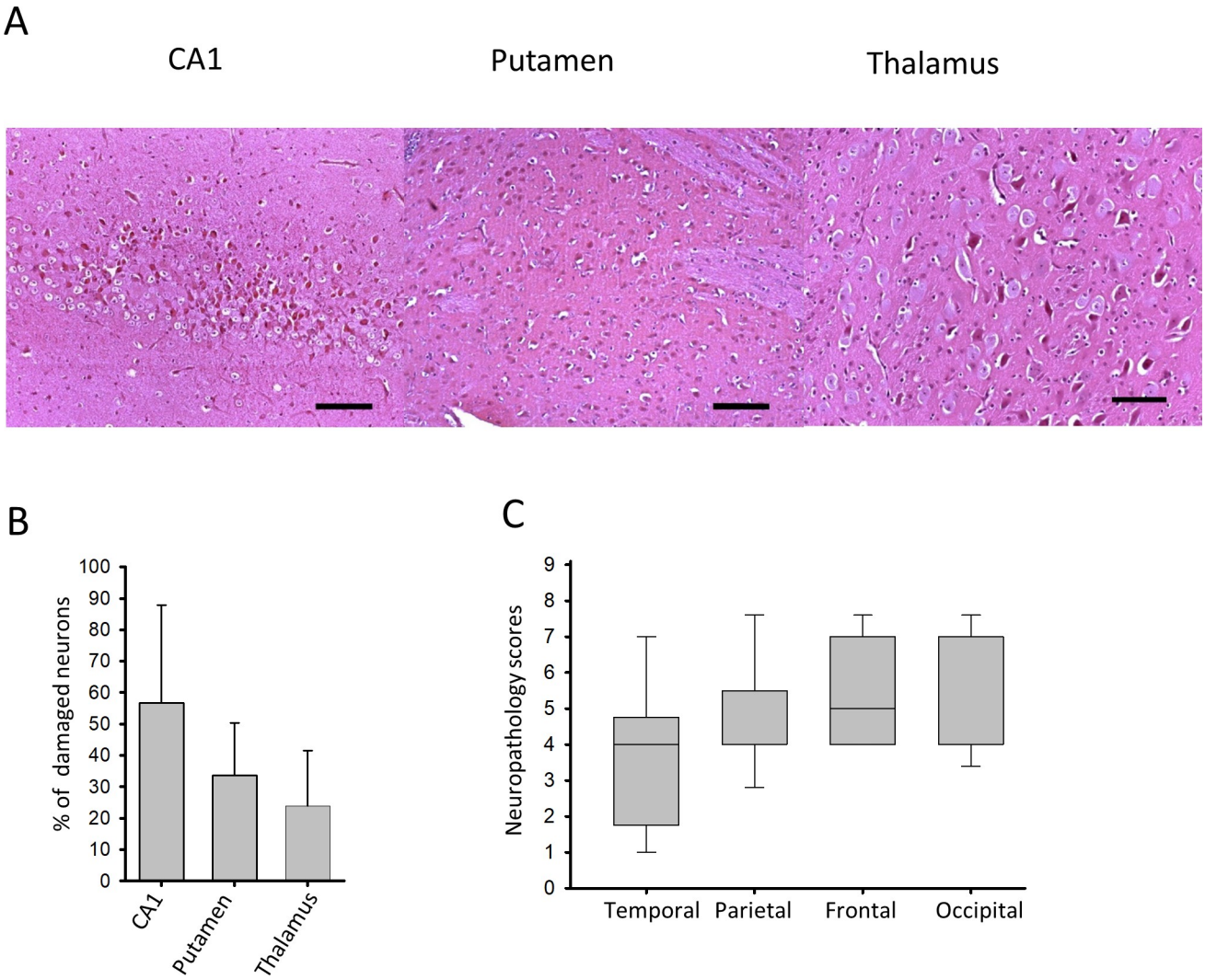

Fig 4. Neuronal injury evaluated at 24 hours after PA. (A) Representative photomicrographs showing injured red neurons at 24-hours of after asphyxia in the CA1 hippocampal region, the putamen, and the thalamus (scale bar: 100μm) (B) Cell counting revealed moderate neuronal damage in these regions (n = 8, mean±SEM). (C) Asphyxia also induced moderate/severe neocortical damage shown by medium/high neuropathology scores (lines, boxes, and whiskers represent the median, the 25^{th}-75^{th}, and the 5^{th}-95^{th} percentiles, respectively).

https://doi.org/10.1371/journal.pone.0233851.g004

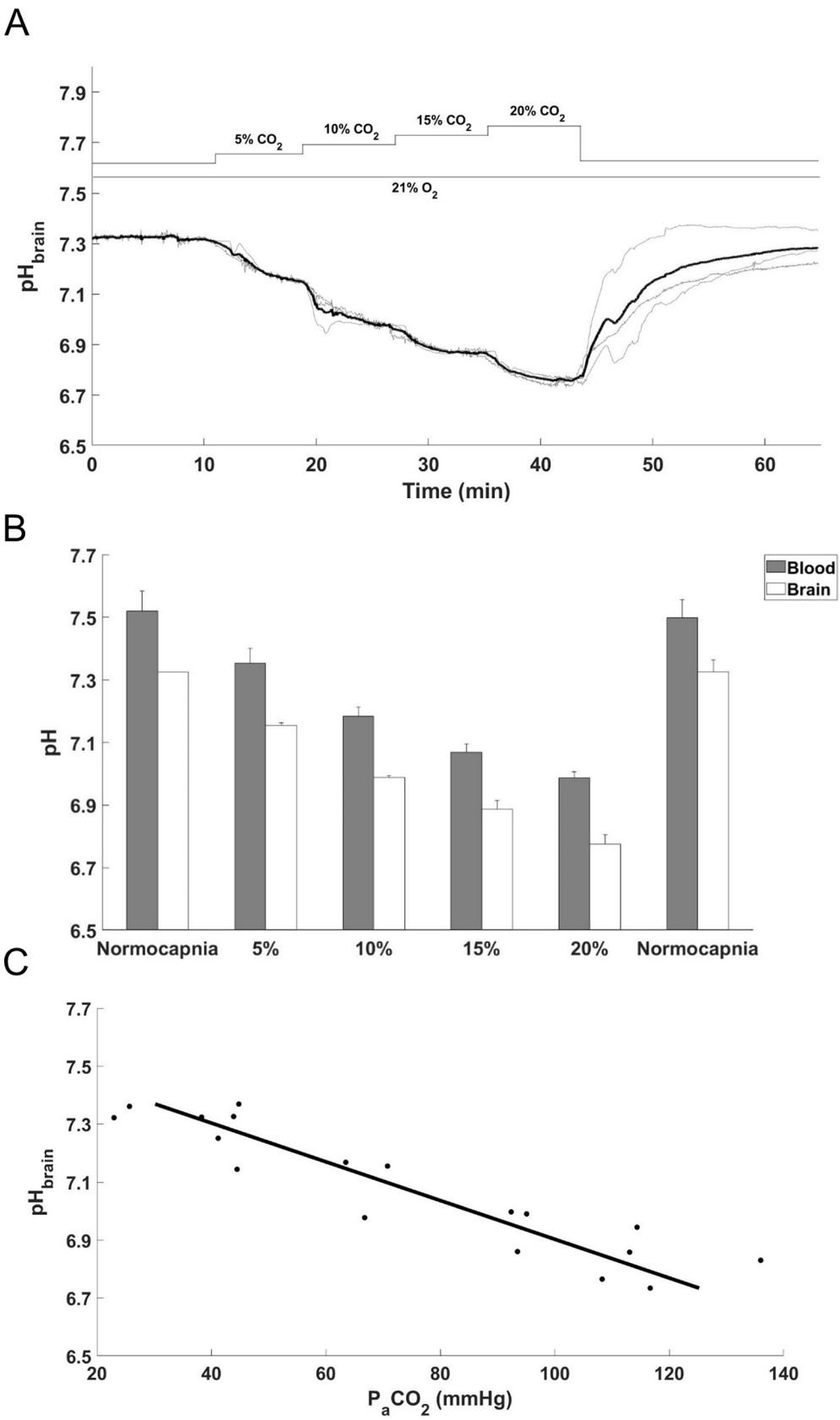
A
7.9
7.7
7.5
7.3
7.1
6.9
6.7
6.5
pH brain
5% CO2
10% CO2
15% CO2
20% CO2
21% O2
0
10
20
30
40
50
60
Time (min)
B
7.7
7.5
7.3
7.1
6.9
6.7
6.5
pH
Blood
Brain
Normocapnia
5%
10%
15%
20%
Normocapnia
C
7.7
7.5
7.3
7.1
6.9
6.7
6.5
pH brain
20
40
60
80
100
120
140
PaCO2 (mmHg)

Fig 5. Cerebral acidosis induced by graded normoxic hypercapnia. (A) pH_{brain} changes during graded normoxic hypercapnia induced by ventilation with 5–20% CO_2 followed by restoration of normocapnia (grey lines–individual tracings, bold black line–mean). (B) Simultaneous reductions in pH_a and pH_{brain} during graded normoxic hypercapnia were in accordance with the elevations in P_aCO_2, the values were (mmHg) 5%: 59.6±7.8, 10%: 84.7±9.0, 15%: 107.0 ±6.7, 20%: 120.3±8.2, (mean±SEM; n = 3). Corresponding P_aO_2 values were (mmHg) 5%: 75.5±12.8, 10%: 78.2±11.3, 15%: 85.5±8.2, 20%: 84.5±9.8, (mean±SEM; n = 3). (C) Linear regression shows close correlation between P_aCO_2 and pH_{brain} ($R^2 = 0.8546$) values obtained during graded hypercapnia (5–20% CO_2).

https://doi.org/10.1371/journal.pone.0233851.g005

analysis revealed similar graded reductions in pH_a, thus the difference between pH_{brain} and pH_a remained unchanged during hypercapnia (Fig 5B). Maximal changes were observed during the inhalation of 20% CO_2 when pH_a dropped from 7.52±0.06 to 6.98±0.02, whereas pH_{brain} from 7.32±0.01 to 6.77±0.02. The pH_{brain} and pH_a changes were fully reversed by restoration of normocapnia.

Discussion

In this study we present *in vivo* real-time recorded pH_{brain} values during PA and the subacute phase of HIE in a translational piglet PA/HIE model. The major findings of the present study are the following: (1) our experimental model elicited PA reflecting its major hallmarks and triggered neuronal injury corresponding to moderate/severe HIE revealed by neuropathology; (2) cerebrocortical pH_{brain} dropped drastically in response to PA, the acidosis exceeding one pH unit in the brain compared to the arterial blood; (3) reventilation/reoxygenation allowed the restoration of pH_{brain} to baseline levels, then pH_{brain} remained stable around baseline levels without major shifts over the 24h observation period.

Every PA/HIE model using postnatal animals inevitably carries the limitation that PA is induced after and not before/during the cardiorespiratory adaptation to extrauterine life. However, we believe that in our study this disadvantage has been minimized by two factors. First, we used truly newborn piglets, thus their vulnerability to PA was least likely to have considerably changed by postnatal development. Second, we elicited PA that resulted in severe enough arterial pH and blood gas alterations that are known to signal human HIE development. This statement is justified by a clinical study that reported significant differences in the degree of acidosis (pH_a: 6.75±0.18 vs 6.90±0.18) and hypercapnia (P_aCO_2: 141±37 vs P_aCO_2: 94±22 mmHg) between asphyxiated babies presenting vs not presenting with HIE [24]. In our model the corresponding values were pH_a: 6.79±0.02 and P_aCO_2: 160±6 mmHg, closely matching the data from human HIE patient group. Interestingly, virtually identical values from umbilical artery blood samples (pH_a: 6.69±0.04 and P_aCO_2: 156±4 mmHg) were obtained in piglets undergoing spontaneous PA during delivery also indicating the translational value of the piglet as a PA/HIE model species [25]. We have developed and used this PA/HIE protocol to test the putative neuroprotective effect of molecular hydrogen [11]. We report virtually identical neocortical, hippocampal, and subcortical neuronal injury in the present study compared to those in [11]. Based on the similar neuropathology findings, we can assume that the surgical manipulations associated with pH_{brain} measurements did not affect HIE development in this study, lending support to the translational value of the present pH_{brain} findings.

The importance of pH_{brain} determining neurological outcome following hypoxic-ischemic stress has long been acknowledged [26]. However, quantitative data on pH_{brain} changes during/after PA in piglet PA/HIE models are very scarce in the literature [16,27,28]. Bender *et al.* [16] assessed pH_{brain} using a similar technique in 1–3 days old piglets. PA was induced also with a hypoxic-hypercapnic gas mixture (5–8%O_2-7%CO_2) for 30 min. At the end of PA, the measured pH_{brain} was 6.26±0.14, which is about 0.3 pH unit higher than in our study and likely

at least part due to the much lower P_aCO_2 values (61±1 *vs*. 160±6 mmHg [16] *vs* present study, respectively). After PA, the reventilation commenced with 100% O_2 ventilation, in addition, sodium bicarbonate (2 mEq/kg, iv) was infused for rapid correction of arterial pH. Both of these interventions are likely to decrease the translational value of the study by Bender *et al*. [16] as they are not included in current guidelines of neonatal care, and they may have affected the recovery of pH_{brain} that was completed in 90 min. Moreover, there was no significant neuronal injury compared to sham operated animals, except experiments where PA was combined with hemorrhagic hypotension, suggesting that the applied PA as such was not severe enough to elicit HIE. Corbett *et al*. [27] used MRS in 8±3 day old piglets to determine pH_i during and after ischemia but not genuine PA. Incomplete cerebral ischemia was elicited by combining bilateral carotid artery occlusion and hemorrhagic hypotension for 25 min followed by 90 min of reperfusion [28]. Severe acidosis developed during the ischemia that was dependent on blood glucose levels during the stress. Brain pH_i dropped below 5.6 in fed piglets that responded to ischemia with hyperglycemia (9.4-15 mmol/L), whereas in fasted piglets responding with hypoglycaemia (1.4-2.6 mmol/L) the nadir at the end of ischemia was mere $pH_i \cong 6.6$. Upon reperfusion, pH_i was again normalized within the 90 min observation period.

From the above discussed studies it is clear that higher levels of hypercapnia, cerebral blood flow, and blood glucose all promote the development of cerebral acidosis during PA. Increases in P_aCO_2 to 140–160 mmHg observed both in human and piglet PA will alone reduce pH_i to 6.5–6.6 under normoxic conditions [29]. Also in the present study, we provide evidence that under normoxic conditions the inhalation of 20% CO_2 alone (P_aCO_2:120 mmHg) results in a pH_{brain} drop to 6.8. Using linear regression (Fig 4C), we then calculated that the developing hypercapnia (at P_aCO_2: 160 mmHg) alone results in a pH_{brain} drop to 6.50 in our PA model, in full agreement with previous results. Further acidification during PA will be dominantly determined by the increases in the rate of anaerobic glycolysis fuelling the subsequent lactic acid production. The rate of glycolysis is limited by glucose delivery to the hypoxic brain, as its reduction by either reducing cerebral blood flow [16] or blood glucose levels [28] attenuated the development of acidosis. We have previously shown that in our PA model significant cerebral ischemia does not develop [11] as in most animals the drop in MABP during the 20 min PA (Fig 4) does not reach the lower limit of blood flow autoregulation [30]. Admittedly, PA in our model has not been long enough for the development of hypotension and bradycardia commonly seen in severely asphyxiated infants, however, it can nicely represent the PA phase before the cardiovascular adaptation mechanisms are exhausted and likely the most pronounced pH_{brain} alterations occur. In summary, our current study provides new compelling experimental evidence that not only cerebral ischemia but *bona fide* PA combining clinically relevant levels of hypoxia, hypercapnia and hyperglycemia is sufficient to elicit cerebral acidosis that is severe enough ($pH_{brain} < 6.0$) to strongly affect neuronal viability [31]. The developing ≅0.8 pH unit difference between pH_{brain} and pH_a signals a >6-fold H^+ gradient across the blood-brain barrier that is in compliance with previous findings that the blood-brain barrier is mature in newborn pigs and not severely compromised by PA [32].

Alterations in pH_{brain} may play important pathophysiological roles not only during acute PA, but also after reventilation/reoxygenation. Previously, pH_{brain} was reported to be stable in piglets after restoration from PA, but it was not followed up beyond four hours of recovery [16]. In contrast, our current study extended the post-asphyxia observation period to 24 hours. We found no major secondary alterations in pH_{brain} in this piglet PA/HIE model during the 24-hour period after PA. Our present findings are in compliance with previous pH_i data obtained with MRS in a piglet HIE model using hypoxic-ischemic stress instead of PA [33]. In this study, pH_i remained at baseline levels after restoration from the ischemic stress for 48 hours, furthermore, the development of secondary energy failure was not reflected in pH_i

alterations in this time period. In a human MRS study, pH_i was also reported to be normal (7.13±0.05) in asphyxiated normocapnic newborns during the first day of life [34], in accordance with our present study. Importantly, brain alkalosis developed during the following days, and then persisted for weeks, even months [13,34]. However, we would like to point out that our PA/HIE piglet model represents the subgroup of asphyxiated babies that require intubation and respiratory support, but not those who breathe spontaneously. While the mechanically ventilated babies stay normocapnic, the spontaneously breathing babies often hyperventilate and may develop hypocapnia [24]. This response can reflect a relative hyperventilation, secondary to the induction of hypoxic hypometabolism resulting in reduced CO_2 production [35]. Reduction in P_aCO_2 due to hyperventilation tends to elevate pH_{brain} and this notion is of special interest as hypocapnia has been identified as an independent risk factor for adverse neurological outcome [36,37]. In piglets, moderate hypocapnia was sufficient to elicit a reduction in cerebral perfusion with a simultaneous increase in pH and lactate levels even in the absence of asphyxia [38]. Indeed, our findings indirectly suggest that maintenance of normocapnia/ slight hypercapnia may prevent secondary pH_{brain} alterations. In a recent work aimed to establish a translationally valid small-animal model of birth asphyxia in rats and guinea pigs, higher P_aCO_2 levels during simulated birth asphyxia and gradual restoration of normocapnia afterwards were found to elicit beneficial effects on cerebral metabolic acidosis, oxygen and lactate levels [39]. Clearly, further studies are warranted to explore these effects in the piglet model. Our current study had some additional limitations. We collected pH_{brain} data from the neocortex using only one level of asphyxia, leaving other brain regions and levels of stress unexplored.

Conclusions

Our translational piglet PA/HIE model reproduces all major hallmarks of birth asphyxia and elicits significant neuronal injury without employing carotid artery occlusions and/or hemorrhagic hypotension. In this model, pH_{brain} drops below 6.0, ≅0.8 pH unit lower than pH_a during PA, establishing a pathogenetic role of severe acidosis in neuronal injury. However, secondary pH_{brain} alterations after restoration of baseline levels were not observed during the 24-hour subacute period, perhaps due to the prevention of secondary hypocapnia by controlled mechanical ventilation.

Author Contributions

Conceptualization: János Németh, Viktória Varga, Viktória Kovács, Valéria Tóth-Szűki, Kai Kaila, Juha Voipio, Ferenc Domoki.

Formal analysis: Gábor Remzső, János Németh, Kai Kaila, Juha Voipio, Ferenc Domoki.

Methodology: Gábor Remzső, János Németh, Viktória Varga, Viktória Kovács, Valéria Tóth-Szűki, Kai Kaila, Juha Voipio, Ferenc Domoki.

Supervision: János Németh, Viktória Varga, Viktória Kovács, Valéria Tóth-Szűki, Kai Kaila, Juha Voipio, Ferenc Domoki.

Validation: Kai Kaila, Juha Voipio, Ferenc Domoki.

Visualization: Gábor Remzső.

Writing – original draft: Gábor Remzső.

Writing – review & editing: Kai Kaila, Juha Voipio, Ferenc Domoki.

References

1. Lawn JE, Manandhar A, Haws RA, Darmstadt GL. Reducing one million child deaths from birth asphyxia—A survey of health systems gaps and priorities. Heal Res Policy Syst. 2007; 5: 1–10. https://doi.org/10.1186/1478-4505-5-4 PMID: 17506872
2. Volpe JJ. Neonatal encephalopathy: An inadequate term for hypoxic-ischemic encephalopathy. Ann Neurol. 2012; 72: 156–166. https://doi.org/10.1002/ana.23647 PMID: 22926849
3. Azzopardi D V., Strohm B, Edwards AD, Dyet L, Halliday HL, Juszczak E, et al. Moderate hypothermia to treat perinatal asphyxial encephalopathy. N Engl J Med. 2009; 361: 1349–1358. https://doi.org/10.1056/NEJMoa0900854 PMID: 19797281
4. Thoresen M. Who should we cool after perinatal asphyxia? Semin Fetal Neonatal Med. 2015; 20: 66–71. https://doi.org/10.1016/j.siny.2015.01.002 PMID: 25667126
5. Yager JY, Ashwal S. Animal Models of Perinatal Hypoxic-Ischemic Brain Damage. Pediatr Neurol. 2009; 40: 156–167. https://doi.org/10.1016/j.pediatrneurol.2008.10.025 PMID: 19218028
6. Bustad LK, McClellan RO. Swine in Biomedical Research. Science. 1966; 152: 1526–1530. https://doi.org/10.1126/science.152.3728.1526 PMID: 17788035
7. Book SA, Bustad LK. The Fetal and Neonatal Pig in Biomedical Research. Am J Anim Sci. 1974; 38: 997–1002.
8. Conrad MS, Johnson RW. The Domestic Piglet: An Important Model for Investigating the Neurodevelopmental Consequences of Early Life Insults. Annu Rev Anim Biosci. 2015; 3: 245–264. https://doi.org/10.1146/annurev-animal-022114-111049 PMID: 25387115
9. Dobbing J, Sands J. Comparative aspects of the brain growth spurt. Early Hum Dev. 1979; 311: 79–83. https://doi.org/10.1016/0378-3782(79)90022-7
10. Busija DW. Cerebral Circulation of the Fetus and Newborn. In: Bevan RD, Bevan JA, editors. The Human Brain Circulation. Humana Press; 1994. pp. 259–269.
11. Nemeth J, Toth-Szuki V, Varga V, Kovacs V, Remzso G, Domoki F. Molecular hydrogen affords neuroprotection in a translational piglet model of hypoxic-ischemic encephalopathy. J Physiol Pharmacol. 2016; 67: 677–689.
12. Azzopardi D, Wyatt JS, Cady EB, Delpy DT, Baudin J, Stewart AL, et al. Prognosis of Newborn Infants with Hypoxic-Ischemic Brain Injury Assessed by Phosphorus Magnetic Resonance Spectroscopy. Pediatr Res. 1989; 25: 445–451. https://doi.org/10.1203/00006450-198905000-00004 PMID: 2717259
13. Robertson NJ, Cox IJ, Cowan FM, Counsell SJ, Azzopardi D, Edwards AD. Cerebral Intracellular Lactic Alkalosis Persisting Months after Neonatal Encephalopathy Measured by Magnetic Resonance Spectroscopy. Pediatr Res. 1999; 46: 287–296.
14. Robertson NJ, Cowan FM, Cox IJ, Edwards AD. Brain alkaline intracellular pH after neonatal encephalopathy. Ann Neurol. 2002; 52: 732–742. https://doi.org/10.1002/ana.10365 PMID: 12447926
15. Helmy MM, Tolner EA, Vanhatalo S, Voipio J, Kaila K. Brain alkalosis causes birth asphyxia seizures, suggesting therapeutic strategy. Ann Neurol. 2011; 69: 493–500. https://doi.org/10.1002/ana.22223 PMID: 21337602
16. Bender TM, Johnston JA, Manepalli AN, Mink RB. Association between brain tissue pH and brain injury during asphyxia in piglets. Resuscitation. 2003; 59: 243–254. https://doi.org/10.1016/S0300-9572(03)00207-7
17. Laptook AR, Stonestreet BS, Oh W. The effect of carotid artery ligation on brain blood flow in newborn piglets. Brain Res. 1983; 276: 51–54. https://doi.org/10.1016/0006-8993(83)90547-4
18. Voipio J, Kaila K. Interstitial PCO2 and pH in rat hippocampal slices measured by means of a novel fast CO2/H+-sensitive microelectrode based on a PVC-gelled membrane. Pflügers Arch Eur J Physiol. 1993; 423: 193–201. https://doi.org/10.1007/BF00374394 PMID: 8391679
19. Voipio J, Pasternack M, MacLeod K. Ion-sensitive microelectrodes. 2nd editio. Microelectrode Techniques–The Plymouth Workshop Handbook. 2nd editio. Cambridge: The Company of Biologists Limited; 1994. pp. 275–316.
20. Foster KA, Colditz PB, Lingwood BE, Burke C, Dunster KR, Roberts MS. An improved survival model of hypoxia/ischaemia in the piglet suitable for neuroprotection studies. Brain Res. 2001; 919: 122–131. https://doi.org/10.1016/S0006-8993(01)03011-6
21. Oláh O, Tóth-Szki V, Temesvári P, Bari F, Domoki F. Delayed neurovascular dysfunction is alleviated by hydrogen in asphyxiated newborn pigs. Neonatology. 2013; 104: 79–86. https://doi.org/10.1159/000348445 PMID: 23859876
22. Randall GCB. Studies on the effect of acute asphyxia on the fetal pig in utero. Biol Neonate. 1979; 36: 63–69. https://doi.org/10.1159/000241208 PMID: 38863

23. Randall GCB. pH Values and Blood-Gas Tensions in the Normal Piglet during the First 48 Hours of Life. Biol Neonate. 1972; 20: 68–73. https://doi.org/10.1159/000240447 PMID: 5063638

24. Engle WD, Laptook AR, Perlman JM. Acute changes in arterial carbon dioxide tension and acid-base status and early neurologic characteristics in term infants following perinatal asphyxia. Resuscitation. 1999; 42: 11–17.

25. Randall GC. The relationship of arterial blood pH and pCO2 to the viability of the newborn piglet. Can J Comp Med. 1971; 35: 141–146.

26. Siesjö BK. Acid-Base Homeostasis in the Brain: Physiology, Chemistry, and Neurochemical Pathology. Prog Brain Res. 1985; 63: 121–154. https://doi.org/10.1016/S0079-6123(08)61980-9

27. Corbett RJT, Laptook AR, Nunnally RL, Hassan A, Jackson J. Intracellular pH, Lactate, and Energy Metabolism in Neonatal Brain During Partial Ischemia Measured In Vivo by 31P and 1H Nuclear Magnetic Resonance Spectroscopy. J Neurochem. 1988; 51: 1501–1509. https://doi.org/10.1111/j.1471-4159.1988.tb01118.x PMID: 3171590

28. Laptook AR, Corbett RJT, Nunnally RL. Effect of Plasma Glucose Concentration on Cerebral Metabolism During Partial Ischemia in Neonatal Piglets. Stroke. 1990; 21: 435–440. https://doi.org/10.1159/000448585

29. Corbett RJT, Laptook AR, Hassan A, Nunnally RL. Quantitation of acidosis in neonatal brain tissue using the 31P NMR resonance peak of phosphoethanolamine. Magn Reson Med. 1988; 6: 99–106. https://doi.org/10.1002/mrm.1910060112 PMID: 3127649

30. Laptook A, Stonestreet BS, Oh W. Autoregulation of brain blood flow in the newborn piglet: Regional differences in flow reduction during hypotension. Early Hum Dev. 1982; 6: 99–107. https://doi.org/10.1016/0378-3782(82)90063-9

31. Li P-A, Shamloo M, Katsura K, Smith M-L, Siesjö BK. Critical values for plasma glucose in aggravating ischaemic brain damage: correlation to extracellular pH. Neurobiol Dis. 1995; 2: 97–108. https://doi.org/10.1006/nbdi.1995.0010 PMID: 8980013

32. Stonestreet BS, Burgess GH, Cserr HF. Blood-brain barrier integrity and brain water and electrolytes during hypoxia/hypercapnia and hypotension in newborn piglets. Brain Res. 1992; 590: 263–270. https://doi.org/10.1016/0006-8993(92)91104-M

33. Lorek A, Takei Y, Cady EB, Wyatt JS, Penrice J, Edwards AD, et al. Delayed ("Secondary") Cerebral Energy Failure after Acute Hypoxia-Ischemia in the Newborn Piglet: Continuous 48-Hour Studies by Phosphorus Magnetic Resonance Spectroscopy. Pediatr Res. 1994; 36: 699–706. https://doi.org/10.1203/00006450-199412000-00003 PMID: 7898977

34. Hope PL, Cady EB, Tofts PS, Hamilton PA, Costello AMDL, Delpy DT, et al. Cerebral Energy Metabolism Studied With Phosphorus NMR Spectroscopy In Normal And Birth-Asphyxiated Infants. Lancet. 1984; 324: 366–370.

35. Mortola JP. How newborn mammals cope with hypoxia. Respiration Physiology. 1999. pp. 95–103. https://doi.org/10.1016/S0034-5687(99)00038-9

36. Lingappan K, Kaiser JR, Srinivasan C, Gunn AJ. Relationship between PCO2 and unfavorable outcome in infants with moderate-to-severe hypoxic ischemic encephalopathy. Pediatr Res. 2016; 80: 204–208. https://doi.org/10.1038/pr.2016.62 PMID: 27049290

37. Pappas A, Shankaran S, Laptook AR, Langer JC, Bara R, Ehrenkranz RA, et al. Hypocarbia and adverse outcome in neonatal hypoxic-ischemic encephalopathy. J Pediatr. 2011; 158: 752–758. https://doi.org/10.1016/j.jpeds.2010.10.019 PMID: 21146184

38. Ringer SK, Clausen NG, Spielmann N, Weiss M. Effects of moderate and severe hypocapnia on intracerebral perfusion and brain tissue oxygenation in piglets. Paediatr Anaesth. 2019; 29: 1114–1121. https://doi.org/10.1111/pan.13736 PMID: 31472089

39. Pospelov AS, Puskarjov M, Kaila K, Voipio J. Endogenous brain-sparing responses in brain pH and P O2 in a rodent model of birth asphyxia. Acta Physiol (Oxf). 2020; e13467. https://doi.org/10.1111/apha.13467 PMID: 32174009

II.

SCIENTIFIC REPORTS
nature research

OPEN

NMDA attenuates the neurovascular response to hypercapnia in the neonatal cerebral cortex

Gábor Remzső, János Németh, Valéria Tóth-Szűki, Viktória Varga, Viktória Kovács & Ferenc Domoki*

Cortical spreading depolarization (SD) involves activation of NMDA receptors and elicit neurovascular unit dysfunction. NMDA cannot trigger SD in newborns, thus its effect on neurovascular function is not confounded by other aspects of SD. The present study investigated if NMDA affected hypercapnia-induced microvascular and electrophysiological responses in the cerebral cortex of newborn pigs. Anesthetized piglets were fitted with cranial windows over the parietal cortex to study hemodynamic and electrophysiological responses to graded hypercapnia before/after topically applied NMDA assessed with laser-speckle contrast imaging and recording of local field potentials (LFP)/neuronal firing, respectively. NMDA increased cortical blood flow (CoBF), suppressed LFP power in most frequency bands but evoked a 2.5 Hz δ oscillation. The CoBF response to hypercapnia was abolished after NMDA and the hypercapnia-induced biphasic changes in δ and θ LFP power were also altered. MK-801 prevented NMDA-induced increases in CoBF and the attenuation of microvascular reactivity to hypercapnia. The neuronal nitric oxide synthase (nNOS) inhibitor (N-(4 S)-4-amino-5-[aminoethyl] aminopentyl-N′-nitroguanidin) also significantly preserved the CoBF response to hypercapnia after NMDA, although it didn't reduce NMDA-induced increases in CoBF. In conclusion, excess activation of NMDA receptors alone can elicit SD-like neurovascular unit dysfunction involving nNOS activity.

Spreading depolarizations (SDs) are repeatable, slowly (3–4 mm/min) propagating waves of almost complete neuronal and glial depolarization at the wavefront with simultaneous depression of cortical electrical activity (cortical spreading depression). These electrophysiological changes are accompanied by transient elevations in interstitial H^+, K^+, glutamate levels and by a characteristic triphasic, in intact brains dominantly hyperemic microvascular response, the latter presumably helping to meet the increased metabolic demand necessary for the recovery of transmembrane ion gradients. In various neurological disorders, such as ischemic stroke or traumatic brain injury, SDs have been shown to play critical roles in the development of cerebrocortical lesions[1], therefore it is of great interest to identify the mechanisms by which SDs may contribute directly or indirectly to cortical neuronal injury.

One of the important injury mechanisms of SDs can be the induction of neurovascular unit dysfunction. SDs have been long reported to alter cortical microvascular reactivity, for instance, a single SD can abolish the normal microvascular reactivity to hypercapnia in virtually all species studied including cats[2], rats[3] and mice[4]. However, the mechanism of SD-induced microvascular dysfunction remains unclear.

N-methyl-D-aspartate (NMDA), the prototypical selective activator of the NMDA subtype of ionotropic glutamate receptors, has been shown to trigger SDs when applied topically onto the surface of the cerebral cortex in adult mice[5] and rats[6]. In addition, functional NMDA receptors are clearly required for triggering SDs with other stimuli and also for SD propagation[7,8]. Interestingly, SDs cannot be elicited in neonates, despite expressing functional NMDA receptors. In the newborn pig, local application of NMDA has been shown to dilate pial arterioles and to increase cortical blood flow in a dose-dependent fashion without confounding SDs[6].

In the present study, we set out to investigate the effect of topical cortical application of NMDA on the cerebrocortical microvascular response to graded hypercapnia in a neonatal piglet model using laser-speckle

Department of Physiology, Faculty of Medicine, University of Szeged, Szeged, Hungary. *email: domoki.ferenc@med.u-szeged.hu

contrast imaging (LSCI). Using a neonatal model, we wished to assess only one aspect of SD – the NMDA receptor activation- on neurovascular unit function without the confounding features of an actual SD triggered by NMDA in adult brains. As we found a significant attenuation of CO_2-reactivity after NMDA application similar to those previously observed in adult animal models following SDs, we used the NMDA-receptor inhibitor MK-801 and the selective neuronal nitric oxide synthase (nNOS) inhibitor (N-(4 S)-4-amino-5-[aminoethyl] aminopentyl-N′-nitroguanidin; AAAN) to pharmacologically characterize this effect. Furthermore, we sought to determine and describe for the first time the cortical layer-specific changes in electrical activity triggered by local NMDA application in this neonatal model recorded with multi-channel microelectrodes.

Materials and Methods

Animals and surgery. Newborn (<24 h old) male Landrace piglets (n = 31, body weight: 1.5–2 kg) were obtained from a local company (Pigmark Ltd., Co., Szeged, Hungary). The experimental procedures were approved by the National Ethical Committee on Animal Experiments (ÁTET, I.74–7/2015), and then the necessary permit to obtain the animals was issued by the National Food Chain Safety and Animal Health Directorate of Csongrád county, Hungary (permit nr: XIV./1414/2015). The procedures were performed according to the guidelines of the Scientific Committee of Animal Experimentation of the Hungarian Academy of Sciences (updated Law and Regulations on Animal Protection: 40/2013. (II. 14.) Gov. of Hungary), following the EU Directive 2010/63/EU on the protection of animals used for scientific purposes and reported in compliance with the ARRIVE guidelines.

The animals were restrained and anesthetized with intraperitoneal sodium thiopental injection (45 mg/kg; Sandoz, Kundl, Austria). The animals were placed on a servo-controlled heating pad (Blanketrol III, Cincinnati SUB-zero, Cincinnati, Ohio, USA), keeping their core temperature in the physiological range (38.5 ± 0.5 °C). The piglets were intubated through a tracheostomy then mechanically ventilated with humidified medical air occasionally supplemented with oxygen (FiO_2: 0.21–0.25) with the following ventilation parameters: respiration rate (RR): 30–35/min; peak inspiratory pressure (PIP): 12–14 cmH_2O. A catheter was inserted into the right femoral vein under aseptic conditions and anesthesia/analgesia was switched to intravenous morphine (100 μg/kg bolus then 10 μg/kg/h; Teva, Petach Tikva, Israel) and midazolam (250 μg/kg bolus then 250 μg/kg/h; Torrex Pharma, Vienna, Austria) as used previously[9,10] along with supportive fluid therapy (0.45% NaCl, 5% glucose; 3 ml/kg/h). A second catheter was inserted into the right carotid artery for taking blood samples, monitoring the mean arterial blood pressure (MABP) and heart rate (HR). As shown previously, unilateral carotid artery occlusion does not affect cerebral blood flow (CBF) and preferable to catheterization of the femoral artery causing very severe hindlimb ischemic damage[11]. Blood samples (300 μl) were analyzed for pH, gases, electrolytes and metabolites with an epoc® Blood Analysis System (Epocal Inc., Ottawa, Canada). We monitored the peripheral saturation (SpO_2) using pulse oximetry.

After instrumentation, the heads of the animals were fixed into a stainless steel stereotactic frame (RWD Life Science, Shenzhen, Guangdong Province, China). For the LSCI studies, we implanted a stainless steel closed cranial window (d = 1.8 cm) over the parietal cortex which was sealed with bone wax and cemented with dental acrylic[12]. For the electrophysiology studies, we obtained an open cranial window over the left parietal bone for electrode insertion and we also drilled two holes into the frontal bone positioning the reference and ground electrodes, respectively. The dura mater was carefully removed avoiding the blood vessels. If necessary, the smaller veins were cauterized. The location of the cranial window and the electrode insertion point was determined by stereotactic reference points (window d = 0.8 cm; measured from Bregma: anterior-posterior (AP) axis:-1.2-(−1.4) cm, medial-lateral (ML) axis: 1.1–1.3 cm). The subarachnoidal space was filled with warmed (37 °C) artificial cerebrospinal fluid (aCSF) containing 0.22 g/l KCl, 0.132 g/l $MgCl_2$, 0.221 g/l $CaCl_2$, 7.71 g/l NaCl, 0.402 g/l urea, 0.665 g/l dextrose and 2.066 g/l $NaHCO_3$, and was equilibrated with a gas mixture containing 6.3% O_2, 6.2% CO_2, and 87.5% N_2, respectively. At the end of the experiments the animals were euthanized with an overdose of pentobarbital sodium (300 mg, Release; Wirtschaftsgenossenschaft deutscher Tierärzte eG, Garbsen, Germany).

Experimental protocol. LSCI and electrophysiology studies were performed in separate animals. For the LSCI measurements the animals were divided into 4 groups (Fig. 1). Randomization was performed by coin flip between Group 1 and 2, or 3 and 4, respectively. In each group after obtaining baseline, the microvascular response to graded hypercapnia induced by mechanical ventilation with 5% and 10% CO_2 for 7 min for each concentration was recorded. In Group 1 (n = 6), the graded hypercapnia was repeated after recovery time matching the NMDA-treated groups. In Group 2–4, after the first graded hypercapnia increasing concentrations (0.1 and 1 mM) of N-methyl-D-aspartate (NMDA; Sigma Aldrich, St. Louis, MO, US) dissolved in aCSF were applied topically on the cortical surface, each NMDA stimulus lasted for 7 min (Fig. 1). Between and after the NMDA applications, the cranial window was washed with aCSF for 10 min to allow CoBF and the electrical activity to return to baseline. The second graded hypercapnia was elicited 1 h after completion of the NMDA application. In Group 2 (n = 7), the effect of NMDA was studied, in Group 3 (n = 4), the cortex was locally pre-treated with the NMDA receptor antagonist MK-801 (0.1 mM dissolved in aCSF; Research Biochemicals International, Natick, MA, US) and the NMDA was also co-applied with 0.1 mM MK-801. Finally in Group 4 (n = 7), before the start of the LSCI protocol the animals were given a selective neuronal nitric oxide synthase (nNOS) inhibitor (N-(4 S)-4-amino-5-[aminoethyl]aminopentyl-N′-nitroguanidin; AAAN; Santa Cruz Biotechnology, Dallas, TX, US; dissolved in saline, 0.4 mg/kg iv)[13]. In each group, LSCI was recorded for additional 5 min after euthanasia to determine the biological zero.

Electrophysiology studies were performed with the same protocol as in Group 2 (n = 7). We tested if the cerebrocortical response to NMDA markedly differed in the absence of preceding graded hypercapnia in two additional animals, but we did not observe any differences (data not shown).

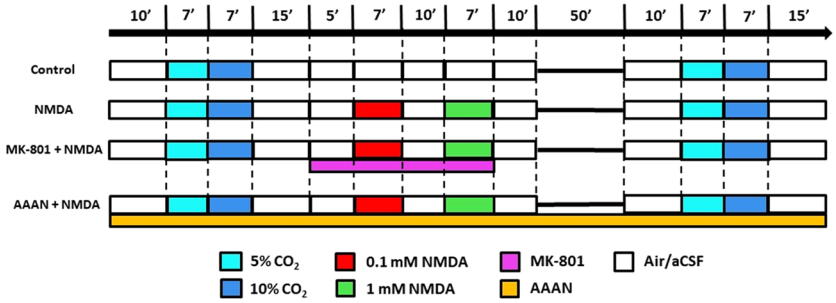

Figure 1. Experimental groups and protocol. The animals fitted with closed cranial windows for laser-speckle contrast imaging and analysis were divided into 4 groups. In the control group, (Group 1, n = 6) graded hypercapnia was induced with 5-10% CO_2 that was repeated after 1 h. In Group 2 (n = 7), increasing concentrations (0.1–1 mM) of NMDA dissolved in artificial cerebrospinal fluid (aCSF) were applied topically to the cortex between the two hypercapnic stimuli. In Group 3 (n = 4), the protocol was the same as in the second, only the NMDA-receptor inhibitor MK-801 (0.1 mM dissolved in aCSF) was pre- and co-applied with NMDA. In Group 4 (n = 7), the protocol was also similar to Group two except that the animals were intravenously treated with the selective neuronal nitric oxide synthase inhibitor N-(4 S)-4-amino-5-[aminoethyl] aminopentyl-N′-nitroguanidin (AAAN; 0.4 mg/kg) before the first graded hypercapnia. An additional group of animals (n = 7) fitted with open cranial windows served for the electrophysiology studies using the same protocol as for the NMDA-treated second group.

LSCI measurements and analysis. The brain was illuminated with near infrared polarized light (λ = 808 nm, 200 mW) with a laser diode (DL-8141-002 SANYO Electric Co., Japan). The images were recorded with a monochrome camera (PL-B741F; PixeLINK® Ottawa, Canada; 1280 × 1024 pixels) which is using a polarizer and a color filter. The raw speckle images were sampled at 1 Hz, 1 ms exposure time with 1 frame/s rate during all the vascular stimuli.

The LSCI analysis was performed offline in LabVIEW (National Instruments Co., Austin, TX, USA). The contrast maps were calculated from the raw speckle images using a 5 × 5 pixel window. In each animal we selected 4 parenchymal region of interests (ROIs; 5 × 5 pixels ~1200 μm^2) over the cortical parenchyma avoiding pial vessels. The τ correlations were calculated using Eq. (1), where K(T) is each ROIs' speckle contrast, β is the coherence factor and T is the exposure time.

$$K(T) = \sqrt{\beta}\left\{\frac{\tau^2}{2T^2}\left[exp\left(\frac{-2T}{\tau}\right) - 1 + \frac{2T}{\tau}\right]\right\}^{\frac{1}{2}} \quad (1)$$

For each image, the calculated 1/τ values were normalized and expressed as percentages of the baseline, and values from all 4 ROIs were averaged in each animal.

Pial arteriolar diameters were determined at selected time points where peak changes in CoBF to the applied stimuli were detected. To obtain better resolution, 30 images were averaged then the Otsu filtering method was applied to reduce noise. In each experiment, four arterioles were selected and the internal diameter of the arterioles were determined using edge detection and Euclidean distance measurement in MATLAB (Mathworks Inc., Natick, US)[14]. The arteriolar diameter data were normalized and expressed as percentages of the baseline, and values from all 4 arterioles were averaged in each animal.

Neurophysiological recordings. Electrophysiological recordings were taken with 16-channel, acute single shank planar silicone electrodes (l = 10 mm, base width = 50 μm) with 177 μm^2 recording sites spaced 100 μm apart (A1x16-10mm-100-177-A16; Neuronexus Technologies. AnnArbor, MI, US, http://neuronexus.com/electrode-array/a1x16-10mm-100-177/). Data acquisition was performed with RHD2000 Evaluation System. The recorded signals were preamplified with a 16-channel headstage/amplifier board (RHD2132 amplifier board, Intan Technologies, Los Angeles, US) under Faraday-cage then the signals were sent through an interface cable to the interface board (RHD2000 USB interface board, Intan Technologies, Los Angeles, US). All recorded data were sampled at 20 kHz, the broad band signals were filtered with a 1-9000 Hz bandpass filter and a notch filter was also applied to eliminate the 50 Hz electrical noise. All data were analyzed off-line in MATLAB environment with implemented toolboxes (Chronux, http://chronux.org/; FMAtoolbox, http://fmatoolbox.sourceforge.net) and custom written scripts.

LFP spectral analysis. The recorded broad band signals (20 kHz) were downsampled to 1250 Hz and filtered with an infinite impulse response (IIR) 4th order Butterworth filter to generate the local field potential (LFP) and to eliminate spiking activity. After LFP generation, we decomposed the signal into the physiological frequency ranges - delta (1–4 Hz), theta (4–8 Hz), alpha (8–13 Hz), beta (13–30 Hz) – to calculate the power spectral density (PSD). We applied a 30 s window on the signals which moves onward with 1 s steps calculating the Fast Fourier Transform (FFT) of the signals using a Gaussian window. The PSDs were determined for each channels,

	1st stimulus			2nd stimulus		
	Baseline	5% CO_2	10% CO_2	Baseline	5% CO_2	10% CO_2
pCO_2 (mmHg)	39 ± 6	63 ± 11	91 ± 14	42 ± 5	69 ± 7	99 ± 9
pO_2 (mmHg)	69 ± 9	79 ± 21	82 ± 26	67 ± 12	77 ± 25	82 ± 29
pH	7.51 ± 0.06	7.32 ± 0.07	7.17 ± 0.05	7.48 ± 0.05	7.29 ± 0.06	7.15 ± 0.05
HCO_3^- (mmol/l)	30.5 ± 3.7	32.2 ± 3.9	33.0 ± 3.9	31.1 ± 3.0	33.2 ± 2.8	34.4 ± 3.2
BE(b) (mmol/l)	6.9 ± 3.6	5.1 ± 3.8	3.3 ± 3.6	7.0 ± 3.1	5.6 ± 3.1	4.0 ± 3.5
SpO_2	97 ± 2	95 ± 4	94 ± 3	96 ± 3	94 ± 4	94 ± 4
MABP (mmHg)	62 ± 9	70 ± 10	75 ± 14	55 ± 8	67 ± 11	74 ± 14
HR (bpm)	139 ± 18	147 ± 28	161 ± 29	140 ± 17	149 ± 25	168 ± 29

Table 1. Arterial pCO_2, pO_2, pH, HCO_3^-, base excess BE(b), oxygen saturation (SpO_2), mean arterial blood pressure (MABP) and heart rate (HR) values during the 1st and 2nd stimulation with graded hypercapnia (mean ± SD) (n = 31).

frequency bands, conditions and animals. The calculated PSDs were summed for each frequency bands. All the PSDs were averaged and normalized to the baseline activity.

Addressing the 'inverse problem' of LFP, we computed the second spatial derivative, the current source density (CSD) to reveal how the different sources contribute to the mixed signal. We explored and segmented the data into 2.5 s epochs using Neuroscope[15]. We used the standard CSD method for the computation. All CSDs were calculated with the FMAtoolbox's built-in function and the spectra were averaged.

Spike sorting and unit classification. Spike sorting was done with the Klusta package (https://github.com/kwikteam/klusta) that performs automatic spike sorting and clustering. Single units were detected from digitally 1–5000 Hz high-pass filtered LFP using a threshold crossing-based algorithm (Spikedetekt2; https://github.com/klusta-team/spikedetekt2). The detected spikes were automatically clustered using masked Expectation-Maximization (EM) algorithm for Gaussian mixtures which is implemented into KlustaKwik2[16] (https://github.com/klusta-team/klustakwik2/). Clustering was followed by manual adjustment of the clusters using phy KwikGUI software (https://github.com/kwikteam/phy) which is an improved version of KlustaViewa[17]. The noise, as well as multi-unit and poor quality clusters were discarded from the analysis. The putative interneurons and pyramidal cells were identified by their waveform characteristics and autocorrelograms (ACG)[18–20] with the further examination of their cross-correlograms (CCG) to reveal the monosynaptic interactions with other single units[19,21].

Statistical analysis. All the LSCI statistical analysis were performed in IBM SPSS Statistics 22, using two-way ANOVA with repeated measures, followed by Tukey's *post hoc* test. All results show mean ± SD, respective to the baseline. $p < 0.05$* was considered as significant.

The electrophysiological statistical analysis was performed with IBM SPSS Statistics 22. We performed one-way ANOVA with repeated measures, followed by Bonferroni *post hoc* test. All results show mean ± SD, respective to the baseline. $p < 0.05$* and $p < 0.01$** were considered as significant. For the Z-score computation we used MATLAB's statistics toolbox. Relative PSD changes were determined as significant above/below $Z \geq \pm 2$* and $Z \geq \pm 4$** with the further examination of the ANOVA results ($p < 0.05$*, $p < 0.01$**).

Results

Effects of graded hypercapnia on physiological parameters. Ventilation with 5–10% CO_2 resulted in graded hypercapnia that was similar in all experimental groups both for LSCI and for electrophysiology experiments (Table 1). Graded elevations in arterial pCO_2 were accompanied by the expected development of marked respiratory acidosis and a slight increase in plasma HCO_3^- levels, however, arterial pO_2, blood oxygen saturation, MABP and HR were all maintained during graded hypercapnia. The stimulus was highly repeatable, repeated ventilation with 5-10% CO_2 resulted in virtually identical changes in blood gases compared to the first application (Table 1).

The cerebrocortical microvascular response to graded hypercapnia and NMDA. LSCI provided two-dimensional maps of cortical perfusion (Fig. 2a–c) that served to determine changes in parenchymal perfusion (Figs. 2d–g, 3a–c) and pial arteriolar diameters (Fig. 3d).

The first exposure to graded hypercapnia resulted in similar, CO_2 concentration-dependent increases in CoBF in all groups (Fig. 2d–g), the peak CoBF values (Fig. 3a), the integrated hyperemic CoBF response (Fig. 3b), and the pial arteriolar diameter changes (Fig. 3d) were all similar.

Topical application of 0.1 mM NMDA resulted in a significant increase in CoBF (peak CoBF was 151 ± 14% of baseline) and pial arteriolar diameters (138 ± 31% of baseline) that peaked within 3–4 min (Figs. 2e, 3a,b,d), the elevated CoBF returned to baseline levels after perfusing the cranial window with aCSF. Repeating the stimulation with 1 mM NMDA resulted only in slightly higher elevations both in the peak (172 ± 23%) and the total CoBF responses and the arteriolar diameters (145 ± 20%), and all these changes were reversible upon removal of NMDA. Topical application of the NMDA receptor inhibitor MK-801 did not affect CoBF (Fig. 2f), however, coapplication of MK-801 with either NMDA doses completely abolished the hyperemic and the pial arteriolar

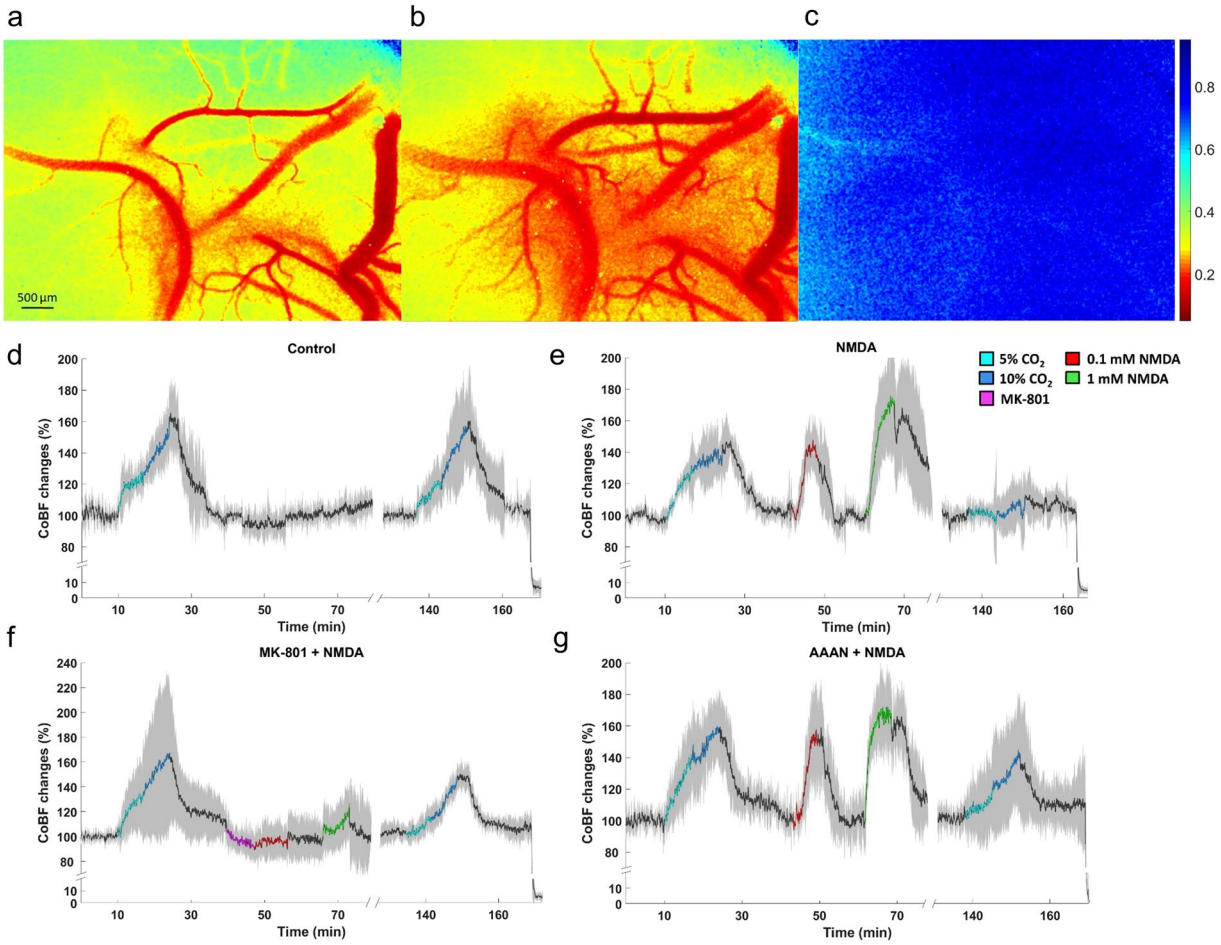

Figure 2. Cortical blood flow (CoBF) changes to graded hypercapnia and NMDA using laser-speckle contrast imaging and analysis. (**a–c**) Representative LSCI contrast images obtained through the closed cranial window (**a–c**) with the corresponding contrast scales. Lower contrast values represent higher flow velocity in the cortical microcirculation. (**a**) baseline condition; (**b**) NMDA (1 mM) showing pial arteriolar vasodilation and increased parenchymal flow as well. (**c**) biological zero after euthanasia characterized by high and stable speckle contrast values marking the disappearance of the perfusion. (**d–g**) Summarized recordings of individual experiments, colored/black lines represent the group mean values during/between stimuli, the gray area represent the SD. (**d**) in the control group graded hypercapnia resulted in concentration-dependent repeatable increases in CoBF relative to the baseline. (**e**) Both doses of NMDA reversibly elevated CoBF, however, the CoBF response to graded hypercapnia was virtually absent after NMDA. (**f**) Pre- and co-treatment of MK-801 with NMDA abolished the CoBF response to NMDA and prevented the attenuation of the CoBF response to graded hypercapnia. (**g**) AAAN did not affect the CoBF response to hypercapnia or NMDA, however, at least partially prevented the attenuation of the microvascular response to graded hypercapnia by NMDA.

response to NMDA (Fig. 3a,b,d). Systemic administration of the selective nNOS inhibitor AAAN did not affect the CoBF response to NMDA (Figs. 2g; 3a,b), however, it caused a significant reduction in the pial arteriolar dilation to NMDA (Fig. 3d).

NMDA eliminates the hypercapnia-induced cortical microvascular response. In the control group, the CoBF response to the second exposure to graded hypercapnia was virtually identical to the first stimulation (Fig. 2d), the peak and the integrated CoBF values were very similar (Fig. 3a,b), and the cerebrovascular reactivity to either CO_2 concentration was fully preserved (Fig. 3c). In sharp contrast, cerebrovascular reactivity to the second exposure to graded hypercapnia was abolished in the NMDA-treated group (Figs. 2e, 3). Pre- and coapplication of MK-801 with NMDA prevented the attenuation of the CoBF response to graded hypercapnia (Figs. 2f, 3a,b), cerebrovascular reactivity was preserved (Fig. 3c). In the nNOS inhibitor treated group, the CoBF response to graded hypercapnia was attenuated but not abolished after NMDA (Figs. 2g, 3a,b), thus cerebrovascular reactivity was partially ($68 \pm 35\%$) preserved in this group (Fig. 3c).

LFP changes induced by graded hypercapnia. Induction of hypercapnia with 5% CO_2 elicited first increases then decreases in LFP power, especially in the delta (δ) and theta (θ) ranges (Fig. 4a,b). Highest increases in δ were observed at cortical depths 100–400 µm and in θ at 100–600 and at 1000–1200 µm (Table 2). The subsequent reduction in power started in the deeper cortical layers (below 900 µm) gradually shifting upward.

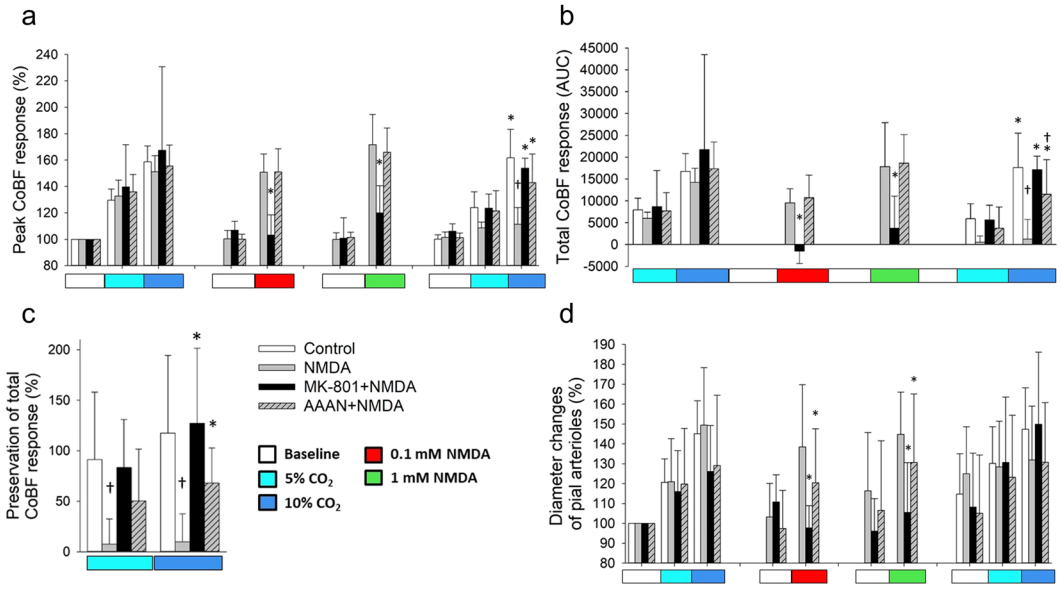

Figure 3. Summary of the cortical microvascular responses to graded hypercapnia and NMDA assessed with laser-speckle contrast imaging and analysis. (**a**) Peak increases in CoBF to graded hypercapnia (n = 6) were significantly blunted after NMDA-treatment (n = 7) alone but not after MK-801 + NMDA coapplication (n = 4) or AAAN pretreatment (n = 7). NMDA-induced peak increases in CoBF were also attenuated by MK-801 ($F_{group} = 3.785$; $\eta^2 = 0.066$; $p = 0.012$), but not by AAAN, furthermore AAAN clearly had no effect on the microvascular response to graded hypercapnia. (**b**) determination of the integrated (area under the curve, AUC) CoBF response shows also the severe attenuation of microvascular reactivity to graded hypercapnia in the NMDA-treated animals. Also, the inhibitory effect of MK-801 on NMDA-induced cortical hyperemia is striking ($F_{group} = 4.464$; $\eta^2 = 0.411$; $p = 0.0001$). (**c**) Cortical microvascular reactivity to hypercapnia is expressed as the ratio of the total CoBF response to the first and second graded hypercapnia. The response was fully preserved in the control and in the MK-801 + NMDA treated animals, however, virtually abolished in the animals exposed to NMDA alone. Pretreatment with AAAN resulted in a partial preservation of the response ($F_{group} = 8.428$; $\eta^2 = 0.441$; $p = 0.0001$). (**d**) Relative (%) changes in pial arteriolar diameters show that pial arteriolar responses to graded hypercapnia were not significantly different among the four groups. However, NMDA-induced pial arteriolar vasodilation was fully prevented by MK-801 and also significantly attenuated by AAAN ($F_{group} = 4.741$; $\eta^2 = 0.113$; $p = 0.004$), $p < 0.05$, * vs. NMDA, † vs. control.

Switching to 10% CO_2 further reduced LFP power both in the δ and θ ranges (Fig. 4). These depressions were largely reversed upon restoration of normocapnia, and the LFPs were not significantly different from the baseline values. LFP power in the alpha (α) and beta (β) ranges was quite small under these experimental conditions and clear hypercapnia-related changes could not be observed (data not shown). LFP changes to graded hypercapnia following the stimulation with NMDA were markedly different, most strikingly the early increases in θ LFP power did not develop (Table 2, Fig. 4b). δ LFP powers were also significantly altered (Table 2), and the pattern of LFP changes appeared to have disorganized.

NMDA evokes delta (δ) oscillation. NMDA (1 mM) selectively increased δ LFP power only in the upper layers (100–700 µm; Fig. 4a; Table 1) however, activity in the θ range were simultaneously suppressed (Fig. 4b). Similar suppression was observed in the α and β ranges as well (e.g. at 600 µm cortical depth reductions were 58.8 ± 1.2 and 44.9 ± 1.7% of baseline, respectively). This characteristic increase in the δ was identified as a ~2.5 Hz δ oscillation) down to 600 µm (Fig. 5a). CSD analysis identifying the contributing sinks and sources of cortical extracellular currents showed that NMDA (1 mM) altered significantly the size of the sinks and sources (Fig. 5b) causing the activation first in layer I. then layer II/III and IV. This NMDA-induced activation was δ band-limited.

Neuronal spiking in response to graded hypercapnia and NMDA. All recorded neurons (n = 149; total spike count = 152,089) fired with low frequency (~0.3–3 Hz, Fig. 6a–e). The ACGs identified major neuronal types of the parietal cortex such as interneurons (Fig. 6a), bursting (Fig. 6bde) and regular spiking pyramidal cells (Fig. 6c). CCGs helped to identify the most characteristic cell connections that were typically excitatory with 3–4 ms latency (Fig. 6g–i). We observed only a few inhibitory connections or reciprocal excitation/inhibition between the cells (Fig. 6h).

Graded hypercapnia and NMDA increased spiking activity mainly in the II/III. and IV. layers down to 900 µm. Increased firing allowed more precise identification of interneuronal connections, from the total 164 connections 71% have been associated with layer II/III including intralaminar connections as well. Under the first hypercapnia the recorded spike counts were much higher compared to baseline condition (5% CO_2: 36,245 spikes, 146/149 active cells; 10% CO_2: 24,043 spikes, 142/149 active cells). In the subsequent normocapnic period the spiking

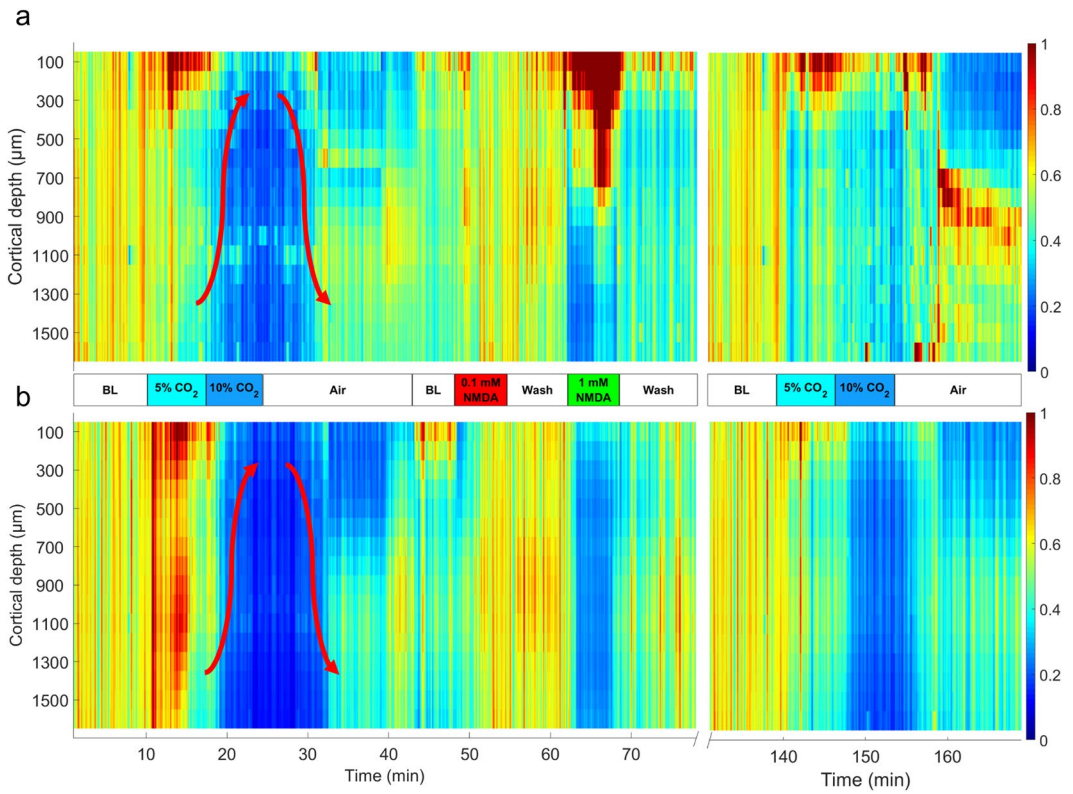

Figure 4. Representative heat map images of (**a**): delta (δ) and (**b**) theta (θ) band power spectral densities (PSDs) obtained from the local field potential recordings with a 16-channel electrode representing 100–1600 μm cortical depths with the corresponding intensity scales (0-1) from an animal of the NMDA-treated group. (**a**) during hypercapnia, 5% CO_2 tended to increase δ in the superficial cortical layers, but activity diminished after switching to 10% CO_2 starting in the deep cortical layers gradually shifting upwards (arrow pointing up). After restoration of normocapnia, δ activity was also restored (arrow pointing down). NMDA, especially the higher dose strongly increased δ activity predominantly in the upper cortical layers ($F_{group} = 1363.103$ (1 mM NMDA); $\eta^2 = 0.8614$; $p = 0.00001$**). The second stimulation with graded hypercapnia showed a somewhat similar pattern, however, the δ depression during the deeper level of hypercapnia, and also the restoration of activity upon normocapnia was less clear-cut than before NMDA. (**b**) during hypercapnia, 5% CO_2 resulted in a quite widespread increase in cortical θ activity ($F_{group} = 726.632$ (5% CO_2); $\eta^2 = 0.7623$; $p = 0.00001$**) that was attenuated and reversed to depression after switching to 10% CO_2 similarly to the pattern observed for δ (arrows). NMDA (1 mM) resulted in an almost complete suppression of θ in all cortical layers. After NMDA, the second graded hypercapnia lacked the θ activation associated with 5% CO_2. BL: baseline.

activity has returned almost to the baseline activity (19,443 spikes, 133/149 active cells). NMDA (1 mM) suppressed neuronal activity in ~60% of neurons, the number of active cells dropped to 73/149, but the remaining ~40% of neurons were excited that total spike count remained similar to the baseline (15,400 spikes). During the second hypercapnia, few cells remained responsive CO_2 (5% CO_2: 41/149 active cells, 8985 spikes; 10% CO_2: 17/149 active cells, 5130 spikes).

Discussion

The major novel findings of the present study are the following: (1) Graded hypercapnia elicits repeatable, concentration-dependent increases in CoBF that was attenuated by topical application of NMDA. (2) The attenuation of the hemodynamic response to hypercapnia after NMDA was prevented fully by MK-801 and partially by AAAN indicating an exclusive role for the NMDA receptor and a significant role for nNOS activation in mediating this response. (3) The attenuated cerebrovascular response after NMDA was associated with an altered electrophysiological response to hypercapnia, more specifically, the increased PSD in the δ and θ bands of the LFP was greatly attenuated. (4) NMDA, however, was shown to elicit strong, ~2.5 Hz delta oscillations peaking at 5–700 μm from the cortical surface indicating the major cortical targets of topically applied NMDA.

The cortical microvascular response to NMDA. The newborn pig is an established translational large animal model of the term neonate, thus the study of cerebrocortical microvascular reactivity to various stimuli as well as its alterations following hypoxic/ischemic stress in this model are of great interest to investigative neonatology[22,23]. Accordingly, the closed cranial window/intravital microscopy technique has been used extensively to study the cerebrocortical microcirculation. NMDA-induced pial arteriolar vasodilation was indeed first described in this species[24], later also confirmed in other species studied such as in rabbits[25] and rats[26]. Based

Delta (%)						
Cortical depth (µm)	**5% CO_2**	**10% CO_2**	**0.1 mM NMDA**	**1 mM NMDA**	**5% CO_2**	**10% CO_2**
100	140.9 ± 14.3*	58.6 ± 17.4	76.2 ± 10.2	252.1 ± 54.3**	51.2 ± 5.1	50.5 ± 12.3
200	130.4 ± 9.2*	20 ± 3.1	44.7 ± 5.1	243.6 ± 49.2**	46.0 ± 8.2	22.3 ± 2.0
300	123.9 ± 23.6*	18.7 ± 3.1	46.8 ± 4.1	187.0 ± 14.3**	45.3 ± 10.3	39.5 ± 11.3
400	127.9 ± 28.7*	46.5 ± 8.2	113.4 ± 11.3	305.0 ± 78.9**	78.5 ± 12.3	68.2 ± 23.6
500	79.8 ± 13.3	54.3 ± 8.2	92.5 ± 5.1	191.1 ± 14.3**	66.6 ± 11.3	59.6 ± 18.4
600	71.1 ± 7.2	44.1 ± 12.3	90.3 ± 7.2	197.7 ± 15.4**	60.8 ± 16.4	50.3 ± 25.6
700	38.0 ± 3.1	24.1 ± 7.2	49.9 ± 5.1	160.6 ± 11.3**	24.4 ± 2.0	34.8 ± 8.2
800	73.4 ± 14.3	60.4 ± 29.7	113.0 ± 10.2	140.9 ± 18.4*	82.1 ± 8.2	77.0 ± 5.1
900	52.1 ± 5.1	46.1 ± 10.2	67.3 ± 3.1	66.7 ± 10.2	97.9 ± 21.5	65.6 ± 13.3
1000	29.7 ± 4.1	26.6 ± 6.1	37.7 ± 1.0	54.2 ± 7.2	31.6 ± 8.2	31.0 ± 6.1
1100	83.0 ± 7.2	39.3 ± 10.2	103.8 ± 5.1	74.0 ± 19.5	61.7 ± 9.2	53.3 ± 10.2
1200	40.8 ± 6.1	31.5 ± 10.2	33.7 ± 3.1	40.7 ± 7.2	27.2 ± 4.1	52.1 ± 14.3
1300	65.7 ± 5.1	40.6 ± 8.2	56.4 ± 2.0	75.7 ± 14.3	42.3 ± 4.1	50.6 ± 7.2
1400	55.3 ± 6.1	41 ± 7.2	45.1 ± 2.0	80.8 ± 21.5	38.4 ± 3.1	65.3 ± 12.3
1500	52.7 ± 3.1	27.7 ± 2.0	60.1 ± 3.1	58.4 ± 9.2	45.8 ± 8.2	36.3 ± 8.2
1600	64.2 ± 5.1	35.2 ± 4.1	61.6 ± 7.2	84.0 ± 14.3	40.1 ± 4.1	34.5 ± 7.2
Theta (%)						
100	184.4 ± 14.3**	32.1 ± 5.1	61.9 ± 3.1	59.0 ± 11.3	43.2 ± 4.1	24.7 ± 3.1
200	174.2 ± 13.3**	22.7 ± 2.0	80.5 ± 6.1	38.1 ± 9.2	42.4 ± 3.1	21.6 ± 3.1
300	163.7 ± 14.3**	19.1 ± 1.0	59.0 ± 4.1	51.3 ± 8.2	37.9 ± 3.1	31.5 ± 4.1
400	160.1 ± 18.4**	24.5 ± 3.1	76.8 ± 6.1	57.7 ± 11.3	42.2 ± 4.1	30.6 ± 4.1
500	157.5 ± 14.3**	30.3 ± 5.1	51.2 ± 3.1	42.5 ± 8.2	31.3 ± 3.1	29.1 ± 6.1
600	165.4 ± 18.4**	21.7 ± 2.0	108.9 ± 9.2	61.7 ± 11.3	42.4 ± 4.1	31.8 ± 3.1
700	105.0 ± 15.4	58.5 ± 12.3	77.7 ± 6.1	67.1 ± 11.3	41.1 ± 3.1	38.4 ± 4.1
800	105.1 ± 12.3	19.9 ± 1.0	81.2 ± 6.1	56.8 ± 10.2	49.1 ± 7.2	40.9 ± 7.2
900	114.1 ± 11.3	29.9 ± 3.1	96.9 ± 7.2	57.4 ± 9.2	65.4 ± 4.1	41.9 ± 5.1
1000	167.5 ± 11.3**	22.3 ± 2.0	91.9 ± 6.1	63.9 ± 10.2	53.1 ± 4.1	44.5 ± 8.2
1100	157.7 ± 12.3**	19.4 ± 2.0	86.7 ± 7.2	59.1 ± 9.2	55.6 ± 3.1	50.4 ± 8.2
1200	154.0 ± 12.3**	24.5 ± 2.0	100.8 ± 7.2	55.3 ± 9.2	56.9 ± 3.1	44.0 ± 7.2
1300	114.5 ± 15.4	22.3 ± 2.0	98.1 ± 6.1	54.0 ± 7.2	64.3 ± 4.1	61.9 ± 1.0
1400	109.5 ± 17.4	17.7 ± 1.0	83.9 ± 5.1	52.0 ± 7.2	59.3 ± 3.1	40.9 ± 6.1
1500	101.5 ± 16.4	19 ± 2.0	82.0 ± 6.1	45.8 ± 7.2	60.4 ± 4.1	32.4 ± 4.1
1600	104.1 ± 16.4	32.7 ± 3.1	71.3 ± 5.1	62.5 ± 7.2	56.2 ± 3.1	48.9 ± 6.1

Table 2. Power spectral density changes in the Delta and the Theta band during stimulations with graded hypercapnia and NMDA. Data are expressed as % of baseline (mean ± SD). *$p < 0.05$, **$p < 0.01$.

on its sensitivity to tetrodotoxin[27] and nNOS inhibitors[28,29], the mechanism of NMDA-induced pial arteriolar dilation has been accepted to be mediated by neuronal NO production in piglets and in most other experimental models[30]. The present study simultaneously confirms previous experimental findings but conflicts with the conclusions drawn in previous studies. In the present study nNOS inhibition by AAAN (0.4 mg/kg) resulted in a similar attenuation (~30–40%) of pial arteriolar dilation to NMDA to that found by Bari *et al.* using the nNOS inhibitor 7-nitroindazole (50 mg/kg)[29]. However, we now demonstrated that the attenuated arteriolar vasodilation to NMDA did not coincide with attenuated blood flow response in the underlying parenchyma, indeed the parenchymal flow response was virtually unchanged. We believe that the LSCI used in the present study to assess the cortical microvasculature gives a good estimate of the NMDA-induced microvascular response as our current results showing ~72% increase in CoBF to 1 mM NMDA are in complete agreement with our previous study displaying virtually identical increases in CoBF to this dose of NMDA using laser-Doppler flowmetry[6]. Our results suggest that dilation of intraparenchymal arterioles plays a more decisive role in determining the CoBF response and can compensate for the somewhat smaller pial arteriolar dilation in response to NMDA when nNOS activity is compromised. This finding is in contrast with data obtained in the adult rat, where also the CoBF response to NMDA applied was demonstrated to be critically dependent on nNOS presence and activity[31], and this difference may well represent a species/age-dependent difference. Clearly, additional vasodilatory mechanisms acting perhaps predominantly on intraparenchymal vessels must play a role in mediating the observed increases in CoBF to NMDA in the piglet that can be subject to further research. One such mediator could be adenosine, as adenosine was proposed beside NO to contribute to the NMDA-induced CoBF response in the rat cerebral cortex based on microdialysis data[32]. In the piglet cortex, exogenous adenosine appeared to reduce the pial arteriolar response to NMDA[33], this latter finding is conceivable presuming the adenosine may have had a predominant action of intraparenchymal arterioles that based on the present study can have responses largely independent of the pial vessels.

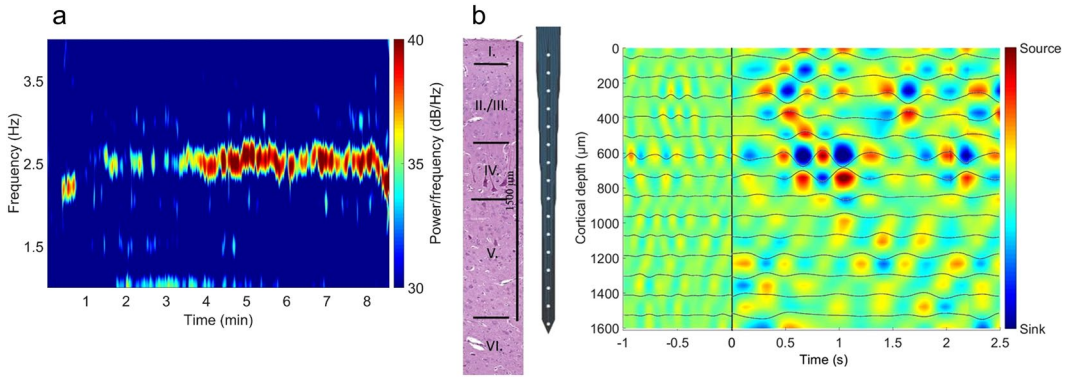

Figure 5. NMDA evokes delta (δ) oscillation in the upper cortical layers. (**a**) Representative δ band spectrogram during NMDA (1 mM) stimulation recorded at 600 µm under the cortical surface. The heat map shows the appearance of a 2.5 Hz frequency oscillation. (**b**) Average current source density (CSD) map of the δ oscillations observed during NMDA (1 mM) stimulation with the δ-filtered LFP superimposed onto the image. The multi-channel electrode (http://neuronexus.com/electrode-array/a1x16–10mm-100-177/) and an H/E-stained section of the piglet cortex are also shown for orientation. CSD analysis show that the oscillation originates chiefly in layers III/IV where the largest amplitude currents appear.

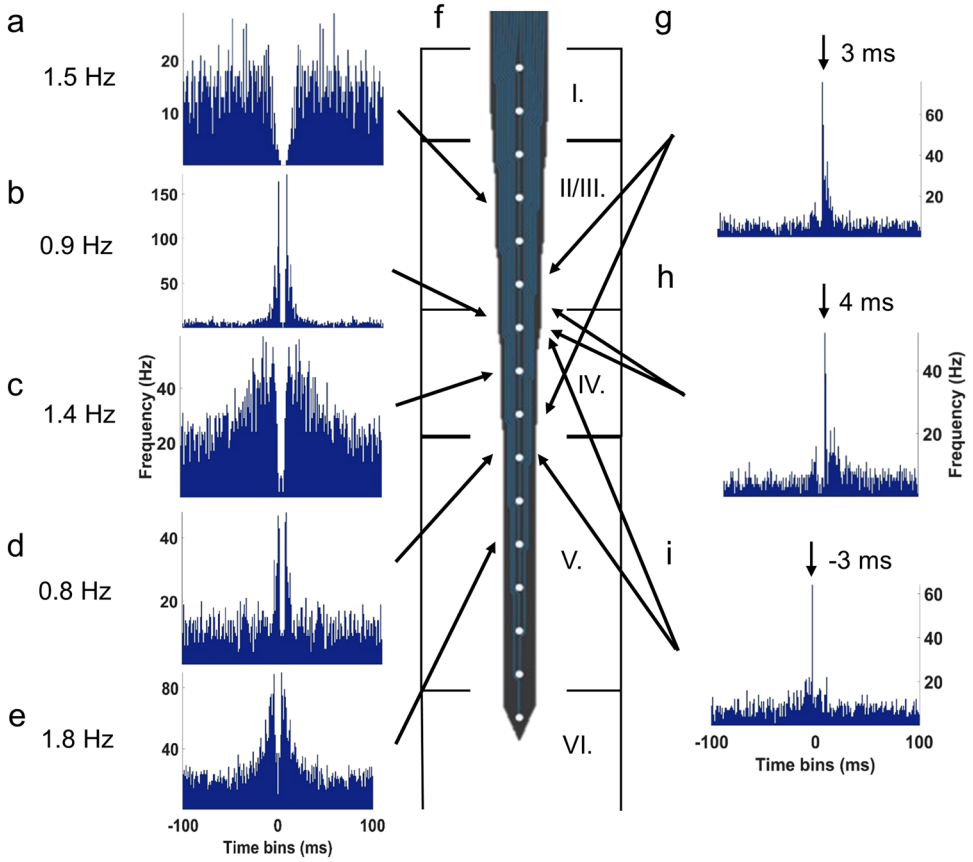

Figure 6. Representative auto- and cross-correlograms (ACGs and CCGs, respectively) of recorded cortical neurons and their connections with their highest firing rates. (**a**) Layer II/III. interneuron. (**b**) Layer IV. bursting pyramidal cell. (**c**) Layer IV. regular spiking pyramidal cell. (**d**,**e**) Layer V. bursting pyramidal cells. (**f**) Representative image of the recording electrode (http://neuronexus.com/electrode-array/a1x16-10mm-100-177/) with its position in the parietal cortex. Excitatory synapses between a (**g**) bursting and a regular spiking, (**h**) interneuron and bursting pyramidal cell, (**i**) two bursting pyramidal cells.

The cortical neuronal response to NMDA. The cortical microvascular response to NMDA in piglets is thought to be mediated by exclusive activation of neuronal NMDA receptors based on two lines of evidence, isolated piglet cortical vessels do not respond to NMDA[34], and functional NMDA receptors are not expressed

in cerebrovascular endothelial cells or microvessels isolated either from rats, humans or piglets[35,36]. However, recent work suggests that in mice abluminally localized endothelial NMDA receptors can contribute to functional hyperemia[37,38]. Unlike the painstakingly analyzed pial arteriolar response to NMDA, the changes in neuronal activity in response to topically applied NMDA were hardly tackled. Topically applied NMDA was demonstrated to elicit an SD characterized by the signature SD-related DC potential shift simultaneously with pial arteriolar changes in adult mice, and the NMDA effect was found concentration-independently linked to the evoked SD[5]. In a subsequent adult rat study, topical NMDA was indeed found to also elicit an SD, but the CoBF response after the SD-related hemodynamic response demonstrated additionally also an NMDA-dose dependent component[6]. The same experimental approach in piglets found only a dose-dependent CoBF response without any confounding SDs[6]. Immunohistochemistry studies in the piglet parietal cortex identified layers II/III as the major site of nNOS-immunoreactive neurons and as these superficial cortical layers were also rich in NMDA-receptor immunoreactive nerve cells[33], they were accordingly assumed to be responsible for the observed effects of NMDA. Our present study is essentially the first that studied the electrophysiological response simultaneously in all cortical layers to topically applied NMDA. Our present findings identified not only the most superficial, but also much deeper cortical structures to be affected by topical NMDA. Thus, the NMDA-induced intense 2.5 Hz δ-oscillation have been found most prominent at 6–800 μm from the cortical surface suppressing LFP power in virtually all other frequency bands. NMDA also had opposing effects on neuronal firing, it suppressed or stimulated spiking in different neuronal populations. We found that after NMDA, the LFP powers were restored to baseline levels, and also no abnormal spikes were recorded during/after NMDA application suggesting that significant excitotoxic lesion to the cortex did not occur during NMDA stimulation. This notion is in accordance with previous findings showing that the neurovascular response to topical NMDA is preserved in piglets (four applications in a 5 hours period)[39]. These results correspond well both with the previous observations of SD-triggering and also with the tetrodotoxin-sensitive actions of topical NMDA application.

NMDA triggers SD-like suppression of the microvascular response to hypercapnia. The cortical microvascular response to graded hypercapnia has been extensively studied in the piglet, but few experiments assessed pial arteriolar diameter and CoBF changes simultaneously[40]. In this study[40], both responses were unaltered by the general NOS inhibitor Nω-nitro-L-arginine methyl ester, indicating that NO plays minor role in the mediation of this response in the newborn pig. This NO-independence appears to be age-restricted in the pig, the pial arteriolar response to hypercapnia has also been shown to be NO-independent in newborns, but to be partially NO-dependent in juvenile (3–4 months old) pigs[41,42]. In the rat, the soluble guanylate cyclase inhibitor 1 H-[1,2,4]oxadiazolo[4,4,-a]quinoxalin-1-one (ODQ) had also no effect on the response to hypercapnia but to NMDA[43]. However, a number of rat studies emphasize the role of nNOS-derived NO in the CoBF response to hypercapnia[44,45]. In accordance with previous newborn pig studies, the nNOS inhibitor AAAN had no effect on the cortical microvascular response to graded hypercapnia in the present study.

The pial arteriolar response to graded hypercapnia has been known to be vulnerable to hypoxic/ischemic stress[46], endothelial injury[47], or seizures[48] making the response a good indicator of neurovascular unit dysfunction. SDs are also known to attenuate the microvascular response to hypercapnia in adult brains[2–4]. In the piglet cortex *bona fide* SDs of course could not be generated, however, an artificially induced 3-min long cortical depolarization (elicited with topical KCl and confirmed with DC recording) did not affect the microvascular response to hypercapnia and other assessed stimuli[49]. In contrast, in the present study, NMDA attenuated the response to graded hypercapnia in the newborn cerebral cortex that is similar to that observed after SD in adult cortex. The microvascular alteration appears to be independent of the direct hemodynamic effect of NMDA-receptor activation but its mechanism appears to involve nNOS activity. However, generalization of our findings to the adult cerebral cortex is prevented by the apparent limitations of developmental differences that actually prevent the triggering of SD in the neonatal brain.

In the present study, we just started to decipher the connections between the well-known cerebrovascular effects of hypercapnia and NMDA and the virtually uncharted neuronal effects of these stimuli in the cerebral cortex of the newborn pig. Using multi-channel silicone probes to study LFP and unit activity changes are widely used in the literature[50,51], although for instance interpretation of LFP data is difficult due to the many sources contributing to the mixed signal[52,53]. There is very little information available about the LFP[54] or the unit activity[55] of the adult pig cerebral cortex let alone of the newborn piglet. Our current findings show layer-specific and concentration-dependent effects of hypercapnia on both the LFP and unit activity that are clearly altered after NMDA. Presently, we cannot make causative statements whether alterations in the neuronal response trigger the observed changes in microvascular reactivity or perhaps vice versa, however, our results are strongly indicating that the mechanism of NMDA-induced attenuation of the microvascular response is not likely to be limited to the cerebral vasculature. NMDA has been also shown to suppress all frequency bands of the LFP (similar to an SD in adult or old rats[56–58]), but it also triggered a 2.5 Hz delta-oscillation. The origin of the arising delta-oscillation is still not clear, however it has been described earlier that these oscillations can be evoked by topical stimulations and different cell types can generate abnormal oscillations in the cortex as well[59–62]. Furthermore, spiking was also suppressed in some, but triggered in other units during NMDA. Again, we cannot determine the significance of these observations in the attenuation of microvascular response to hypercapnia, however, we can hypothesize that different components of the electrophysiological response to NMDA could be responsible for the attenuation of microvascular reactivity to hypercapnia and for the developing marked CoBF response. Clearly, further studies are warranted to identify the neuronal-vascular mechanisms selectively responsible for either effect of topically applied NMDA.

In conclusion, NMDA triggers microvascular dysfunction in the piglet cerebral cortex similar to but not confounded by SD. Understanding the mechanism of this novel observation may help to elucidate the deleterious effects of SD on the neurovascular unit.

Data availability

The datasets generated during the current study are available from the corresponding author on reasonable request.

Received: 23 May 2019; Accepted: 29 November 2019;
Published online: 11 December 2019

References

1. Hartings, J. A. *et al*. The continuum of spreading depolarizations in acute cortical lesion development: Examining Leão's legacy. *J. Cereb. Blood Flow Metab.* **37**, 1571–1594 (2017).
2. Piper, R. D., Lambert, G. A. & Duckworth, J. W. Cortical blood flow changes during spreading depression in cats. *Am. J. Physiol.* **261**, H96–102 (1991).
3. Lacombe, P., Sercombe, R., Correze, J. L., Springhetti, V. & Seylaz, J. Spreading depression induces prolonged reduction of cortical blood flow reactivity in the rat. *Exp. Neurol.* **117**, 278–286 (1992).
4. Uneķawa, M. *et al*. Dynamic diameter response of intraparenchymal penetrating arteries during cortical spreading depression and elimination of vasoreactivity to hypercapnia in anesthetized mice. *J. Cereb. Blood Flow Metab.* **37**, 657–670 (2016).
5. Ayata, C. & Moskowitz, M. A. Cortical spreading depression confounds concentration-dependent pial arteriolar dilation during N-methyl-D-aspartate superfusion. *AJP Hear. Circ. Physiol.* **290**, H1837–H1841 (2006).
6. Lenti, L. *et al*. N-methyl-D-aspartate induces cortical hyperemia through cortical spreading depression-dependent and -independent mechanisms in rats. *Microcirculation* **16**, 629–639 (2009).
7. Marrannes, R., Willems, R., De Prins, E. & Wauquier, A. Evidence for a role of the N-methyl-d-aspartate (NMDA) receptor in cortical spreading depression in the rat. *Brain Res.* **457**, 226–240 (1988).
8. Lauritzen, M. & Hansen, A. J. The effect of glutamate receptor blockade on anoxic depolarization and cortical spreading depression. *J. Cereb. Blood Flow Metab.* **12**, 223–229 (1992).
9. Nemeth, J. *et al*. Molecular hydrogen affords neuroprotection in a translational piglet model of hypoxic-ischemic encephalopathy. *J. Physiol. Pharmacol.* **67**, 677–689 (2016).
10. Kovács, V. *et al*. Active forms of Akt and ERK are dominant in the cerebral cortex of newborn pigs that are unaffected by asphyxia. *Life Sci.* **192**, 1–8 (2018).
11. Laptook, A. R., Stonestreet, B. S. & Oh, W. The effect of carotid artery ligation on brain blood flow in newborn piglets. *Brain Res.* **276**, 51–54 (1983).
12. Domoki, F. *et al*. Comparison of cerebrocortical microvascular effects of different hypoxic-ischemic insults in piglets: A laser-speckle imaging study. *J. Physiol. Pharmacol.* **65**, 551–558 (2014).
13. Ji, H. *et al*. Selective neuronal nitric oxide synthase inhibitors and the prevention of cerebral palsy. *Ann. Neurol.* **65**, 209–217 (2009).
14. Domoki, F. *et al*. Evaluation of laser-speckle contrast image analysis techniques in the cortical microcirculation of piglets. *Microvasc. Res.* **83**, 311–317 (2012).
15. Hazan, L., Zugaro, M. & Buzsáki, G. Klusters, NeuroScope, NDManager: A free software suite for neurophysiological data processing and visualization. *J. Neurosci. Methods* **155**, 207–216 (2006).
16. Kadir, S. N., Goodman, D. F. M. & Harris, K. D. High-Dimensional Cluster Analysis with the Masked EM Algorithm. *Neural Comput.* **26**, 2379–2394 (2014).
17. Rossant, C. *et al*. Spike sorting for large, dense electrode arrays. *Nat. Neurosci.* **19**, 634–641 (2016).
18. Csicsvari, J., Hirase, H. & Czurkó, A. Reliability and State Dependence of Pyramidal Cell – Interneuron Synapses in the Hippocampus: an Ensemble Approach in the Behaving Rat. *Neuron* **21**, 179–189 (1998).
19. Mizuseki, K., Sirota, A., Pastalkova, E. & Buzsáki, G. Theta Oscillations Provide Temporal Windows for Local Circuit Computation in the Entorhinal-Hippocampal Loop. *Neuron* **64**, 267–280 (2008).
20. Stark, E. *et al*. Pyramidal cell-interneuron interactions underlie hippocampal ripple oscillations. *Neuron* **83**, 467–480 (2014).
21. Barthó, P. *et al*. Characterization of Neocortical Principal Cells and Interneurons by Network Interactions and Extracellular Features. *J. Neurophysiol.* **92**, 600–608 (2004).
22. Alonso-Alconada, D. *et al*. Brain cell death is reduced with cooling by 3.5 °C to 5 °C but increased with cooling by 8.5 °C in a piglet asphyxia model. *Stroke* **46**, 275–278 (2015).
23. Sabir, H. *et al*. Xenon depresses aEEG background voltage activity whilst maintaining cardiovascular stability in sedated healthy newborn pigs. *J. Neurol. Sci.* **363**, 140–144 (2016).
24. Busija, D. W. & Leffler, C. W. Dilator effects of amino acid neurotransmitters on piglet pial arterioles. *Am. J. Physiol. Circ. Physiol.* **257**, H1200–H1203 (1989).
25. Faraci, F. M. & Breese, K. R. Nitric oxide mediates vasodilatation in response to activation of N- methyl-D-aspartate receptors in brain. *Circ. Res.* **72**, 476–480 (1993).
26. Mayhan, W. G. & Didion, S. P. Acute Effects of Ethanol on Responses of Cerebral Arterioles. *Stroke* **26**, 2097–2102 (1995).
27. Leffler, C. W., Parfenova, H., Fedinec, A. L., Tcheranova, D. & Basuroy, S. Contributions of astrocytes and CO to pial arteriolar dilation to glutamate in newborn pigs. *Am. J. Physiol. Circ. Physiol.* **291**, H2897–H2904 (2006).
28. Meng, W., Tobin, J. R. & Busija, D. W. Glutamate-Induced Cerebral Vasodilation Is Mediated by Nitric Oxide Through N-Methyl-D-Aspartate Receptors. *Stroke* **26**, 857–863 (1995).
29. Bari, F., Errico, R. A., Louis, T. M. & Busija, D. W. Interaction between ATP-sensitive K+ channels and nitric oxide on pial arterioles in piglets. *J. Cereb. Blood Flow Metab.* **16**, 1158–1164 (1996).
30. Busija, D. W., Bari, F., Domoki, F. & Louis, T. Mechanisms Involved in the Cerebrovascular Dilator Effects of N- methyl-D-aspartate in Cerebral Cortex. *Brain Res. Rev.* **56**, 89–100 (2007).
31. Girouard, H. *et al*. NMDA receptor activation increases free radical production through Nitric Oxide and NOX2. *J. Neurosci.* **29**, 2545–2552 (2009).
32. Kaiser, M. G. & During, M. J. Combining laser doppler flowmetry with microdialysis: a novel approach to investigate the coupling of regional cerebral blood flow to neuronal activity. *J. Neurosci. Methods* **60**, 165–173 (1995).
33. Bari, F., Thore, C. R., Louis, T. M. & Busija, D. W. Inhibitory effects of hypoxia and adenosine on N-methyl-D-aspartate-induced pial arteriolar dilation in piglets. *Brain Res.* **780**, 237–244 (1998).
34. Simandle, S. A. *et al*. Piglet pial arteries respond to N-methyl-D-aspartate *in vivo* but not *in vitro*. *Microvasc. Res.* **70**, 76–83 (2005).
35. Morley, P. *et al*. Evidence that Functional Glutamate Receptors are not Expressed on Rat or Human Cerebromicrovascular Endothelial Cells. *J. Cereb. Blood Flow Metab.* **18**, 396–406 (1998).
36. Domoki, F., Kis, B., Gáspár, T., Bari, F. & Busija, D. W. Cerebromicrovascular endothelial cells are resistant to L-glutamate. *Am. J. Physiol. Integr. Comp. Physiol.* **295**, R1099–R1108 (2008).
37. Lu, L. *et al*. Astrocytes drive cortical vasodilatory signaling by activating endothelial NMDA receptors. *J. Cereb. Blood Flow Metab.* **39**, 481–496 (2019).

38. Hogan-Cann, A. D., Lu, P. & Anderson, C. M. Endothelial NMDA receptors mediate activitydependent brain hemodynamic responses in mice. *Proc. Natl. Acad. Sci. USA* **116**, 10229–10231 (2019).
39. Busija, D. W. *et al*. Effects of ischemia on cerebrovascular responses to N-methyl-D-aspartate in piglets. *Am. J. Physiol. - Hear. Circ. Physiol.* **270** (1996).
40. Domoki, F., Zimmermann, A., Tóth-Szűki, V., Busija, D. W. & Bari, F. Acetazolamide induces indomethacin and ischaemia-sensitive pial arteriolar vasodilation in the piglet. *Acta Paediatr.* **97**, 280–284 (2008).
41. Willis, A. P. & Leffler, C. W. NO and prostanoids: Age dependence of hypercapnia- and histamine- induced dilations of pig pial arterioles. *Am. J. Physiol. - Hear. Circ. Physiol.* **277**, 299–307 (1999).
42. Willis, A. P. & Leffler, C. W. Endothelial NO and prostanoid involvement in newborn and juvenile pig pial arteriolar vasomotor responses. *Am. J. Physiol. - Hear. Circ. Physiol.* **281**, 2366–2377 (2001).
43. Rosenblum, W. I., Wei, E. P. & Kontos, H. A. Dilation of rat brain arterioles by hypercapnia *in vivo* can occur even after blockade of guanylate cyclase by ODQ. *Eur. J. Pharmacol.* **448**, 201–206 (2002).
44. Iadecola, C. Does nitric oxide mediate the increases in cerebral blood flow elicited by hypercapnia? *Proc. Natl. Acad. Sci. USA* **89**, 3913–3916 (1992).
45. Wang, Q., Pelligrino, D. A., Baughman, V. L., Koenig, H. M. & Albrecht, R. F. The role of neuronal nitric oxide synthase in regulation of cerebral blood flow in normocapnia and hypercapnia in rats. *J. Cereb. Blood Flow Metab.* **15**, 774–778 (1995).
46. Leffler, C. W., Busija, D. W., Armstead, W. M., Mirro, R. & Beasley, D. G. Ischemia Alters Cerebral Vascular Responses to Hypercapnia and Acetylcholine in Piglets. *Pediatr. Res.* **25**, 180–183 (1989).
47. Leffler, C. W., Mirro, R., Shanklin, D. R., Armstead, W. M. & Shibata, M. Light/dye microvascular injury selectively eliminates hypercapnia-induced pial arteriolar dilation in newborn pigs. *Am. J. Physiol. Circ. Physiol.* **266**, H623–H630 (1994).
48. Carratu, P., Pourcyrous, M., Fedinec, A., Leffler, C. W. & Parfenova, H. Endogenous heme oxygenase prevents impairment of cerebral vascular functions caused by seizures. *Am. J. Physiol. Circ. Physiol.* **285**, H1148–H1157 (2003).
49. Domoki, F., Veltkamp, R., Bari, F., Louis, T. M. & Busija, D. W. Cerebrovascular reactivity remains intact after cortical depolarization in newborn piglets. *Pediatr. Res.* **45**, 834–837 (1999).
50. Berényi, A. *et al*. Large-scale, high-density (up to 512 channels) recording of local circuits in behaving animals. *J. Neurophysiol.* **111**, 1132–1149 (2014).
51. Fiáth, R. *et al*. Laminar analysis of the slow wave activity in the somatosensory cortex of anesthetized rats. *Eur. J. Neurosci.* **44**, 1935–1951 (2016).
52. Buzsáki, G., Anastassiou, C. A. & Koch, C. The origin of extracellular fields and currents-EEG, ECoG, LFP and spikes. *Nat. Rev. Neurosci.* **13**, 407–420 (2012).
53. Einevoll, G. T., Kayser, C., Logothetis, N. K. & Panzeri, S. Modelling and analysis of local field potentials for studying the function of cortical circuits. *Nat. Rev. Neurosci.* **14**, 770–785 (2013).
54. Tanosaki, M., Ishibashi, H., Zhang, T. & Okada, Y. Effective Connectivity Maps in the Swine Somatosensory Cortex Estimated from Electrocorticography and Validated with Intracortical Local Field Potential Measurements. *Brain Connect.* **4**, 100–111 (2014).
55. Ulyanova, A. V. *et al*. Electrophysiological Signature Reveals Laminar Structure of the Porcine Hippocampus. *Eneuro* **5**, ENEURO.0102–18.2018 (2018).
56. Hertelendy, P. *et al*. Advancing age and ischemia elevate the electric threshold to elicit spreading depolarization in the cerebral cortex of young adult rats. *J. Cereb. Blood Flow Metab.* **37**, 1763–1775 (2017).
57. Menyhárt, Á. *et al*. High incidence of adverse cerebral blood flow responses to spreading depolarization in the aged ischemic rat brain. *Neurobiol. Aging* **36**, 3269–3277 (2015).
58. Makra, P., Menyhárt, Á., Bari, F. & Farkas, E. Spectral and Multifractal Signature of Cortical Spreading Depolarisation in Aged Rats. *Front. Physiol.* **9**, 1–12 (2018).
59. Kiss, T., Feng, J., Hoffmann, W. E., Shaffer, C. L. & Hajós, M. Rhythmic theta and delta activity of cortical and hippocampal neuronal networks in genetically or pharmacologically induced N-methyl-d-aspartate receptor hypofunction under urethane anesthesia. *Neuroscience* **237**, 255–267 (2013).
60. Gireesh, E. D. & Plenz, D. Neuronal avalanches organize as nested theta- and beta/gamma-oscillations during development of cortical layer 2/3. *Proc. Natl. Acad. Sci.* **105**, 7576–7581 (2008).
61. Minlebaev, M., Ben-Ari, Y. & Khazipov, R. NMDA receptors pattern early activity in the developing barrel cortex *in vivo*. *Cereb. Cortex* **19**, 688–696 (2009).
62. Matulewicz, P., Orzeł-Gryglewska, J., Kuśmierczak, M. & Jurkowlaniec, E. NMDA-glutamatergic activation of the ventral tegmental area induces hippocampal theta rhythm in anesthetized rats. *Brain Res. Bull.* **107**, 43–53 (2014).

Acknowledgements

We thank the technical and methodological support to Antal Berényi and Gábor Kozák. This work was supported by grants from the Hungarian Brain Research Program 2.0 (2017-2.1 NKP 2017 00002), the EU-funded Hungarian grant EFOP-3.6.1-16-2016-00008 and the GINOP 2.3.2 15 2016 00034. V.K. is supported by OTKA-PD128464 from the NRDI.

Author contributions

G.R. designed the project, conducted experiments, analysis and interpretation of the hemodynamic and electrophysiological data, statistical analyses, wrote the manuscript. J.N. designed the project, conducted experiments, analysis and interpretation of the hemodynamic data, reviewed the manuscript. V.T.-S. conducted animal experiments, analyzed hemodynamic, reviewed the manuscript. V.V. conducted *in vivo* experiments, reviewed the manuscript. V.K. conducted experiments, reviewed the manuscript. F.D.: drafted and designed the project, drafting, writing and critically revising the manuscript.

Competing interests

The authors declare no competing interests.

Additional information

Correspondence and requests for materials should be addressed to F.D.